Report Number: RHAMM-TR-05-02
December 31, 2005

Extend MANPADS M&S Capabilities to Include Energetic Materials, Fragmentation Effects, and Wing Flutter Response

Ronald L. Hinrichsen, Monty A. Moshier, and Brian D. Choules

RHAMM Technologies LLC
332 Skyland Dr., Bellbrook
OH 45305

Prepared for
United States Air Force
under Contract No. F49620-03-C-0013

REPORT DOCUMENTATION PAGE

Form Approved
OMB No. 0704-0188

1. REPORT DATE *(DD-MM-YYYY)*	2. REPORT TYPE	3. DATES COVERED *(From - To)*
31122005	Final Report	15 January 2003 - 31 December 2005

4. TITLE AND SUBTITLE
Extend MANPADS M&S Capabilities to Include Energetic Materials, Fragmentation Effects, and Wing Flutter Response

5a. CONTRACT NUMBER

5b. GRANT NUMBER
F49620-03-C-0013

5c. PROGRAM ELEMENT NUMBER

6. AUTHOR(S)
Ronald L. Hinrichsen, Monty A. Moshier, and Brian D. Choules

5d. PROJECT NUMBER

5e. TASK NUMBER

5f. WORK UNIT NUMBER

7. PERFORMING ORGANIZATION NAME(S) AND ADDRESS(ES)
RHAMM Technologies LLC
332 Skyland Drive
Bellbrook OH 45305

8. PERFORMING ORGANIZATION REPORT NUMBER

9. SPONSORING/MONITORING AGENCY NAME(S) AND ADDRESS(ES)
USAF/AFRL
AFOSR
875 North Randolph Street
Arlington VA 22203
Dr John Schmisseur

10. SPONSOR/MONITOR'S ACRONYM(S)
AFOSR

11. SPONSOR/MONITOR'S REPORT NUMBER(S)
AFRL-SR-AR-TR-06-0133

12. DISTRIBUTION/AVAILABILITY STATEMENT
Distribution Statement A. Approved for public release; distributin is unlimited.

13. SUPPLEMENTARY NOTES

14. ABSTRACT
The purpose of this effort is to create an analytical physics based aircraft-MANPADS model capability that includes impact, detonation, penetration, and wing flutter response. This work extends an existing body on body missile model to include, energetic materials, fragmentation effects and wing flutter response due to dynamic air loads. The detonation of the high explosive within the missile as well as the expansion of the surrounding fluids was modeled in the Eulerian domain. The Jones-Wilkins-Lee (JWL) equation of state was used to model the explosive and the Gruneisen equation of state was used for the surrounding fluids. Linear Boundary elements based on inviscid, incompressible flow theory were coupled with the wing structure model to simulate air loads. A modular approach was taken to separate the Eulerian domain and the JWL equation model, from the model including the target. Separating the models allows the complex physics to be mapped onto the missile including the target, preserving the physics without the added costs. Evaluation was done of various element failure criteria to increase model robustness Lastly, the model was used to evaluate the dynamic air loads and response of wing flutter. A physics based MANPADS model has been created which includes impact, penetration, detonation, and fragmentation with drag.

15. SUBJECT TERMS

16. SECURITY CLASSIFICATION OF:			17. LIMITATION OF ABSTRACT	18. NUMBER OF PAGES	19a. NAME OF RESPONSIBLE PERSON
a. REPORT	b. ABSTRACT	c. THIS PAGE			19b. TELEPHONE NUMBER *(Include area code)*
U	U	U	UU	99	

Abstract

The purpose of this effort is to create an analytical physics based aircraft-MANPADS model capability that includes impact, detonation, penetration, and wing flutter response. This work extends an existing body on body missile model to include, energetic materials, fragmentation effects and wing flutter response due to dynamic air loads. The detonation of the high explosive within the missile as well as the expansion of the surrounding fluids was modeled in the Eulerian domain. The Jones-Wilkins-Lee (JWL) equation of state was used to model the explosive and the Gruneisen equation of state was used for the surrounding fluids. Linear Boundary elements based on inviscid, incompressible flow theory were coupled with the wing structure model to simulate air loads. A modular approach was taken to separate the Eulerian domain and the JWL equation model, from the model including the target. Separating the models allows the complex physics to be mapped onto the missile including the target, preserving the physics without the added costs. Evaluation was done of various element failure criteria to increase model robustness. Lastly, the model was used to evaluate the dynamic air loads and response of wing flutter. A physics based MANPADS model has been created which includes impact, penetration, detonation, and fragmentation with drag. Wing flutter was included by coupling a boundary element method based on an aerodynamic paneling technique. Recommendations were made to continue to validate and refine the model against test data and incorporate additional features such as jet flow fields and fragment erosion.

Table of Contents

Figures

Tables

Executive Summary

The purpose of this work was to extend the capabilities of an existing body on body physics based Man Portable Air Defense Systems (MANPADS) model to include the effects of explosive materials and fragmentation effects and use them in the evaluation of a wing flutter response analysis.

Blast effects on the missile were evaluated using a coupled Eulerian/Lagrange mesh that included the explosive material and surrounding air. Forces on the fragments and warhead caps were then mapped onto an all Lagrangian model that included the target. Blast effects were included on the target using a collection of conventional weapons effects calculations and curves from TM-5-855-1 Fundamentals of Protective Design of Conventional Weapons (CONWEP). Initial validation of the fragmentation has determined the penetration and overall dispersion of fragments is comparable to test data. Penetrations of the fragments were compared against a static test and proven to be similar. The overall non blast related damage capability of the model compares to the previous body on body analysis.

Aerodynamic loading of the wing target structure was accomplished by coupling a boundary element method based on an aerodynamic paneling technique. Missile impact on the wing structure leads to local structural failure and loss of mass and stiffness. Since the analysis is performed using an explicit time integration technique, the structural changes due to damage are immediately applied and accounted for. Furthermore, since the structural materials are nonlinear with failure criteria assigned, damage progression is also accounted for.

Although initial validation has been performed, additional testing is recommended to obtain a higher level of confidence in various aspects of the model. This validation would require tests specifically designed to capture, impact and penetration of fragments against various targets. Further testing would help validate the blast effects on the missile body using x-ray imagery of a complete missile assembly during static detonation.

In conclusion, the initial MANPADS model incorporates the additional physics in a modular robust package that can be used to evaluate wing flutter or other damage modes of various targets.

1 Introduction

1.1 Background

The world has seen a proliferation of Man Portable Air Defense Systems (MANPADS). These shoulder-launched missiles are both light and portable and pose great risks for military and civilian aircraft. The DoD survivability community has no complete aircraft-MANPADS analysis capability that includes impact, detonation, penetration, and wing flutter response predictions. Because of this, all MANPADS testing such as Live Fire Test and Evaluation (LFT&E) and Joint Live Fire (JLF) and other vulnerability assessments are adversely affected. All aircraft (including both military and civilian) are impacted (no pun intended). This is particularly crucial to the design of new aircraft, such as the Joint Strike Fighter (JSF), because it is the first new aircraft that must be designed to survive a MANPADS encounter. Without a complete analysis capability that includes impact, detonation, penetration, and wing flutter response, designers are compelled to use rudimentary estimates and models that were not intended for use with these complex weapon systems.

1.1.1 Modeling Impact and Penetration of MANPADS

Over the past few years, RHAMM Technologies, LLC has been working with the 46th Test Wing and the Joint Aircraft Survivability Program Office (JASPO) to develop a methodology for modeling the impact and penetration of man portable (MANPADS) missiles on aircraft [1-3]. The Finite Element Method (FEM) in the Lagrangian domain implemented within a dynamic explicit time integration code has been used for this purpose. Figure 1.1.1-1 shows an exploded view of a typical MANPADS missile.

Previously, the FEM model of an aircraft component such as a wing has been clamped at the root and a static load placed on the component model. The MANPADS model is given an initial velocity and orientation and allowed to impact and penetrate the target model. Conventional master-slave contact algorithms using penalty function formulations are used to implement the contact. Element failures are based on a material allowable (stress or strain) and when failure is indicated, erosion of the failed elements is performed. Figure 1.1.1-2 shows the results of such a scenario.

1.1.1.1 MANPADS Impact on Generic Wingtip

In this section we present a sample of a MANPADS impact normal to a wing surface. The model is compared with an actual test. Figure 1.1.1.1-1 shows the finite element model used for this simulation. The model is given an initial velocity of 1040 fps and is allowed to contact the wing at normal incidence. Figure 1.1.1.1-2 shows a snapshot of the impact with VonMises Stress fringes. Note that the missile is penetrating the wing and that the missile is degrading and collapsing under the high impact forces.

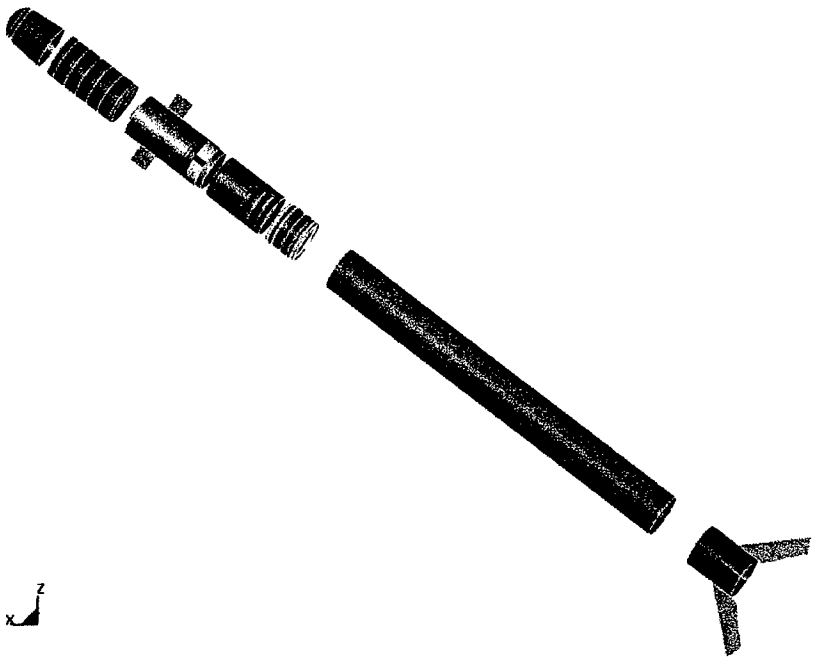

Figure 1.1.1-1. Exploded View of MANPADS

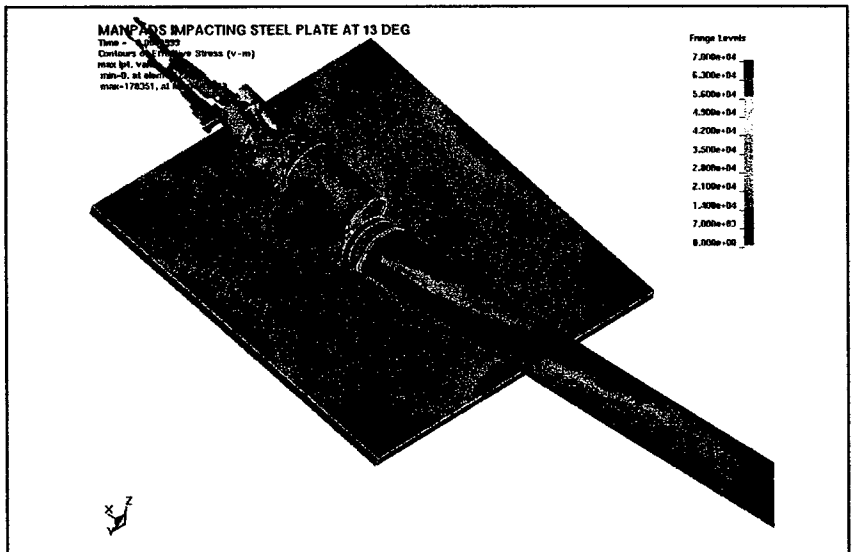

Figure 1.1.1-2. Simulation of MANPADS Impact on Flat Plate

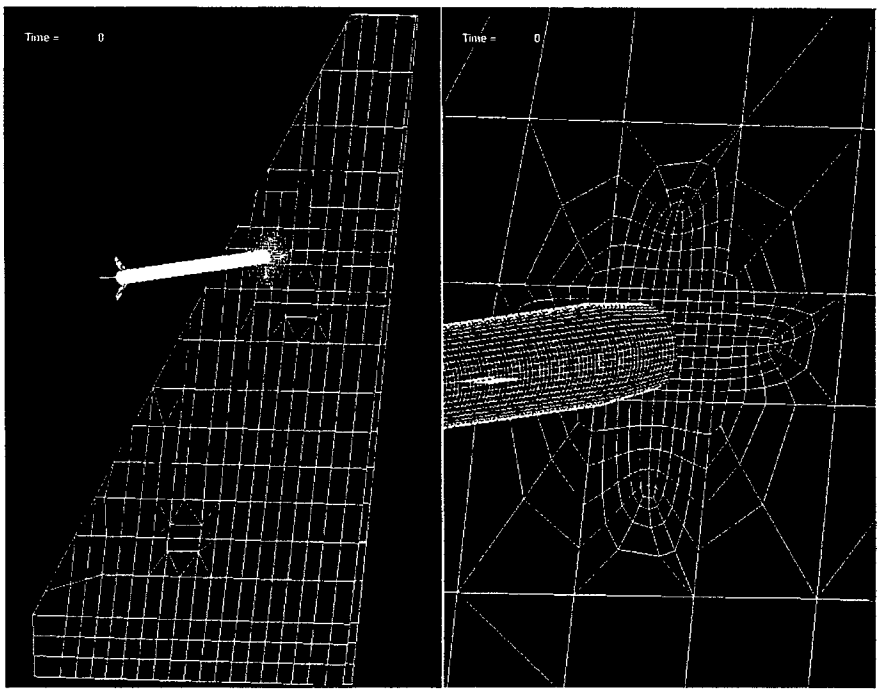

Figure 1.1.1.1-1. Model of MANPADS Impacting Wing at Normal Incidence

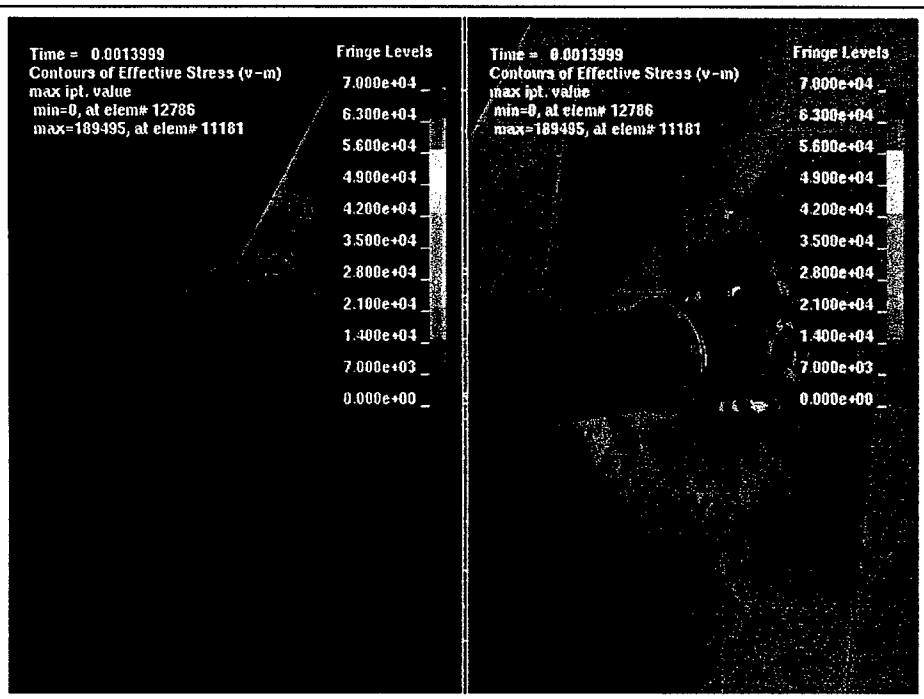

Figure 1.1.1.1-2. Model of MANPADS Impacting Wing at Normal Incidence

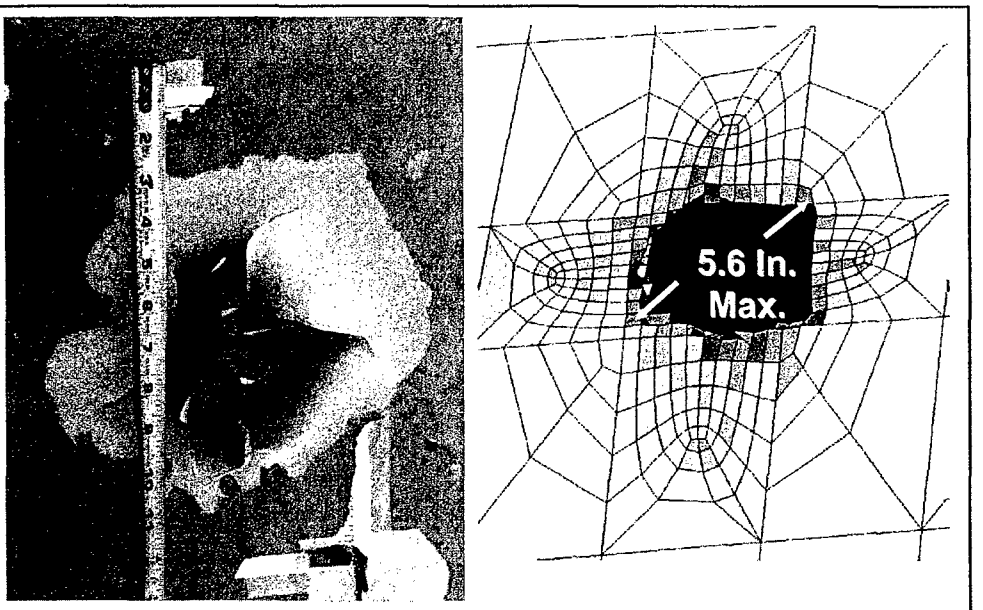

Figure 1.1.1.1-3. Comparison of Model with Test

Figure 1.1.1.1-3 shows a comparison of the entrance side damage predicted (right) with the test that was performed. Note that the model prediction shows an entrance hole of approximately 5.6 inches and the test shows damage of approximately 6 inches.

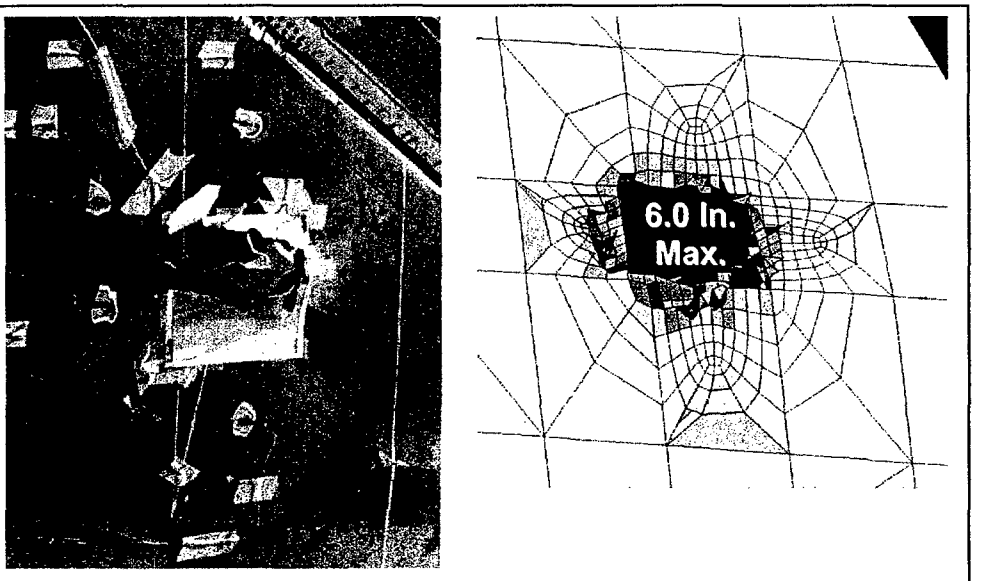

Figure 1.1.1.1-4. Comparison of Model with Test

Figure 1.1.1.1-4 shows a comparison of the exit side damage predicted (right) with the test that was performed. Note that the model prediction shows an exit hole of approximately 6 inches and the test shows damage of approximately 6 inches.

These initial comparisons of this methodology with experimental test results have proven accurate in modeling MANPADS impact tests. The detonation of the warhead is not modeled. This means that the target does not respond to the fragmentation and blast generated by the warhead.

1.1.2 Dynamic Air Load and Wing Flutter

The dynamic response of a damaged wing is primarily a result of the reduced stiffness caused by the damage. Reduced mass, to a lesser extent, is also a factor. A damaged wing can survive and the aircraft continue to fly if 1.) its stiffness is sufficient to withstand the aerodynamic loads (this assumes that sufficient lifting capability is still present) and 2.) damage does not reduce the flutter speed to the point that the wing responds in a manner that it uncontrollably flutters or enters into a limit cycle oscillation and destroys itself.

The current methodology for modeling wing damage is outlined below:

1. A finite element structural model of the lifting surface is generated and coupled with an aerodynamic flow model.
2. A time integrated finite element simulation is performed of the aircraft in flight. During the simulation, at ($t = 0$) g-loading and aerodynamic loading are applied to the model.
3. The model is allowed to come to a steady state condition.
4. At a time when the model is at or near steady state ($t = t_1$) damage is instantaneously inflicted by removing structural elements from the model.
5. The time history of displacements and strains is monitored.

Three cases using this instantaneous damage methodology are presented below.

1.1.2.1 Wing Flutter Sample Case 1

Case 1 investigates the dynamic response of a clean wing damaged near the wing root with moderate damage (Figure 1.1.2.1-1). The model simulation was for the aircraft at an angle of attack of 6 degrees, altitude below 4000 ft. and mach 0.8.

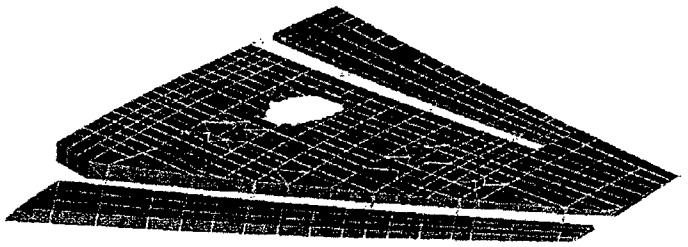

Figure 1.1.2.1-1. Typical Damage – Mach 0.80

This particular case illustrates the structural redundancy of this wing. After the wing reaches steady state, aerodynamic loading causes the undamaged wing to deflect approximately 3.5 inches, as measured at buttline 120 (Figure 1.1.2.1-2). Figure 1.1.2.1-2 also shows that once damage occurs, the instantaneous loss of structural stiffness initiates some brief oscillations followed by a steady state deflection that is approximately 0.5 inches more than the pre-damage state. The stress contour plots for this case are uninteresting since stresses in the wing before and after damage are below the yield stress of the materials used.

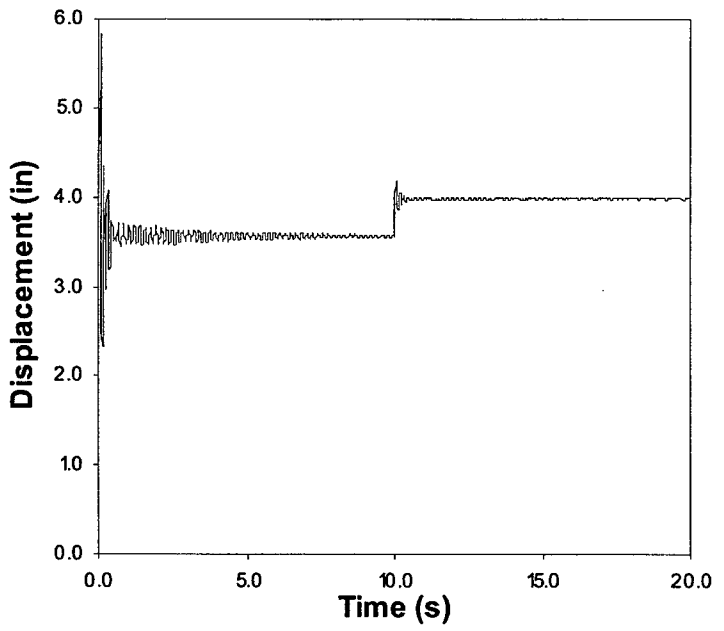

Figure 1.1.2.1-2. Deflection at Baseline 120 for a Clean Wing and Typical Damage – Mach 0.80

Under these simulated flight conditions, the wing's loss of flutter resistance due to damage does not affect the dynamic response of the wing sufficiently to cause catastrophic failure. However, brief oscillations experienced immediately following damage, under the right conditions, may cause additional damage that result in additional flutter resistance loss. It is important to note that the models in this investigation used linear elastic material behavior and that additional failure modes are not included.

The redundancy of this wing can be demonstrated by looking at stresses in the damaged spar caps. Figure 1.1.2.1-3 shows spar cap stresses in spar caps 6 and 7 before and after damage. Portions of spar cap 7, 8, 9, and 10 are eliminated at time t=10 seconds. Before damage is input, spar caps 6 and 7 are loaded to about –12 ksi. After damage, spar cap 6 is loaded to -30 ksi because it carries additional load from the damaged spar caps. The yield stress of aluminum used in modeling the spar caps is 70 ksi. As can be seen from Figure 1.1.2.1-3, the post-damage stresses are far below the allowable yield.

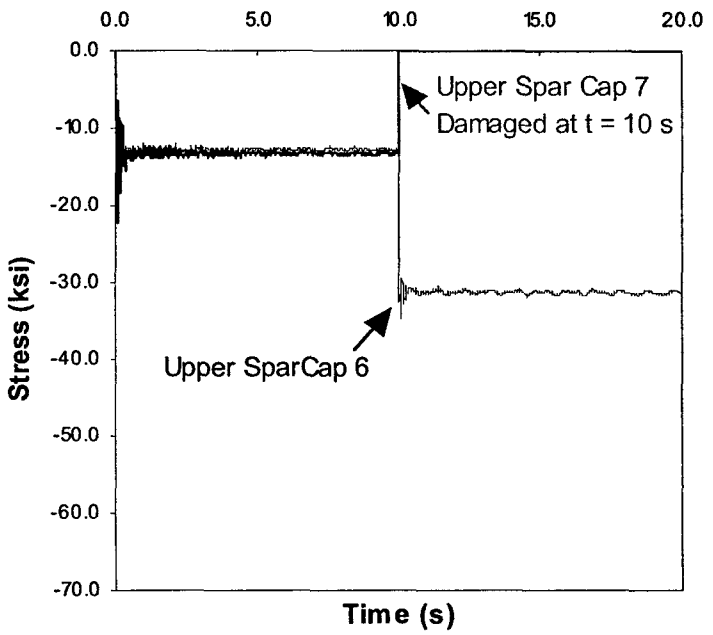

Figure 1.1.2.1-3. Spar Cap Stresses Before and After Damage

1.1.2.2 Wing Flutter Sample Case 2

In Case 2, a 300 lb store was attached to the wing tip and the dynamic response was investigated when the wing was again damaged near the wing root (Figure 1.1.2.2-1). This case used an angle of attack of 3 degrees, altitude below 4000 ft., and mach 0.92. As can be seen in Figure 1.1.2.2-1, the store was modeled as a series of simple beams. Figure 1.1.2.2-1 also shows the wing's deflection and tortuous shape caused by the damage and loss of flutter resistance.

Figure 1.1.2.2-1. Wing Deflection with Typical Damage and Wing Tip Store – Mach = 0.92

Oscillations associated with step loading the wing at the beginning of the simulation require more time to reach steady state than the previous case (Figure 1.1.2.2-2). Additionally, after damage the deflection diverges due to the lower stiffness and reduced flutter speed.

The reduced flutter resistance caused by the damage led to increased deflections resulting in stresses which exceed the allowable yield stresses of the materials used. Figure 1.1.2.2-3 shows the Von Mises stresses for the wing prior to damage. Where the Von Mises stresses are scaled such that blue is 0 ksi and red 70 ksi, corresponding to the maximum allowable yield stress. Prior to damage the Von Mises stresses were all well below the yield stresses. However, after damage and due to the increased deflections caused by flutter, Von Mises stresses exceeded the allowable yield stress in the entire tip region (Figure 1.1.2.2-4). The likely result would be the loss of the wing tip and possible loss of the aircraft.

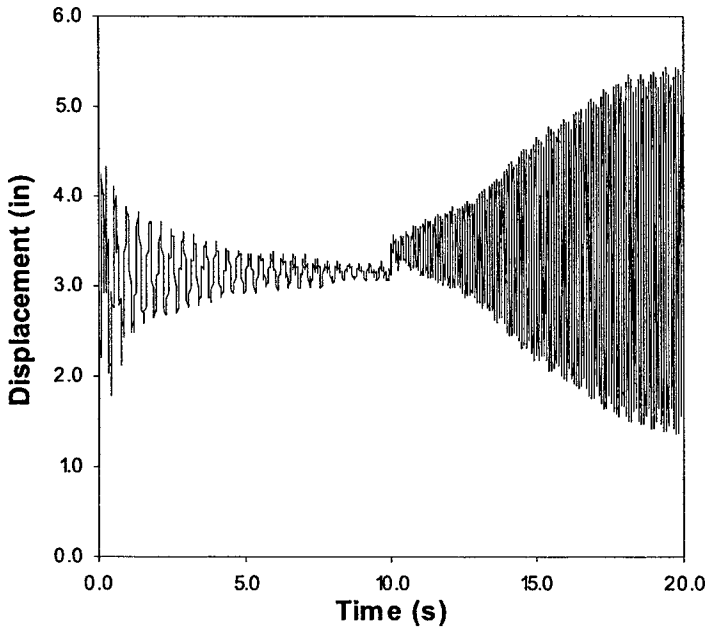

Figure 1.1.2.2-2. Deflection at Baseline 120 for Wing + 300lb. Store and Typical Damage – Mach = 0.92

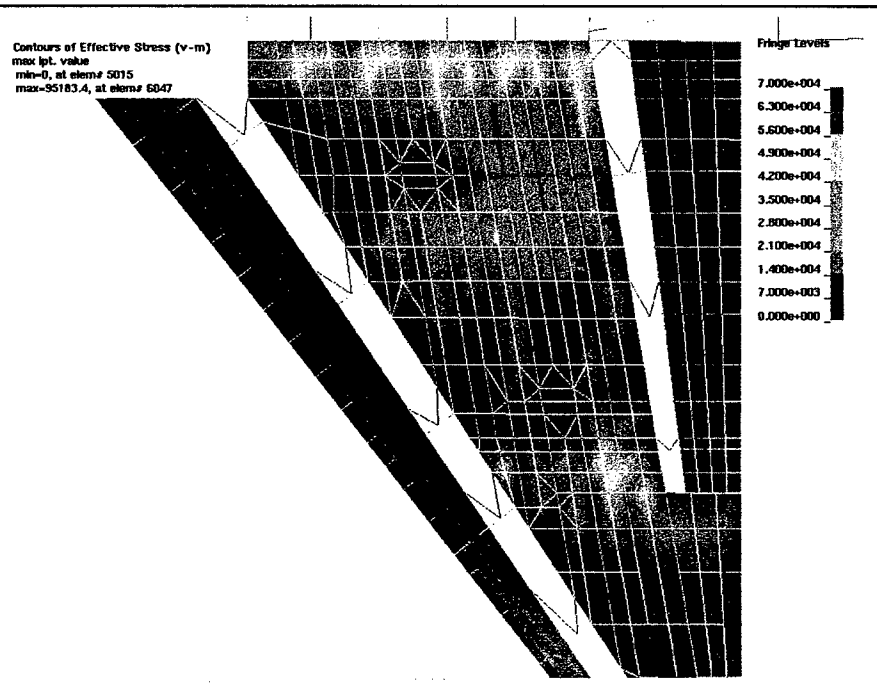

Figure 1.1.2.2-3. Von Mises Stress Contour Plot for Wing Just Before Damage

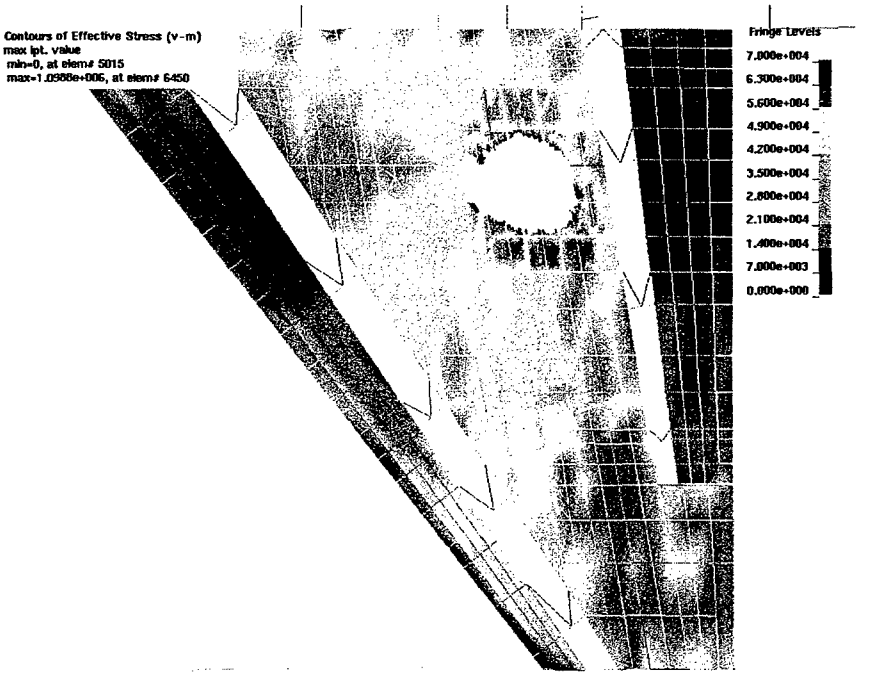

Figure 1.1.2.2-4. Von Mises Stress Contour Plot For Wing After Damage

1.1.2.3 Sample Case 3

In Case 3 the dynamic response of the clean wing was investigated where damage was inflicted near the wing tip (Figure 1.1.2.3-1). This case is for an angle of attack of 3 degrees, altitude below 4000 ft., and mach = 0.95. As can be seen from Figure 1.1.2.3-1, the damage causes severe distortion of the wing.

Deflections in Figure 1.1.2.3-2 reveal that the tip deflections after damage have an oscillation of 50 inches. Before damage the oscillations are a factor of 5 smaller. It is important to note that presented deflections are given at the wing tip and not at baseline 120 as in the previous two cases. In this case, deflections at baseline 120 were much less severe since the damage occurred outside of baseline 120.

Figures 1.1.2.3-3 and 1.1.2.3-4 show Von Mises stresses before and after damage, respectively. Again, Von Mises stresses are scaled such that blue is 0 ksi and red is 70 ksi, with red corresponding to maximum allowable yield stress.

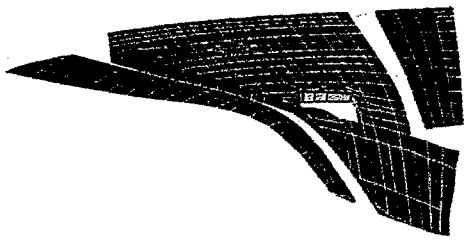

Figure 1.1.2.3-1. Wing Deflection With Typical Wing Tip Damage – Mach = 0.95

As can be seen, the stresses before damage are within the allowable range while stresses after damage are above the allowable for most of the wing. The obvious result from this simulation would be loss of control of the aircraft, unless flight conditions are modified.

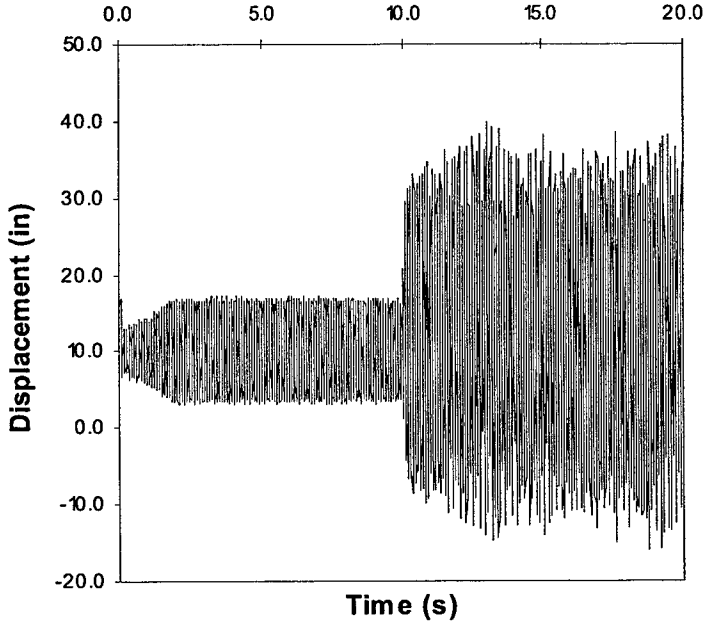

Figure 1.1.2.3-2. Deflection Of Wing Tip -- Typical Damage Located Near Wing Tip – Mach = 0.95

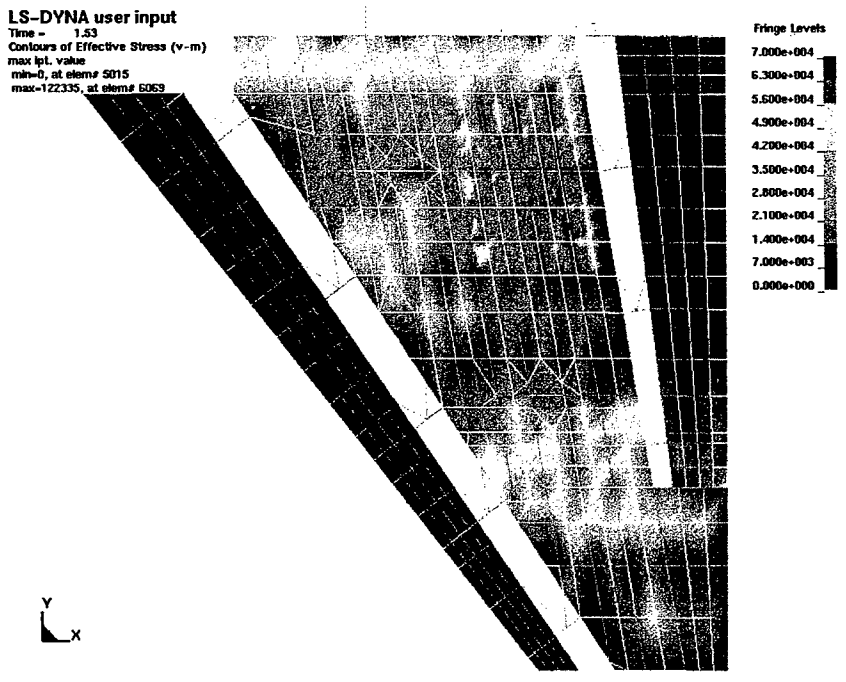

Figure 1.1.2.2-3. Von Mises Stress Contour Plot For Wing Before Damage

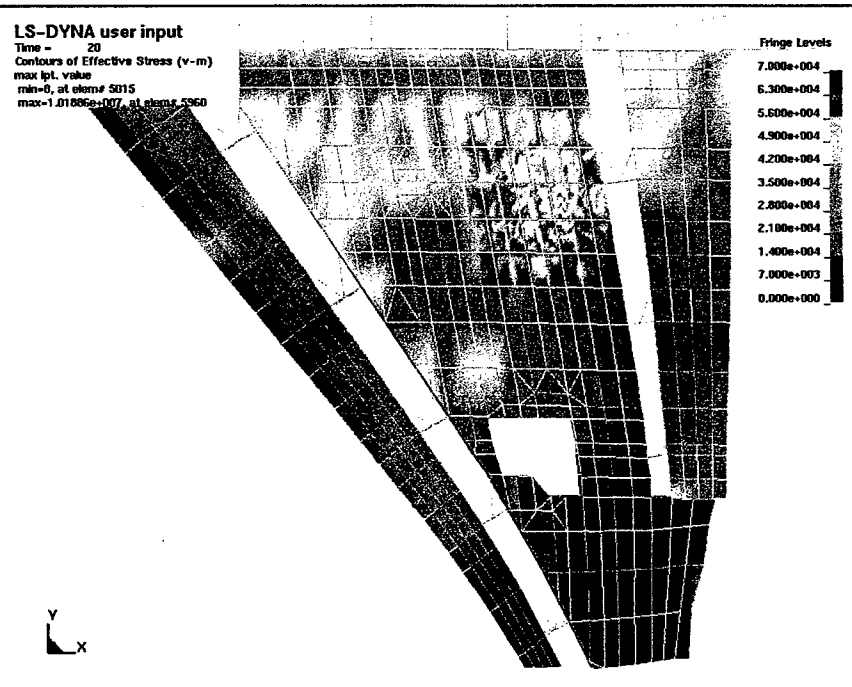

Figure 1.1.2.2-4. Von Mises Stress Contour Plot For Wing After Damage

1.1.3 Present Body on Body Methodology Shortcomings

Sections 1.1.1 and 1.1.2 presented the current methodology. The following shortcomings were identified.

1. The materials in the target are modeled using linear elastic models. Thus damage progression in the target model is not captured.
2. The damage imposed on the target model is simulated by instantaneous removal of material, rather than having the MANPADS threat actually doing the damage.
3. The detonation of the MANPADS warhead is not modeled. This means that the target does not respond to the fragmentation and blast generated by the warhead.

1.2 Project Objectives

There are two main objectives of the present work, both of which build upon the impact methodology that has been developed and solve the shortcomings in the present methodology. They are:

1. Incorporation of dynamic air loads and response of the aircraft component(s) such as wing flutter into the methodology and using the actual MANPADS model with nonlinear material models to simulate target damage.
2. Incorporation of warhead detonation into the methodology so that the fragmentation and blast generated are accounted for in the target response.

1.3 Statement of scope

This work applies to all existing and future aircraft and/or armored vehicle programs where MANPADS are a threat. With a more accurate methodology, structures with higher probability of survival may be designed.

1.4 Report Organization

First, the methodology developed for the warhead detonation with fragmentation including crack elements, drag, impact, and blast modeling is presented in Sections 2.1. The details of the FEM model of the MANPADS missile are presented in Section 2.1.3. The methodology developed to model dynamic airloads and wing flutter is presented in Section 2.2. Results are presented for three models: MANPADS warhead with composite wingbox target model (Section 3.1), MANPADS missile with wingbox showing flutter response (Section 3.2), impact studies of MANPADS on typical transport aircraft outer wingbox.

2 Methods, Assumptions and Procedures

2.1 Warhead Detonation with Fragmentation and Blast

2.1.1 Fragmentation

Three different methods of capturing fragmentation were investigated: Stress/strain with time step failure criterion, tied nodes, and crack elements. These methodologies are described in Section 2.1.1.1, 2.1.1.2, and 2.1.1.3 respectively. Crack elements were found to be the most robust. A methodology for fragmentation drag was also developed and validated as described in Section 2.1.1.4.

2.1.1.1 Element Erosion Stress/Strain coupled with Time Step Failure Criterion

We performed basic research into improving the current stress/strain failure criterion and element erosion techniques which are not robust enough to model fragmentation. It was found that the failure rate of the element solely driven by a strain based failure criteria was not robust. The elements would deform and drive the problem time step down to unreasonable levels. Applying an additional failure criteria based on the elements individually calculated time step added stability during element erosion. Although the strain based criteria was limiting the measured level of strain, the elements were not eroding consistently. Adding the time step based failure criteria provided an additional means for element erosion.

2.1.1.2 Tied Nodes

Another means for element erosion was investigated that incorporated tied nodes. That is, elements which normally would share common nodes at their interfaces would (in the tied node methodology) have node numbers unique to each element that are "tied" together with effective constraint equations. Using this methodology, the tied nodes are separated when a failure criterion is met. Since only the tied equation fails, no erosion of the elements was required and the mass of the system could be maintained. Unfortunately, this method is computationally expensive due to the additional calculations and very large data files.

2.1.1.3 Crack Elements

Another method was created which combines the robustness of the element erosion methods and maintains much of the original mass of the model. This method is based on the smallest existing element size, already in use in the model, and uses it as a size for separating elements. The separating elements or crack elements, divide clusters of at least four elements. Each crack section requires a material property and associated failure criteria. The crack material failure criterion is the same as material of the component. The cluster of elements or fragments has an artificially high failure criterion,

so they can withstand the initial blast wave without eroding. Crack elements have advantages over the tied node methodology. The first advantage is the smallest fragments are composed of multiple elements. Groups of elements are more stable and less likely to vibrate at zero energy modes (hourglassing). The tied node methodology often created single element fragments. The second advantage is the fragment size can be dictated from experimental test data. The tied method generally produced fragments the same size as the individual elements. A disadvantage of the cracked element methodology is the amount of time required to create the crack elements.

2.1.1.4 Fragmentation Air Drag

Since the radius of effective fragment damage, although target dependent, exceeds considerably the radius of effective blast damage in an air burst, we included air drag on the fragment. Air drag can have a significant effect on a fragment with a long flight path.

Accounting for drag of the fragments is accomplished with equation (1). The final velocity, V_f, is given as a function of the air density, ρ, the drag coefficient, C_d, the fragment area, A , mass, m, distance traveled, x, and initial velocity, V_i. This equation assumes a flat trajectory (neglecting gravity). Combining terms into a drag coefficient, k, yields equation (2). The drag coefficient, k, was determined to be 0.04 by comparing modeling results with experimental data at ground level conditions. As drag associated with individual particles could not be correlated to each fragment mass, an average drag coefficient was determined. This average drag coefficient and an average fragment mass were used for the simulated fragments

$$V_f = V_i * \exp\left(-\frac{\rho C_D A}{2m} x\right) \tag{1}$$

$$V_f = V_i * \exp\left(-kx\right) \tag{2}$$

In order to incorporate drag into LS-DYNA, the *DAMPING_PART_MASS option was used. In this option, individual parts can be given a mass proportional damping in the form of a curve and a scale factor. Since each fragment is modeled as an individual part, a number of damping entries equal to the number of fragments is used. Mass damping is used, because it effects not only the elastic deformations of a part, but also the rigid body velocities. Several curve forms were investigated and a line was chosen, as it best fit the experimental data. A scale factor of 460 was found to best match the experimental data (which was taken at sea level). Figure 2.1.1.4-1 shows a comparison of experimentally derived velocity versus distance with that being generated by LS-DYNA at various altitudes. Altitude is accounted for in LS-DYNA by scaling the damping parameter (460 at sea level) according to the density at the altitude of interest.

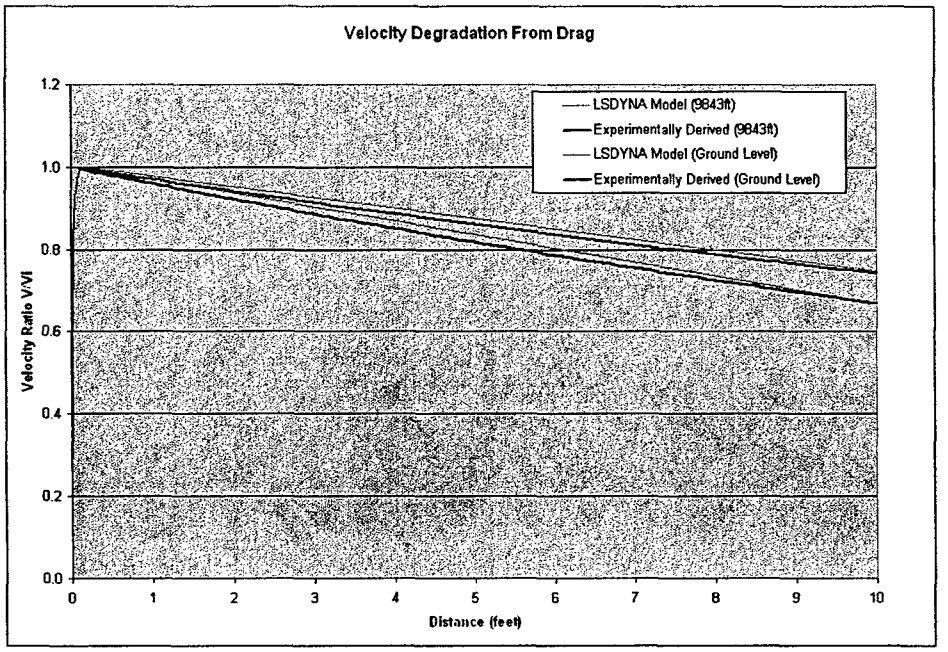

Figure 2.1.1.4-1. Comparison of Experimental to FEA Fragmentation Drag.

Rigid fragments were used to allow the model to be robust. Due to highly ductile flow, modeling the true behavior of a fragment after impact would be very complex and require an extremely fine mesh and state transformations for the more volatile fragment materials. Experience has shown that the high velocity of a fragment modeled by an elastic solid brick element causes severe numerical instabilities that quickly drive the time step below an acceptable level or creates out of range nodal velocities.

2.1.2 Detonation/Blast Modeling

Methodology for warhead blast effects was investigated by examining the Eulerian domain and coupling the explosive and surrounding fluids with the Lagrangian structural components. The Jones-Wilkins-Lee (JWL) equation of state was used for the explosive and the Gruneisen equation of state was used for the surrounding fluids. The Lagrangian structure and the Eulerian fluids were coupled using the Arbitrary Lagrangian Eulerian (ALE) technique. We specifically examined a Coupled Euler Lagrange (CEL) technique where the Eulerian and Lagrangian meshes need not share common nodes (overlapping mesh).

The JWL equation of state is given by:

$$P = A\left(1-\frac{\omega\eta\rho_0}{R_1}\right)e^{-\frac{R_1}{\eta}} + B\left(1-\frac{\omega\eta\rho_0}{R_2}\right)e^{-\frac{R_2}{\eta}} + \omega\eta\rho_0 E \qquad (3)$$

where:

P = predicted pressure,
ρ = overall material density,
ρ_0 = reference density (initial density),
$\eta = \rho/\rho_0$,
E = specific internal energy, and
A, B, ω, R_1 and R_2 are constants.

The Gruneisen equation of state is given by:

$$P = a_0 + a_1\mu + a_2\mu^2 + a_3\mu^3 + \left(a_4 + a_5\mu + a_6\mu^2 + a_7\mu^3\right)\rho_0 e \qquad (4)$$

where:

P = predicted pressure,
ρ = density,
ρ_0 = reference density (initial density),
$\eta = \rho/\rho_0$,
$\mu = \eta - 1$,
e = specific internal energy, and
$a_0 \ldots a_7$= constants.

A technique which incorporates the Jones-Wilkins-Lee (JWL) equation of state for the explosive and the Gruneisen equation of state for the surrounding fluids to model blast effects has been developed that is both modular and robust for the end user.

This method uses a two part system. The first part consists of a model that couples the Lagrangian missile including the warhead with the Eulerian explosive products and surrounding air. The target is not included in the first model to save computational expense. The first model is only used to determine the effects of the explosion on the missile and the warhead including fragmentation. From this model fragment accelerations are extracted. Also pressure on the ends of the warhead can be obtained. This data can be mapped onto the second model using a customized program (see Appendix A3) to convert the standard output rigid body accelerations and masses into rigid body input forces as functions of time. The second model includes the target and the full missile minus the explosive material and surrounding air mesh. Since the missile model will be used with various complex targets and multiple end users, simplifying this model is essential for portability. Including the target with the explosive material and the Eularian air mesh can quickly become unmanageable with the currently available resources and requires a higher level of user interaction to manage the added complexity.

Blast effects are included on the target using a collection of conventional weapons effects calculations and curves from TM-5-855-1 Fundamentals of Protective Design of Conventional Weapons (CONWEP). The CONWEP algorithm has been implemented within LS-DYNA (*LOAD_BLAST). This option uses the CONWEP code, which is an empirical code for predicting pressure. Specifically it is an empirical code of explosives in air on the ground. Inputs include: type of explosive, the weight of the explosive and the

distance(s) at which results are required. The output is the incident and reflected pressure versus time at the selected distances.

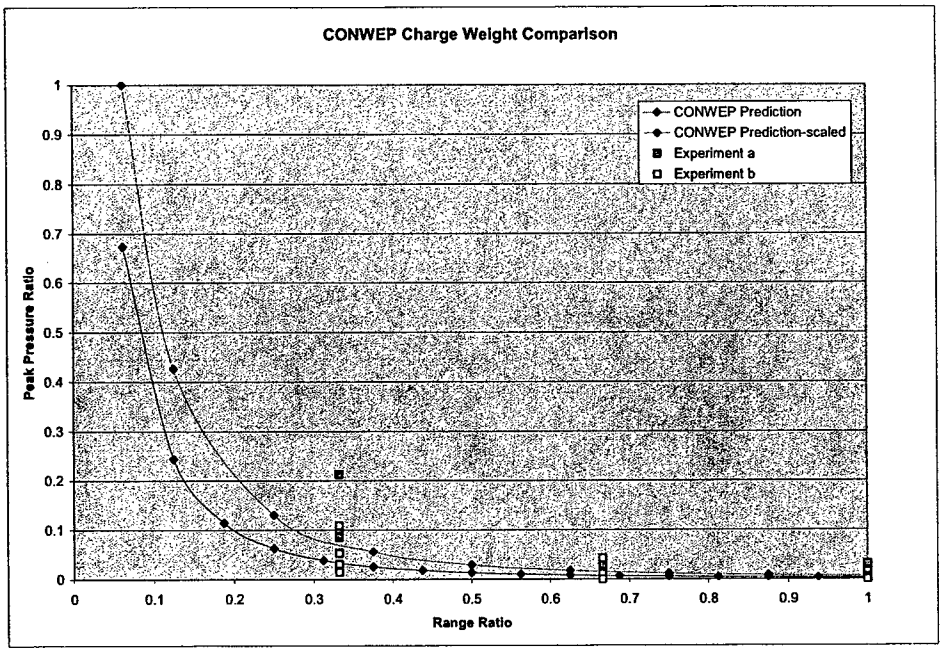

Figure 2.1.2-1. CONWEP Peak Pressure Ratio Comparison with Experimental Data

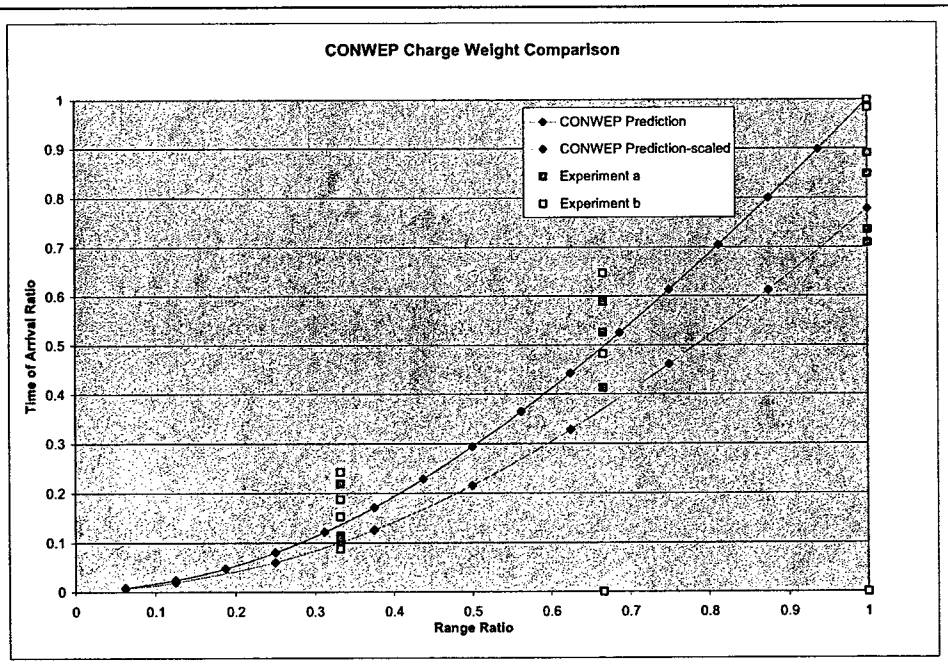

Figure 2.1.2-2. CONWEP Time of Arrival Comparison with Experimental Data

Figures 2.1.2-1 and 2.1.2-2 present a comparison of the CONWEP code with some actual MANPADS detonation data (Seymour, Timothy J., "JTCG/AS-02-V-001", AFRL-WS-WP-TR-2002-9001, Final Report, July, 2002) in terms of peak pressure and arrival time, respectively.

2.1.3 MANPADS Missile Model

A US MANPADS missile is modeled using LSDYNA. It has 187600 nodes, 52802 shell elements with 13 shell materials, 112200 solid elements with 1804 solid materials. The fragments are modeled with 14400 rigid elements.

Figure 2.1.3-1 shows the overall configuration of the US MANPADS missile model. Figures 2.1.3-2 through 2.1.3-5 show close-ups of the individual sections of the model

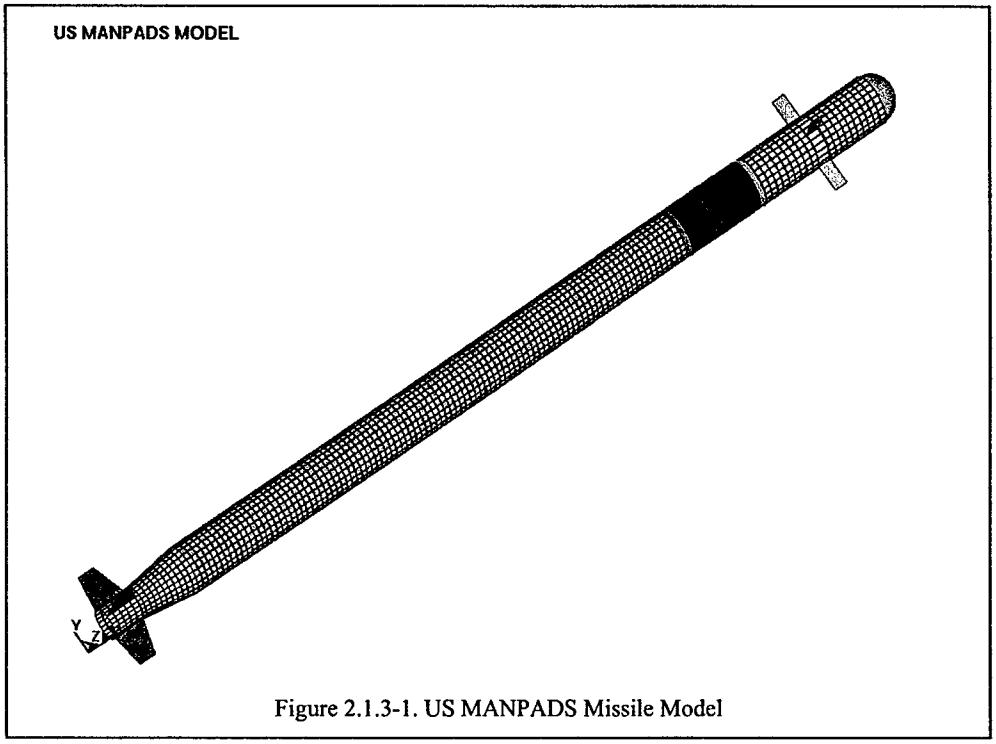

Figure 2.1.3-1. US MANPADS Missile Model

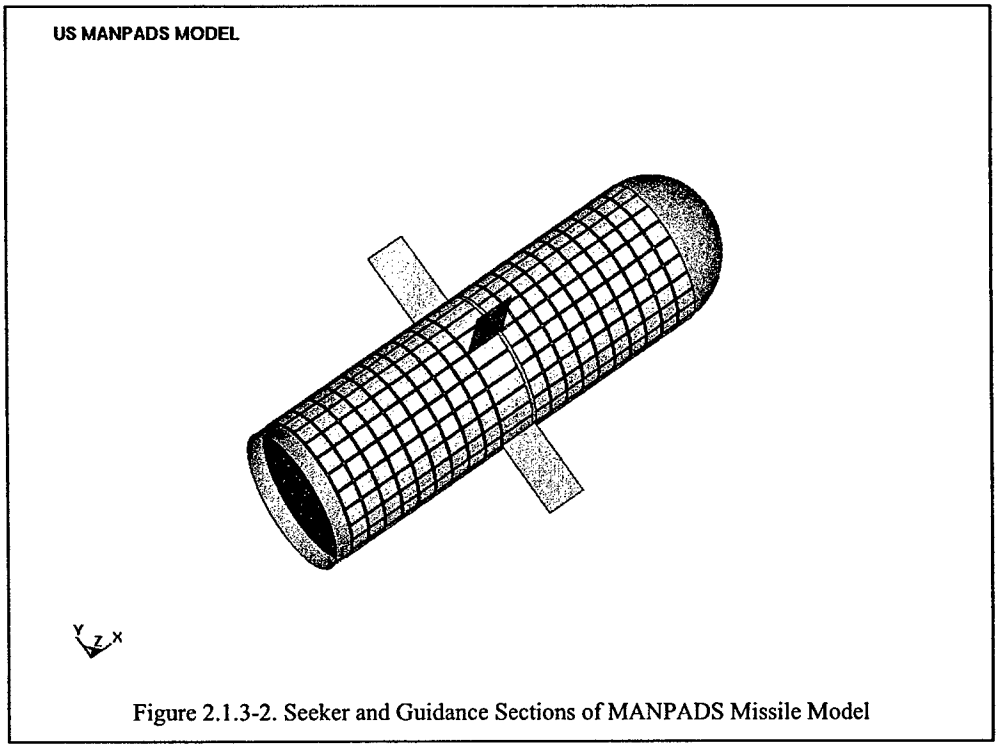

Figure 2.1.3-2. Seeker and Guidance Sections of MANPADS Missile Model

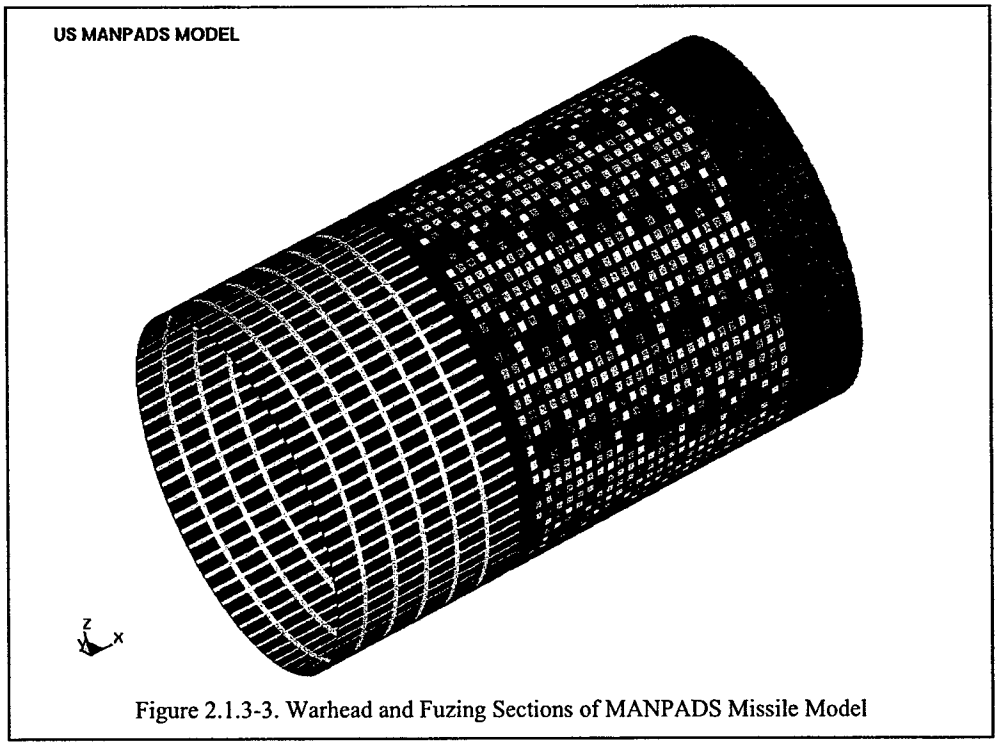

Figure 2.1.3-3. Warhead and Fuzing Sections of MANPADS Missile Model

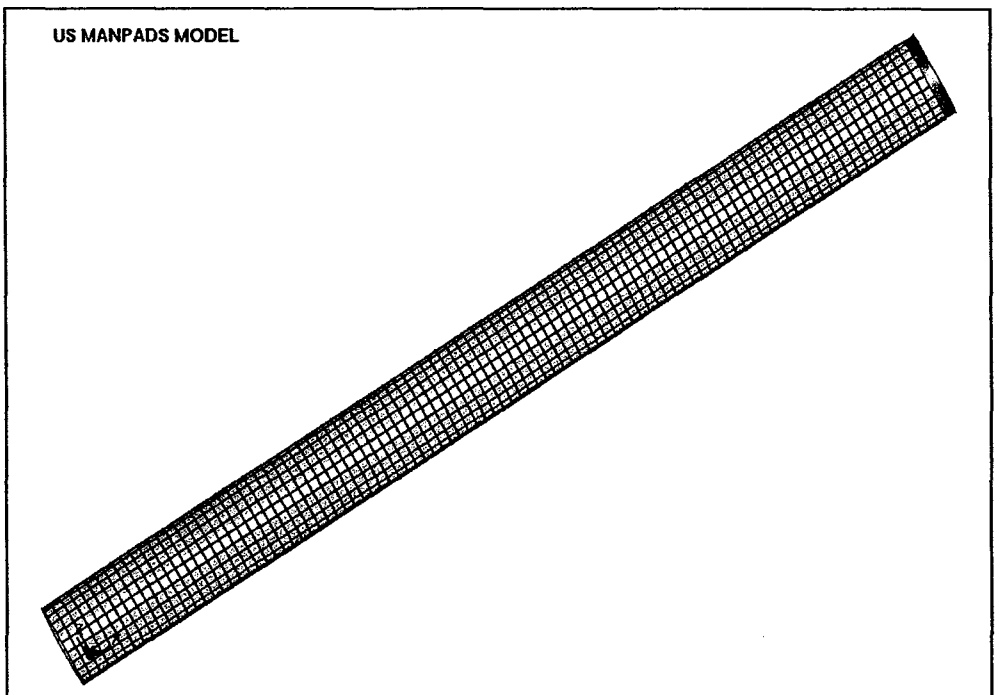

Figure 2.1.3-4. Rocket Motor of MANPADS Missile Model

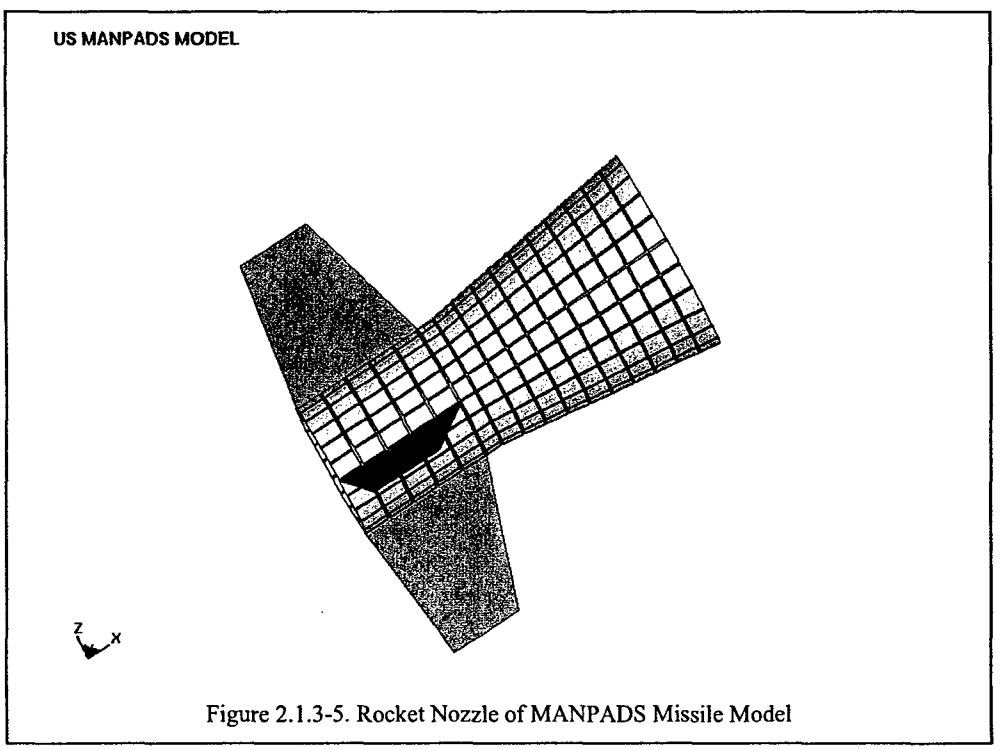

Figure 2.1.3-5. Rocket Nozzle of MANPADS Missile Model

2.2 Dynamic Air Loads and Flutter Evaluation

Dynamic air loads were incorporated into the current impact methodology so that the response of aircraft component(s), such as wing flutter, could be more accurately modeled. A linear boundary element method was incorporated to model the airflow over the aircraft component. The flow model was coupled to the structure model such that the influence of the airflow to the structural members is accounted for. This is accomplished by ensuring that the boundary elements and the structure elements share the same nodes. This ensures the appropriate interaction between the air and structure.

The aerodynamic paneling model was a boundary element method based on theVSAERO code [4]. Since it is based on linear aerodynamic theory, it is applicable for inviscid, incompressible, attached fluid flows. This feature was added to the LS-DYNA [5] code in 1998 and validated against a number of closed form fluid flow problems [6]. Flow separation does not necessarily invalidate the analysis. If well-defined separation lines exist on the body, then wakes can be attached to these separation lines and reasonable results can be obtained. The Prandtl-Glauert rule can be used to correct for non-zero Mach numbers in a gas, so the effects of aerodynamic compressibility can be correctly modeled. The following LS-DYNA keywords were used for the aerodynamic portion of the model:

```
*BOUNDARY_ELEMENT_METHOD_CONTROL
$#    lwake      dtbem     iupbem     farbem
         40 5.0000E-4      10000 10.000000
*BOUNDARY_ELEMENT_METHOD_FLOW
$#     ssid         vx         vy         vz         ro    pstatic       mach
         1 7500.0000 435.00000      0.000 1.1230E-7      0.000  0.570000
*BOUNDARY_ELEMENT_METHOD_WAKE
$#    nelem      nside
       120          2
```

The LS-DYNA input deck with the node and element definitions deleted may be found in Appendix A4. The *BOUNDARY_ELEMENT_METHOD_CONTROL keyword is used to control the execution time of the boundary element method calculation. Forty wake elements were used at the trailing edge of the wing. The BOUNDARY_ELEMENT_METHOD_FLOW keyword is used to turn on the boundary element method calculation and defined the fluid velocity and Mach number. The free-stream fluid velocity was set at 7500 in/s in the direction of travel (x) and 435 in/s in the lift direction (y). A mach number of 0.57 was also used.

A wing structure with an aerodynamic mesh was modeled as shown in Figure 2.2-1. The aero mesh is shown in Figure 2.2-2, while the structural mesh is shown in Figures 2.2-3 and 2.2-4. The aerodynamic mesh uses nodes which are coincident with and numbered the same as the structural model nodes. By imposing the coincidence of the aero and structural nodes, pressures generated by the aero model are directly applied to the structural nodes.

The aerodynamic mesh is also set to straddle the structural mesh where the MANPADS is to impact the wing. This is necessary so that the aero model always has viable structure to which to couple. Without having this viable structure, the aero model deforms wildly and leads to erroneous results.

A MANPADS was also modeled as shown in Figures 2.2-5 and 2.2-6. For the purpose of showing the effect of structural damage due to impact and penetration of the missile on wing flutter, the model of the MANPADSdoes not include blast or fragmentation.

The wing model contains 1,044 shell elements, 654 nodes, 20 spc nodes, 11, and boundary element wake elements. The model of the missile contains 12,280 solid elements, 10 beam elements, 9,901 shell elements and 25,113 nodes.

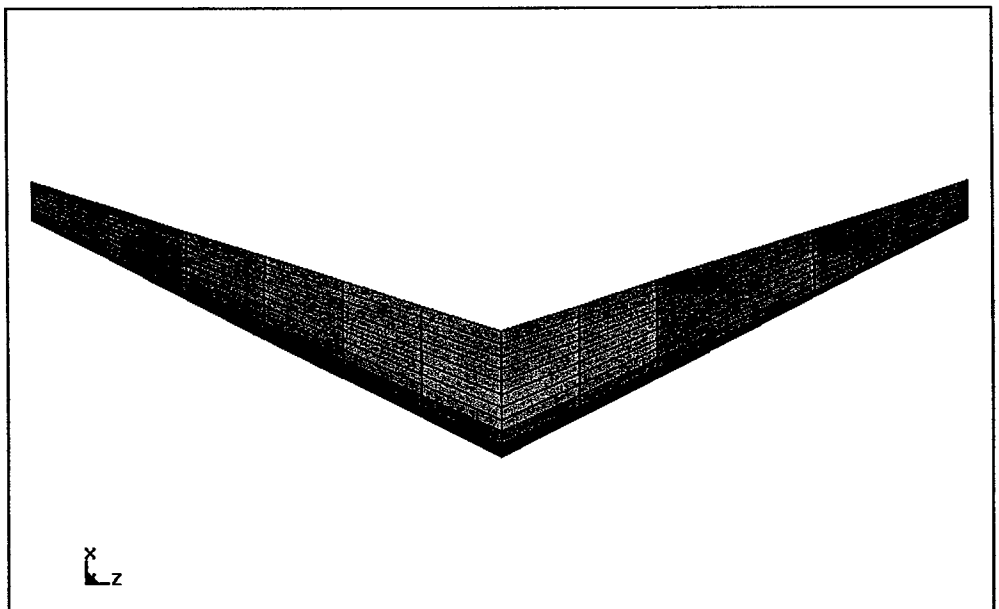

Figure 2.2-1. Aero Mesh of Simple Wing Model: Top View

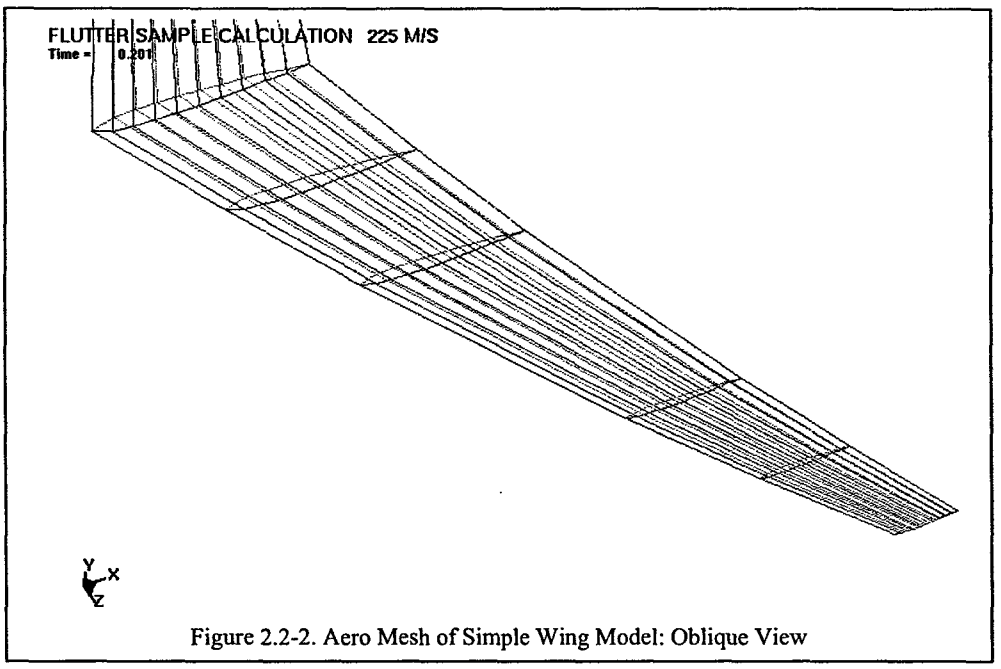

Figure 2.2-2. Aero Mesh of Simple Wing Model: Oblique View

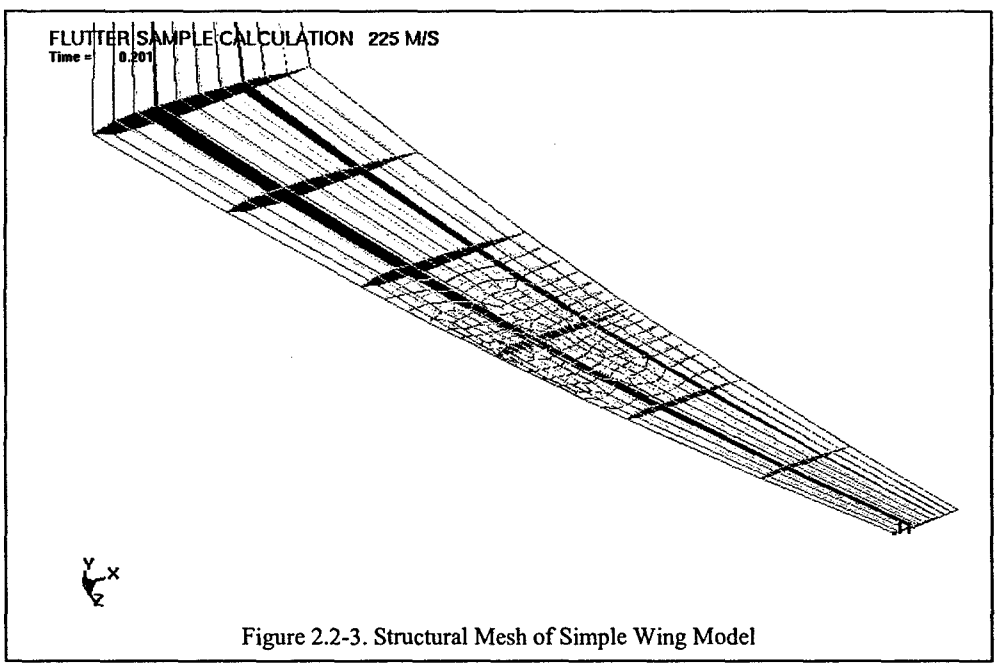

Figure 2.2-3. Structural Mesh of Simple Wing Model

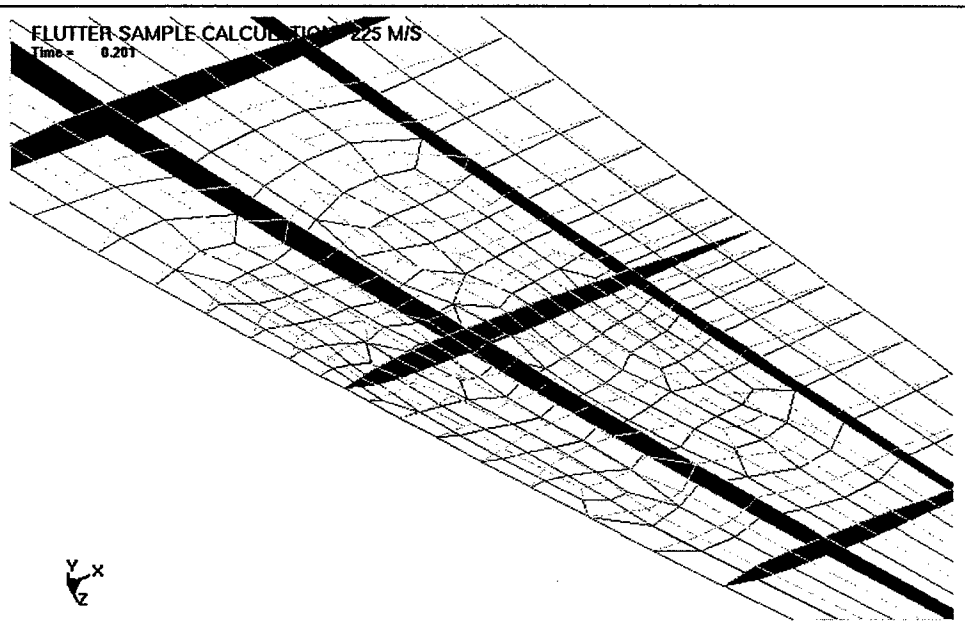

Figure 2.2-4. Structural Mesh of Simple Wing Model: Enlarged View

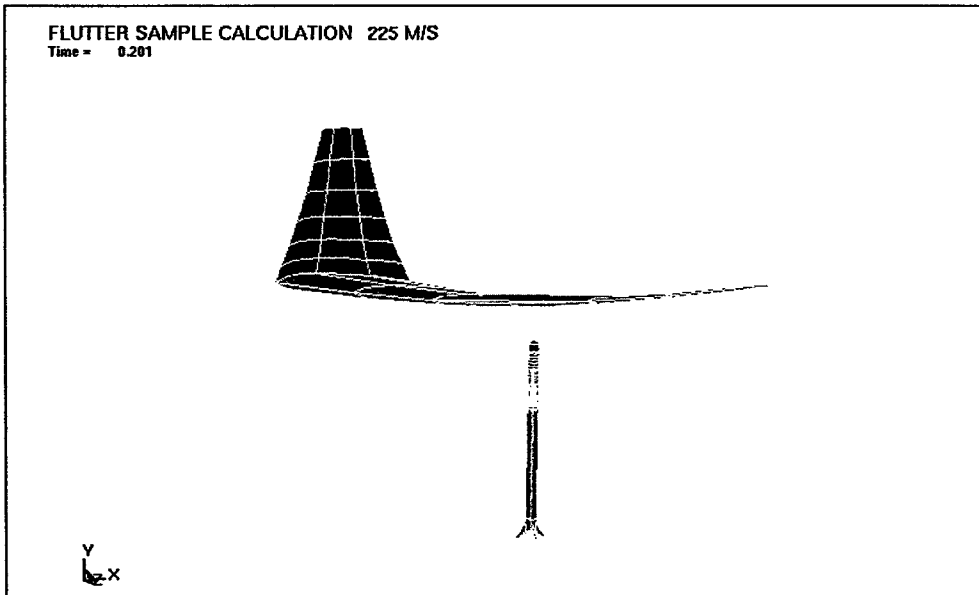

Figure 2.2-5. MANPADS and Simple Wing Model

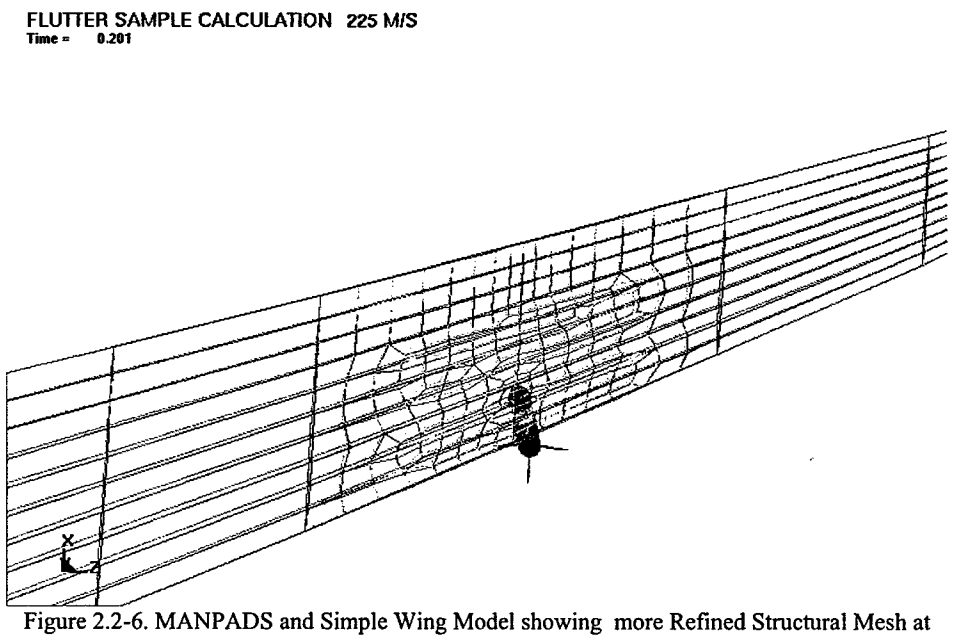

Figure 2.2-6. MANPADS and Simple Wing Model showing more Refined Structural Mesh at Location of MANPADS penetration.

2.3 MANPADS Damage on Transport Aircraft Wing Structures

Mitigating the effects of in-flight damage to commercial transport aircraft caused by terrorist attacks has recently become an area of great research interest. The sources of damage may include ballistic penetrators, high explosive incendiary (HEI) projectiles, and shoulder fired surface to air missiles, or Man Portable Air Defense Systems (MANPADS). Since they are inexpensive and many countries produce them, they can easily be acquired by terrorist groups. Additionally, the urban location of many airports allows terrorists to easily access areas where aircraft are flying at very low altitudes, making the aircraft susceptible to attack.

Currently, commercial aircraft are not equipped with any countermeasures to defend against these attacks. Recent studies by government agencies and aircraft manufacturers have found that the cost of hardening the aircraft or installing countermeasures to defend against these threats is impractical because of the great expense. Therefore, it becomes necessary to determine likely damage scenarios caused by these projectiles to enable the development of techniques to safely land the damaged aircraft using the remaining functional control systems and engines.

The objective of this study is to quantify the damage caused by a projectile impacting aircraft structures using computational simulations. Since there are many potential fusing selections, fragment patterns, impact locations, and incident angles for an attack, experimental testing of all possible damage scenarios is impractical. The use of validated

computational models and commercial software to simulate projectile impact damage is therefore necessary.

The following steps were taken for this damage study. The first step in characterizing the damage caused by a projectile was to investigate the effects of a simple body-on-body impact on the aircraft's wing structure. In this investigation, it was assumed that there was no explosive material involved, and the damage was caused by the kinetic energy of the projectile alone. The second step was to add an explosive to the projectile model to investigate the combined effects of the kinetic energy of the projectile, and the explosive blast at various locations and incident angles.

A finite element model of a typical transport aircraft outer wing was obtained from NASA. Section 3.3 presents the results of this study. An abbreviated input file is presented in Appendix 5.

3 Results and Discussion

3.1 Warhead Blast and Fragmentation Damage on Composite Wingbox

Early on in the program, the 46 TW entered into a Long Term Technical Program on Aircraft Survivability (LTTP/AS) with the UK, France, and Germany. As part of that collaboration, static warhead tests were performed against an all-composite wingbox that had been manufactured by the UK. The wingbox was generic in nature and typical of structural concepts in current use in fighter aircraft. The wingbox consisted of internal spar members and skins that were bonded on one side and bolted on the other.

Static arena tests with the warhead positioned at 0.5 meters from the wingbox bonded surface showed that there was damage from the fragments, but no detectable damage due to the blast effects. Analysts at the Ernst Mach Institute (EMI) used these tests to validate their warhead model. Lessons learned from the EMI warhead model were incorporated in the US version. The fragmentation patterns generated from the EMI and US models were similar. One question that remained was: "We know there is no apparent blast damage on the composite wingbox at 0.5 meters standoff. Is there blast damage at 0.25 meters standoff?"

Both of these cases were simulated dynamically. That is, there was relative velocity between the warhead and target that would result from an actual MANPADS encounter with at target at a relative velocity of 1200 feet per second. Initially, the simulations were performed holding the wingbox model stationary and moving the warhead. When the results of these simulations were presented the the LTTP group, they commented that the blast was not moving relative to the target. This was a result of using the CONWEP technique. The issue was overcome by holding the warhead stationary and moving the wingbox target relative to it. In this way, the CONWEP method, although producing a spherical blast would appear elliptical to the moving target. The use of this technique is acceptable except when the target has rotating parts, in which case the linear motion of the rotating parts introduces some spurious forces in the model.

3.1.1 0.5 Meter Standoff

Figure 3.1.1-1 shows the MANPADS warhead located 0.5 meters away from the typical composite wingbox structure. Figures 3.1.1-2 through 3.1.1-5 present snap shots of the detonation of the warhead. The fragment velocity versus distance plot for a fragment encounter with the typical wingbox is shown in Figure 3.1.1-8. The fragment accelerates to approximately 8700 fps within the first 76 mm, and then decelerates due to aerodynamic drag until it impacts the first layer of the target at approximately 0.5 m. There is a significant velocity reduction as the fragment passes through the first layer. From 0.55m to 0.61m, the fragment decelerates through the air within the wingbox, then hits the second layer of the box, decelerates within the layer significantly and then emerges through the back side and continues decelerating in the air at the back of the wingbox. Figures 3.1.1-6 and 3.1.1-7 show the damage resulting from the blast and penetration of the warhead fragments.

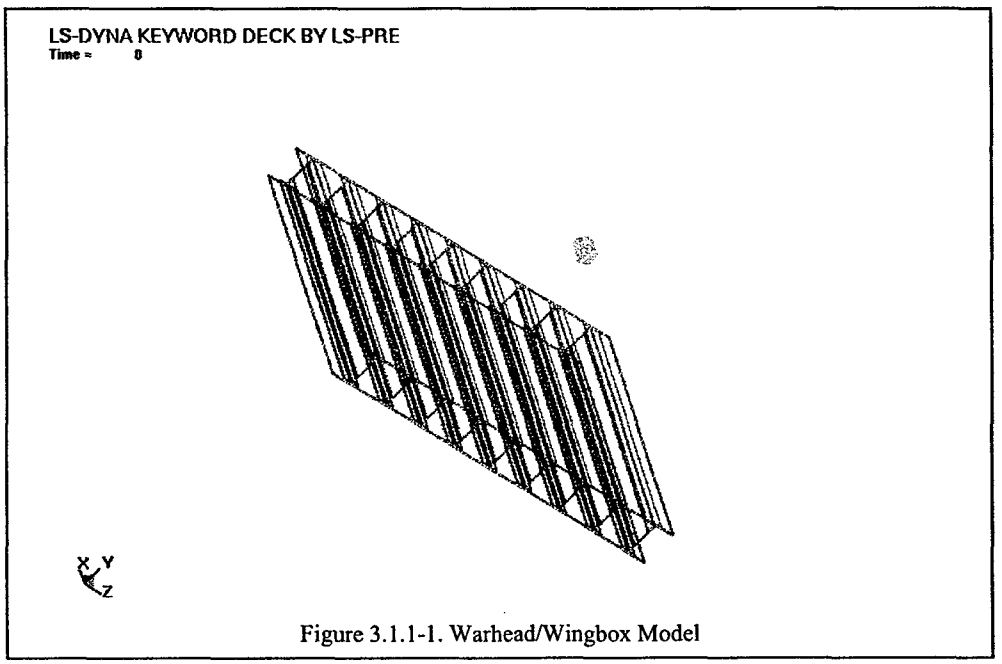

Figure 3.1.1-1. Warhead/Wingbox Model

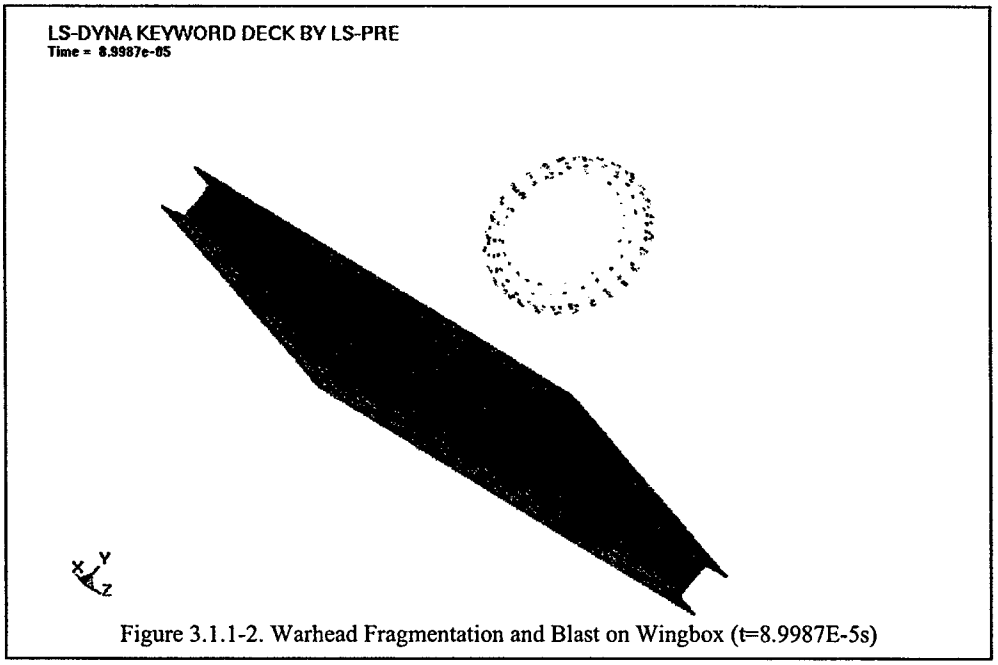

Figure 3.1.1-2. Warhead Fragmentation and Blast on Wingbox (t=8.9987E-5s)

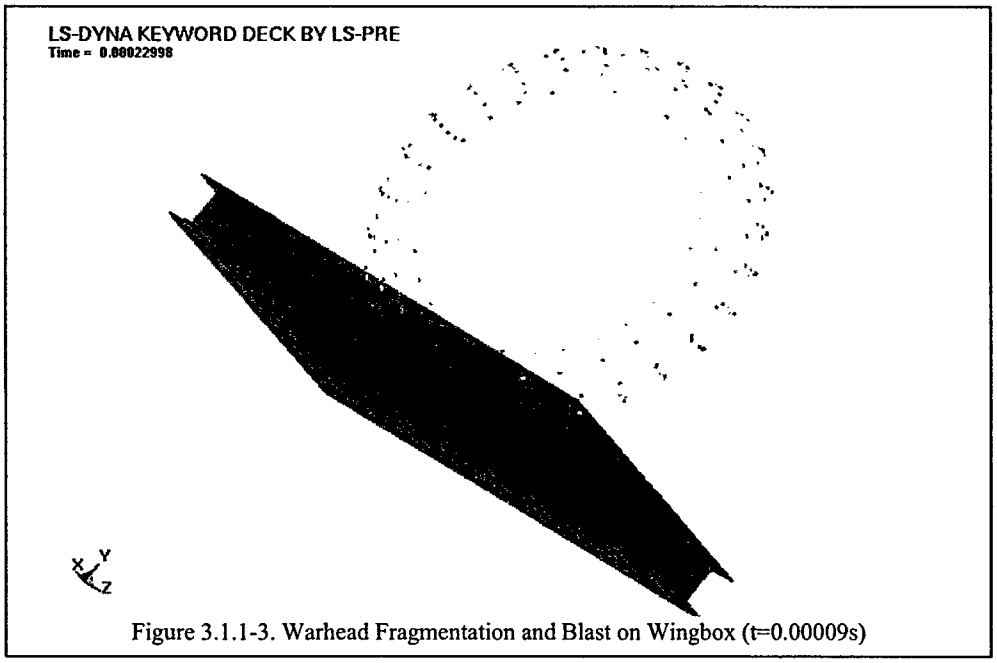

Figure 3.1.1-3. Warhead Fragmentation and Blast on Wingbox (t=0.00009s)

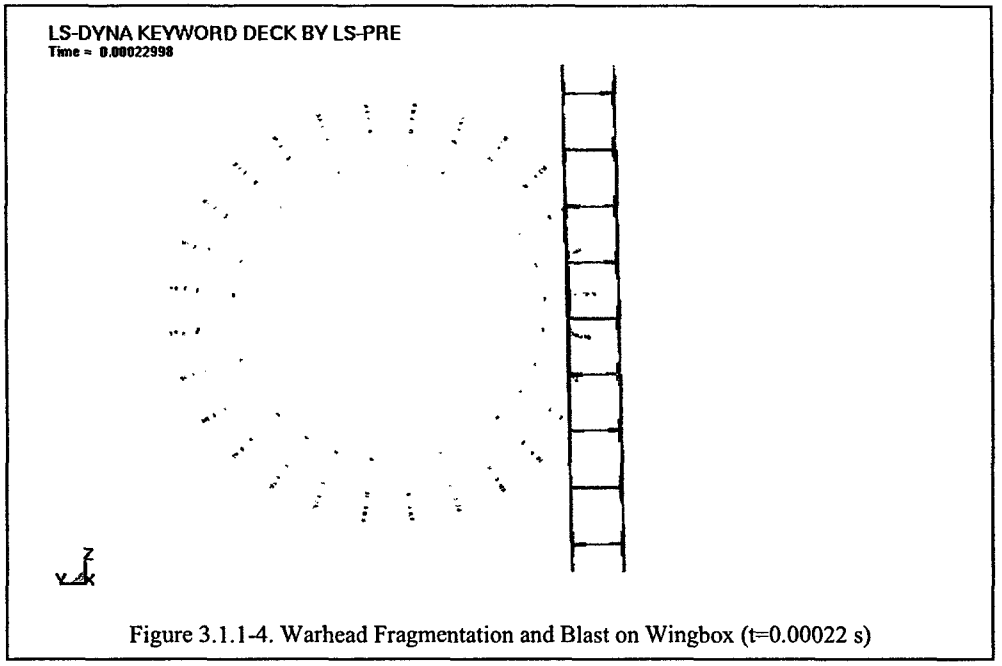

Figure 3.1.1-4. Warhead Fragmentation and Blast on Wingbox (t=0.00022 s)

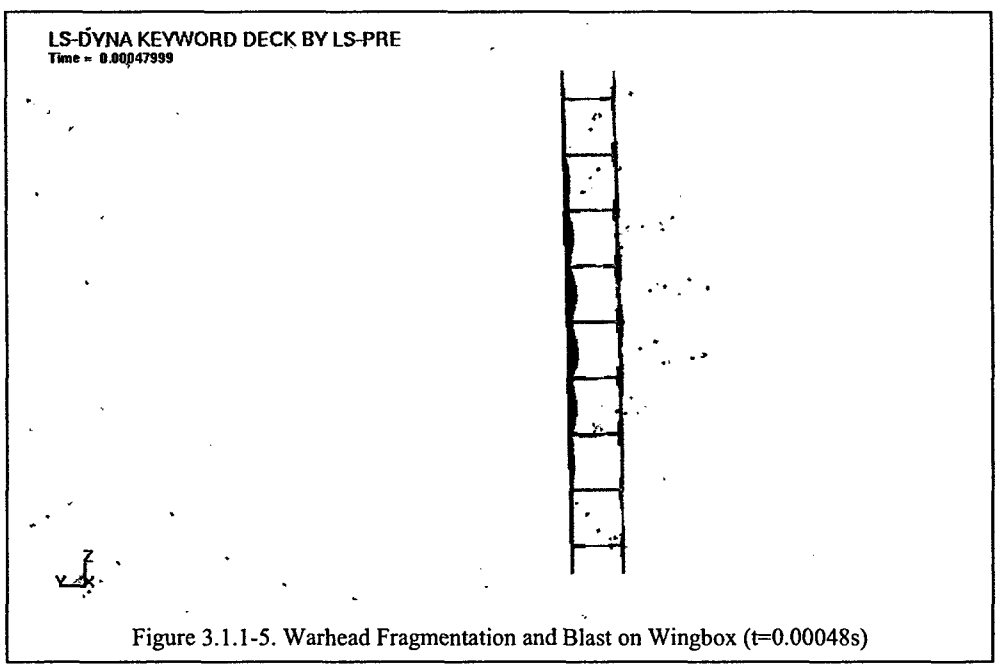

Figure 3.1.1-5. Warhead Fragmentation and Blast on Wingbox (t=0.00048s)

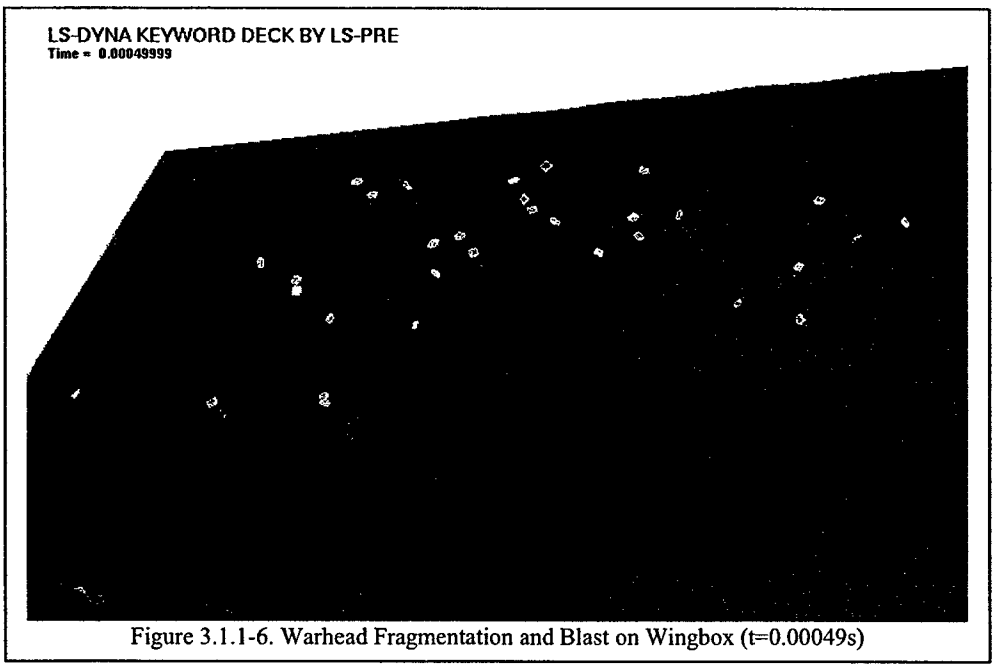

Figure 3.1.1-6. Warhead Fragmentation and Blast on Wingbox (t=0.00049s)


Figure 3.1.1-7. Warhead Fragmentation and Blast on Wingbox (t=0.00054s)

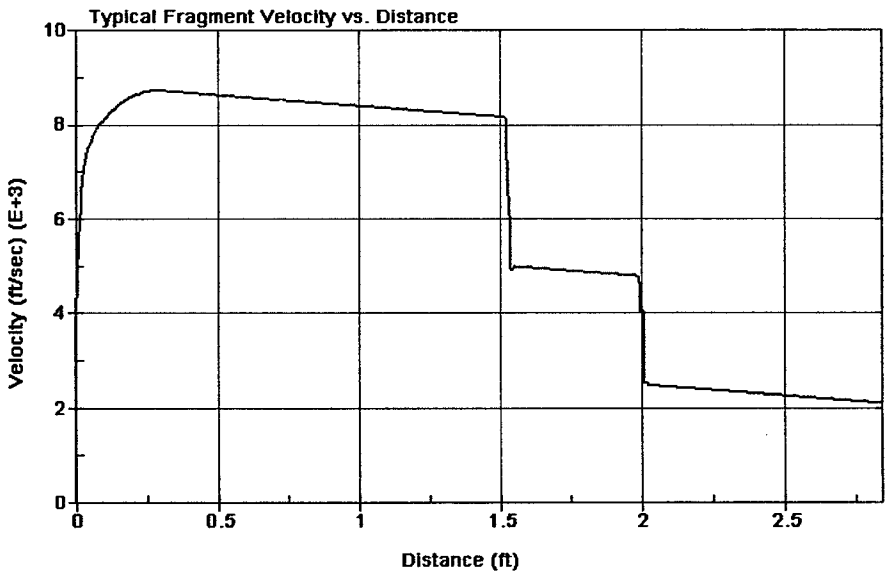

Figure 3.1.1-8. Typical Fragment Velocity versus distance

Examination of the resulting damage to the composite wingbox model indicates that the damage was typical of fragment penetration. There was no apparent damage due to the blast. These observations are consistent with the test that had previously been done.

3.1.2 0.25 Meter Standoff

A second case was run with the warhead located at 0.25m standoff from the target. This was done in order to examine whether or not blast damage would be observed at the target.

Figures 3.1.2-1 through 3.1.2-4 show top view snapshots of the damage in the wingbox from the 0.25 m standoff. Figures 3.1.2-5 through 3.2.1-9 show side view snapshots of the damage.

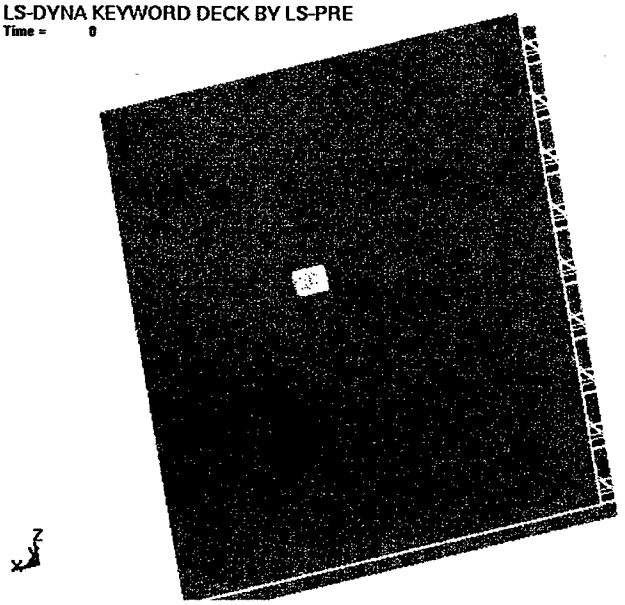

Figure 3.1.2-1. Warhead Fragmentation and Blast on Wingbox (0.25 m standoff)(t=0 s)

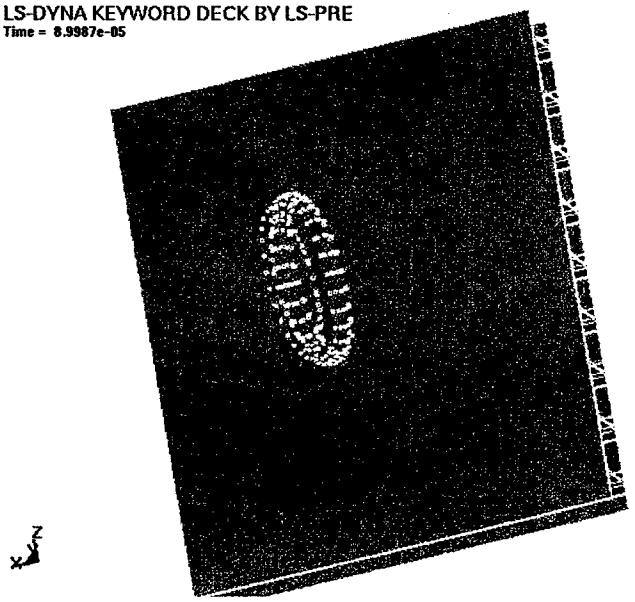

Figure 3.1.2-2. Warhead Fragmentation and Blast on Wingbox (0.25 m standoff)(t=0.00009 s)

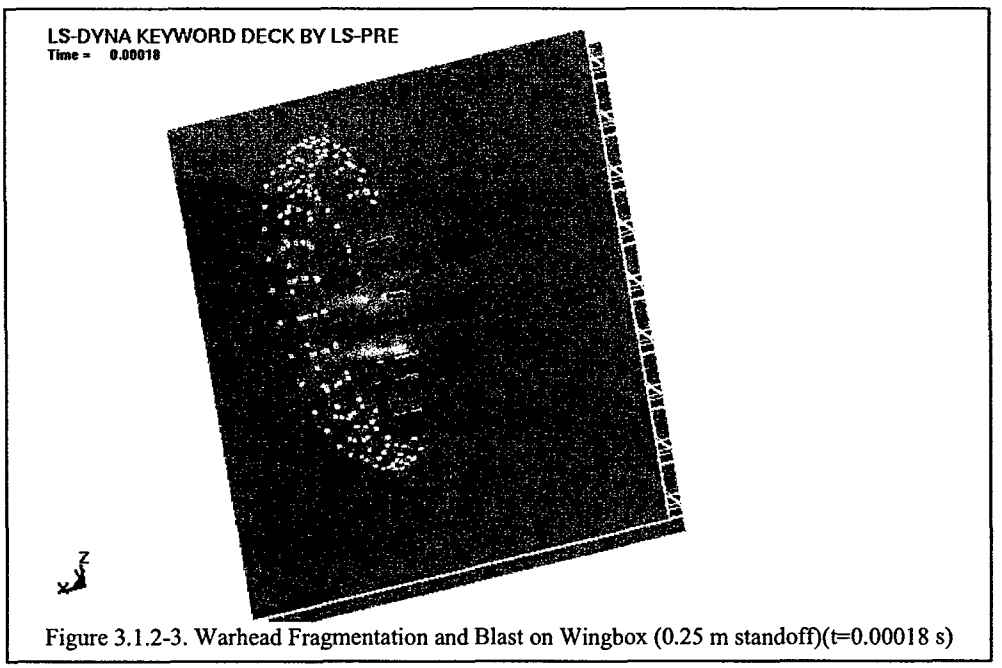

Figure 3.1.2-3. Warhead Fragmentation and Blast on Wingbox (0.25 m standoff)(t=0.00018 s)

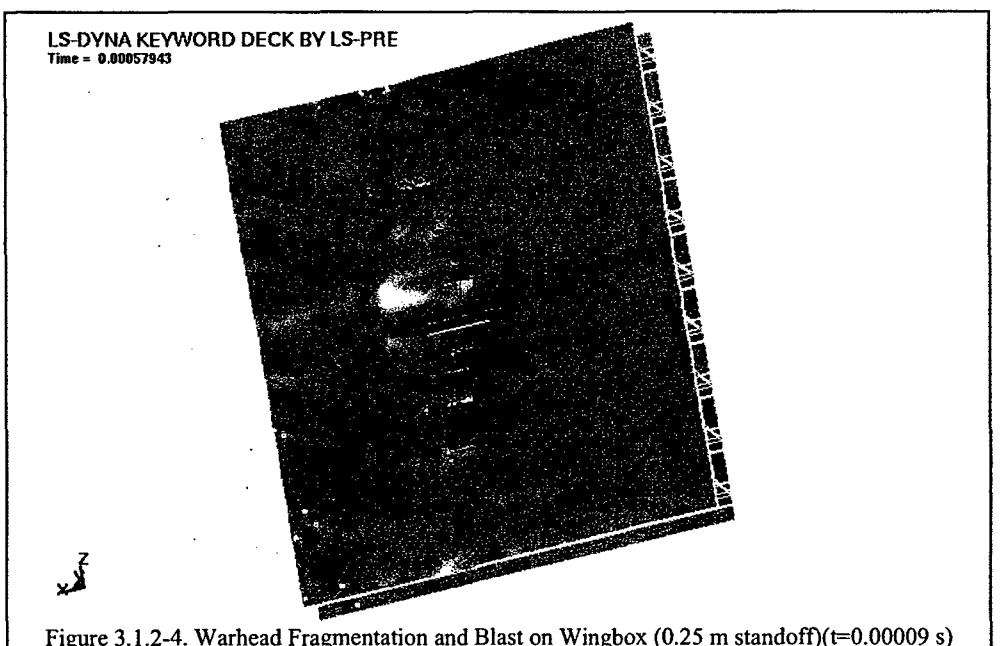

Figure 3.1.2-4. Warhead Fragmentation and Blast on Wingbox (0.25 m standoff)(t=0.00009 s)

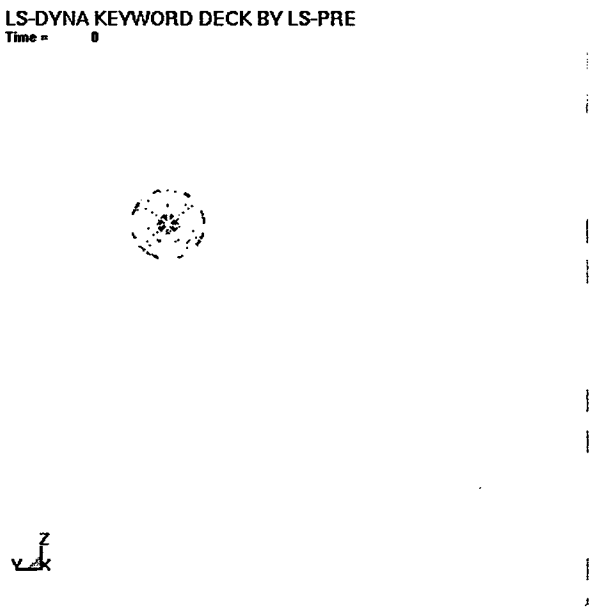

Figure 3.1.2-5. Warhead Fragmentation and Blast on Wingbox Side View (0.25 m standoff)(t=0.0 s)

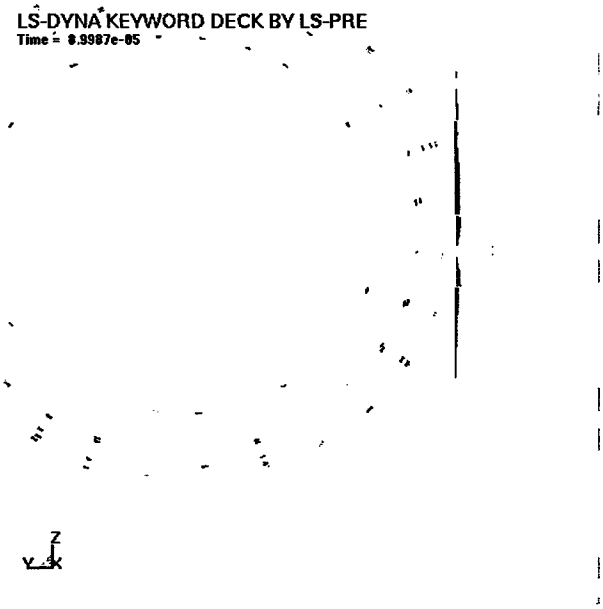

Figure 3.1.2-6. Warhead Fragmentation and Blast on Wingbox Side View (0.25 m standoff)(t=0.00009 s)

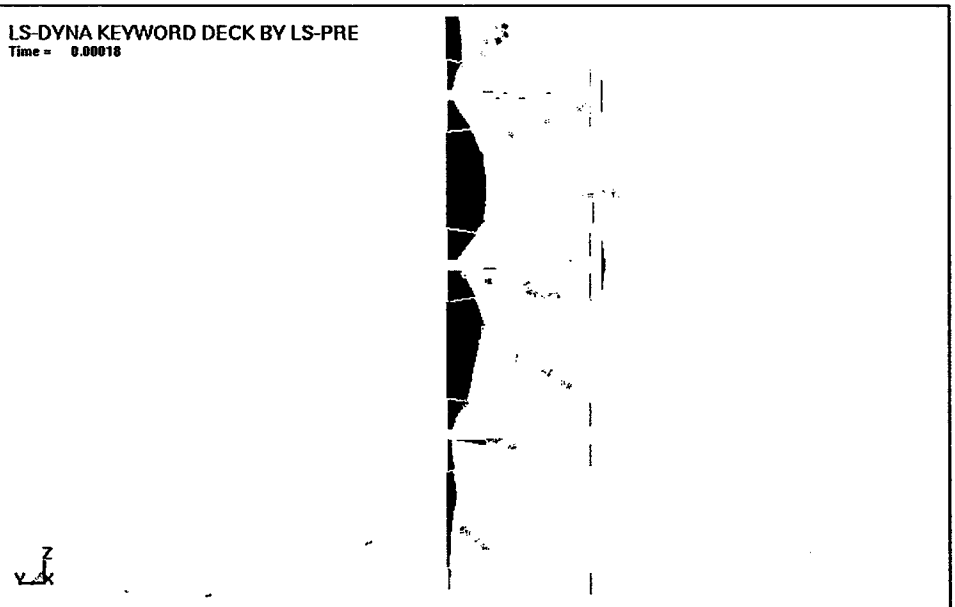

Figure 3.1.2-7. Warhead Fragmentation and Blast on Wingbox Side View (0.25 m standoff)(t=0.00018 s)

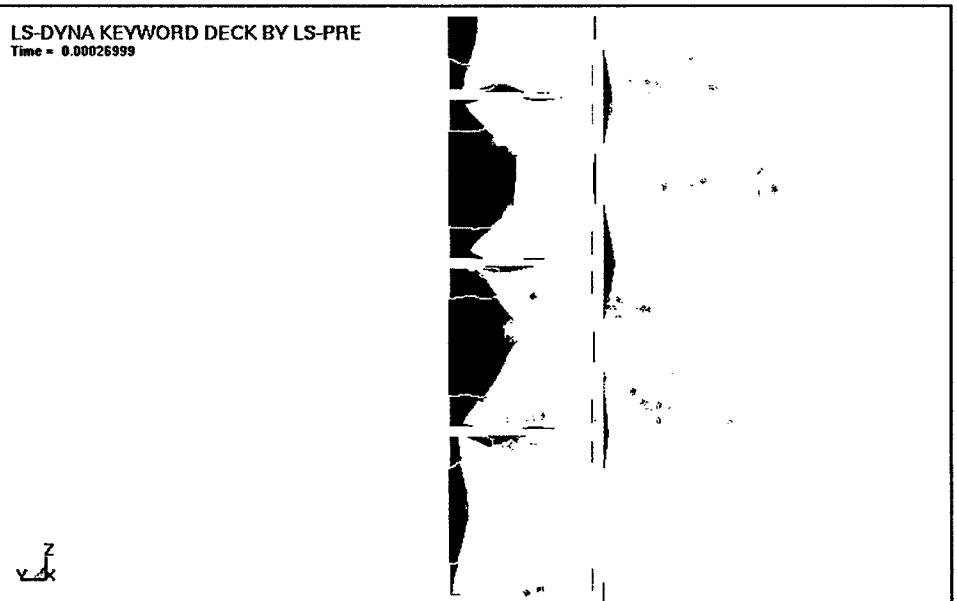

Figure 3.1.2-8. Warhead Fragmentation and Blast on Wingbox Side View (0.25 m standoff)(t=0.000027 s)

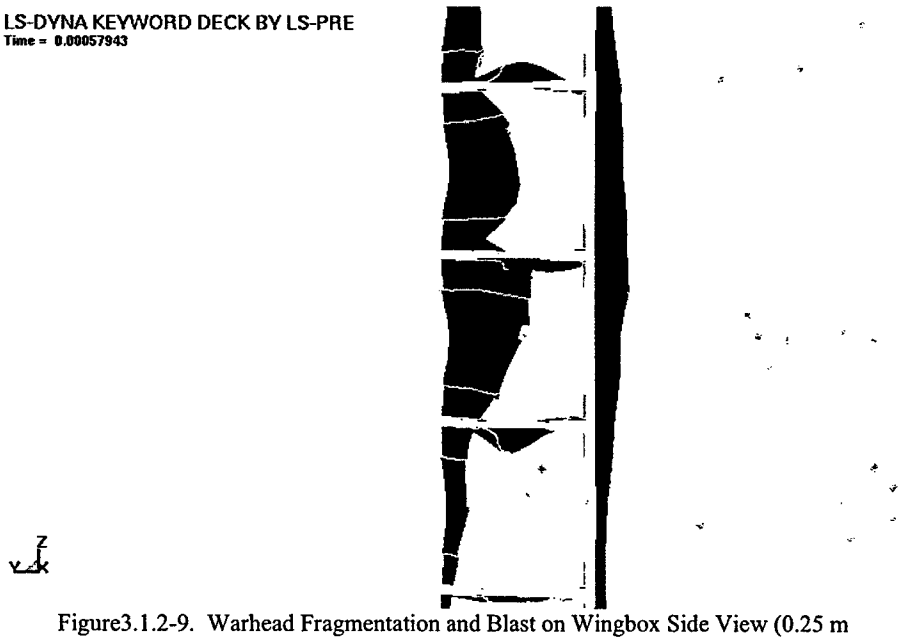

Figure3.1.2-9. Warhead Fragmentation and Blast on Wingbox Side View (0.25 m standoff)(t=0.00058 s)

Examination of Figures 3.1.2-4 and 3.1.2-9 reveals that there is damage at the spar junction with the skin of the wingbox. This is damage not seen in the 0.5 m standoff case and indicates that the damage is due to the warhead blast.

This observation of blast damage occurring at the 0.25m standoff led the authors to propose that a dynamic MANPADS test be performed in which the missile passes over the composite wingbox at 0.25m standoff, at 1200 fps and impact into an array of aluminum plates

3.2 Wing Flutter Study

The results of the validation of the wing flutter mythology are presented in Section 3.2.1. Section 3.2.2 presents the results of the model of a wing structure with an aerodynamic mesh being impacted with a MANPADS missile.

3.2.1 Wing Flutter Model Validation

A validation of the undamaged wing including aerodynamic effects modeled with LS-DYNA was conducted. This was done by comparing the performance of the model against existing data that had been obtained from earlier static and dynamic ground tests.

3.2.1.1 Wing Flutter Static Validation

For the static ground test, the aircraft wing was cantilevered horizontally from a strong back wall and subjected to a static load at buttline 120. Displacement measurements at the loading points were taken. Comparisons of model predictions of the displacements with those obtained during the test are shown in Figure 3.2.1.1-1.

For this comparison, the wing model was detached from the fuselage model and cantilevered to replicate boundary conditions of the ground test. The aerodynamic model was replaced with a concentrated line load at buttline 120. Since LS-DYNA is an explicit time integration code, results are plotted in the time domain. The smooth build-up of displacement vs. time of the LS-DYNA model is the result of a ramped loading in combination with mass scaling and damping application.

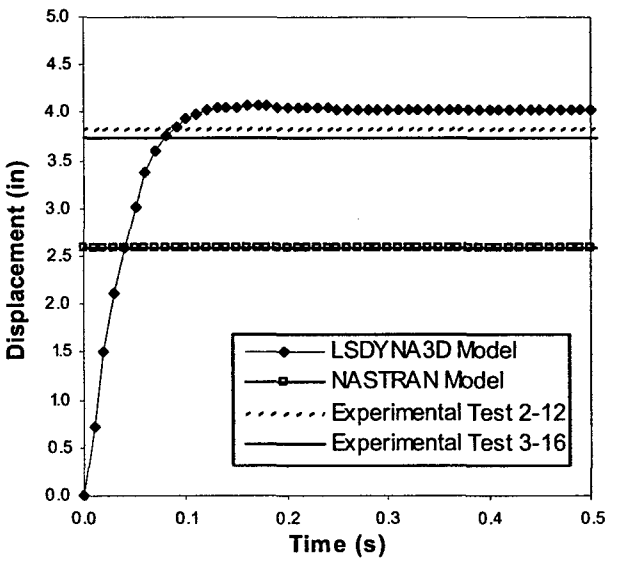

Figure 3.2.1.1-1. Wing model with Aerodynamic Mesh Displacement Comparison

One can see from Figure 3.2.1.1-1 that the LS-DYNA model predicts a displacement approximately 5% greater than ground test. One striking observation is that when compared to the original NASTRAN model [4], the LS-DYNA model is significantly better. The model displacement is quite sensitive to the imposition of the cantilevered boundary condition. Additional refinement of that boundary condition would have led to closer agreement, but it was decided that the 5% difference was acceptable.

3.2.1.2 Wing Flutter Dynamic Validation

For the dynamic ground test, the aircraft wing was cantilevered vertically from a strong back, instrumented, and subjected to a ground vibration/modal analysis test.

Due to the explicit nature of the LS-DYNA code, natural frequencies were determined in the time domain by cantilevering the wing model at the root and "plucking" the wing tip. The time history of displacement in the z direction of selected nodes was extracted and a fast fourier transform (FFT) was applied to obtain the frequency response. Figure 3.2.1.2-1 shows the results of the FFT processing, while Table 1 shows the comparison of natural frequencies.

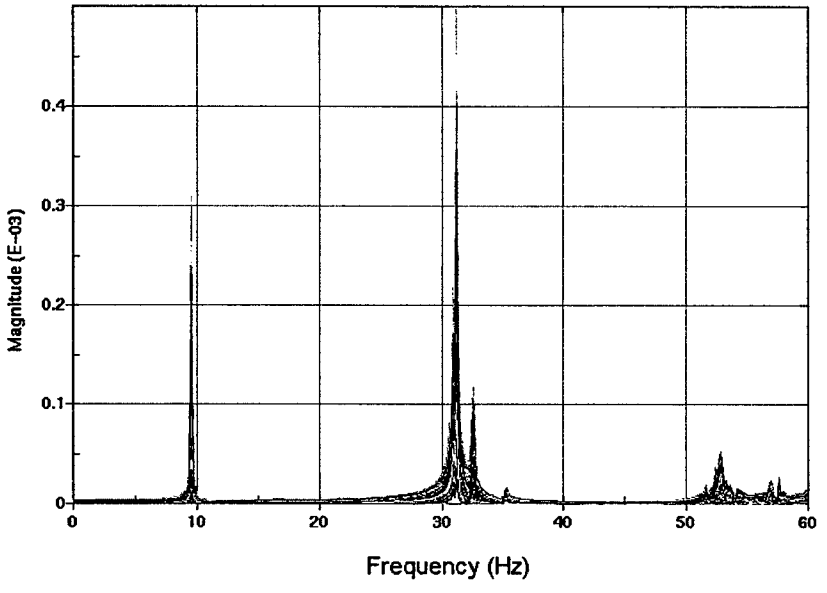

Figure 3.2.1.2-1. LS-DYNA Prediction of Natural Frequencies

Table 1. Natural Frequency Comparison

Mode #	Ground Test (Hz)	LS-DYNA Model (Hz)	NASTRAN Model (Hz)[4]
1	11.39	9.61	10.03
2	34.76	31.20	26.97
3	36.51	32.60	32.99
4	56.16	53.00	41.44

The difference between the LS-DYNA model and the ground test values varies between 6% and 16%.

3.2.2 MANPADS Induced Damage Including Aerodynamic Effects

This section presents the results of the model of a wing structure with an aerodynamic mesh being impacted with a MANPADS as described in Section 2.2. The purpose of the study is to show the ability of this modeling technique to capture wing flutter under

missile imposed damage conditions. This model does not include blast or fragmentation effects.

The model of the missile prior to impact of the wing is presented in Figure 3.2.2-1. Upon impact the missile penetrates through the wing causing structural damage to the wing skin, spars and ribs as shown in Figure 3.2.2-2 through 3.2.2-4. The damage criterion used for the wing and missile is a strain based element erosion technique. Figure 3.2.2-5 shows damage to the spars and ribs as the missile penetrated at a spar-rib joint. Figures 3.2.2-6 through 3.2.2-12 present the resulting wing flutter. After several fluctuations of the wing, the wing completely separates from the main structure. The leading edge wing tip displacements are presented in Figure 3.2.2-13. The undamaged wing displacement oscillates by only a small amount (~±1 in), while the damaged wing oscillates violently (~±20 in) after the impact at 0.2 seconds. The Von Mises stress at 0.273 seconds is presented in Figure 3.2.2-14. High stresses at ~60 ksi are evident due to the wing flutter. These results show that with the boundary element method, wing flutter may be evaluated after missile damage.

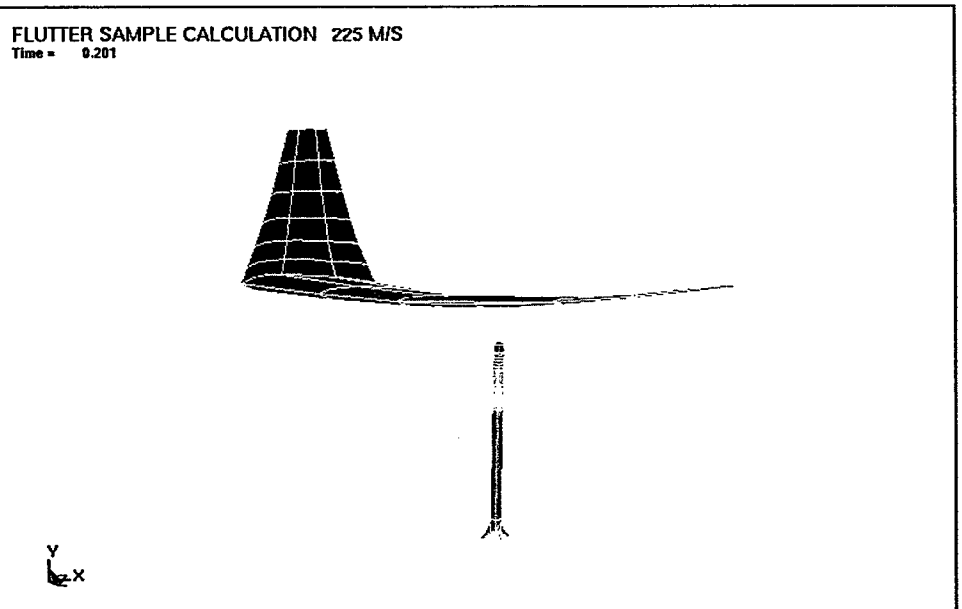

Figure 3.2.2-1 Wing Flutter-MANPADS Model

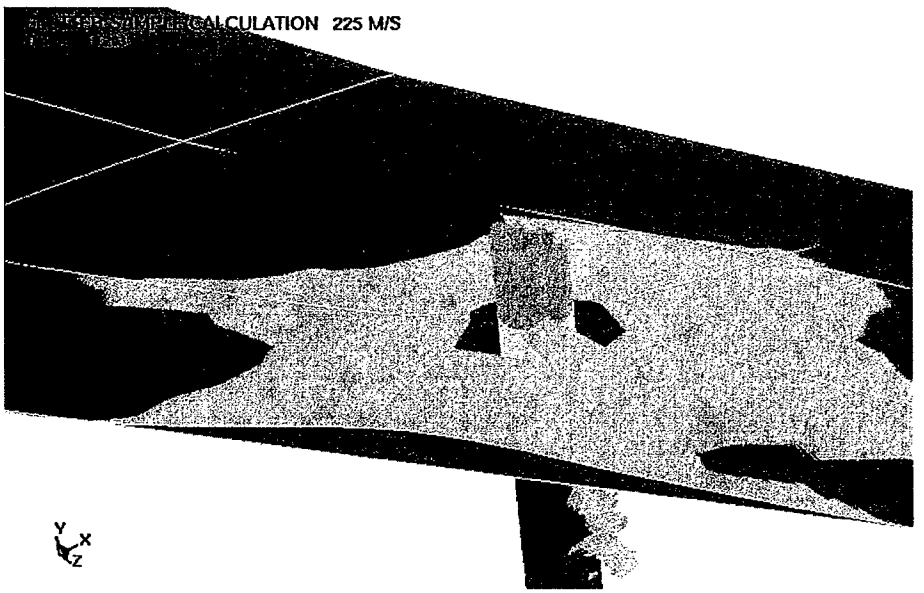

Figure 3.2.2-2 Wing Flutter-MANPADS Model after Penetration and Blast (t=0.203 s)

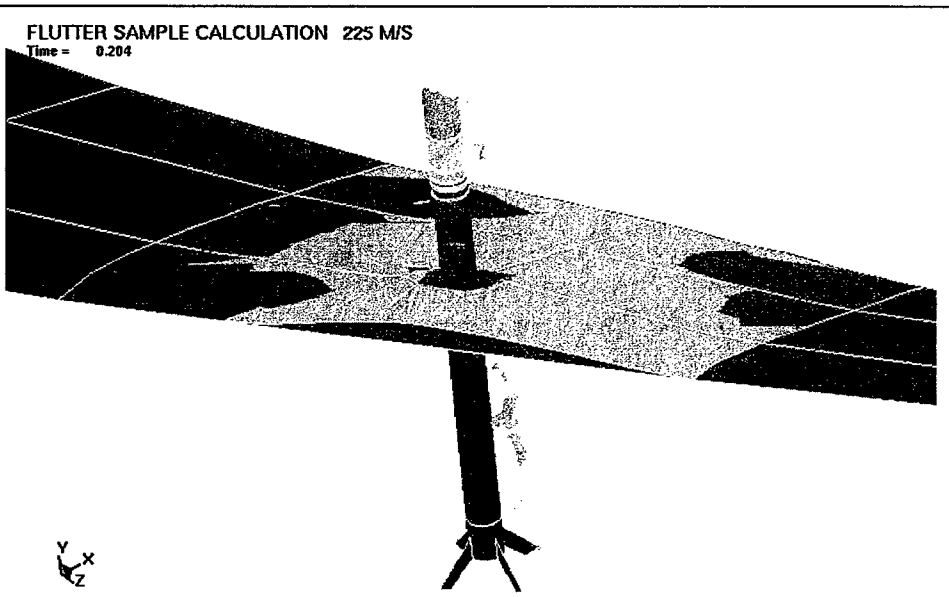

Figure 3.2.2-3 Wing Flutter-MANPADS Model after Penetration and Blast (time=.204 s)

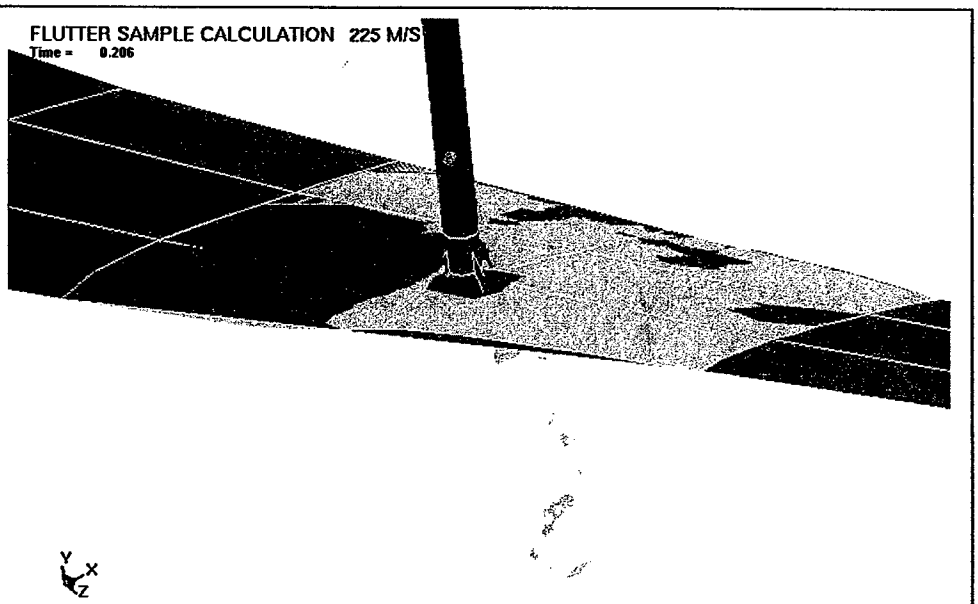

Figure 3.2.2-4. Wing Flutter-MANPADS Model after Penetration and Blast (time=0.206 s)

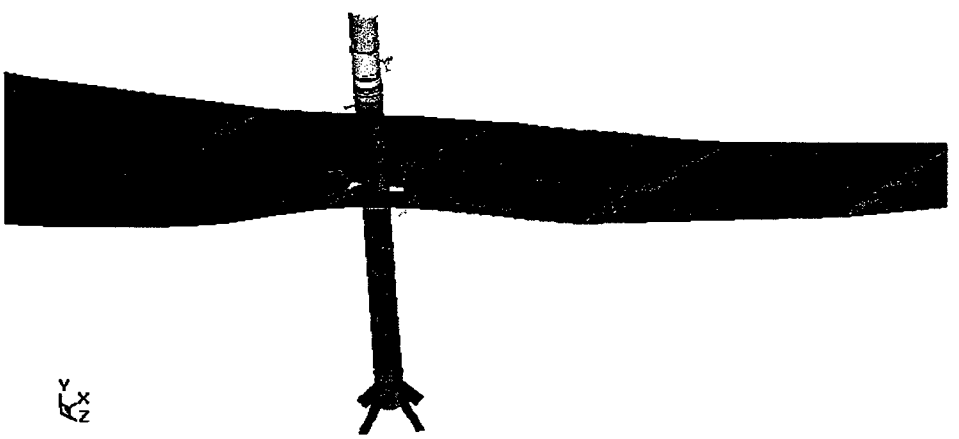

Figure 3.2.2-5. Wing Flutter-MANPADS Model after Penetration and Blast (time=0.283 s)

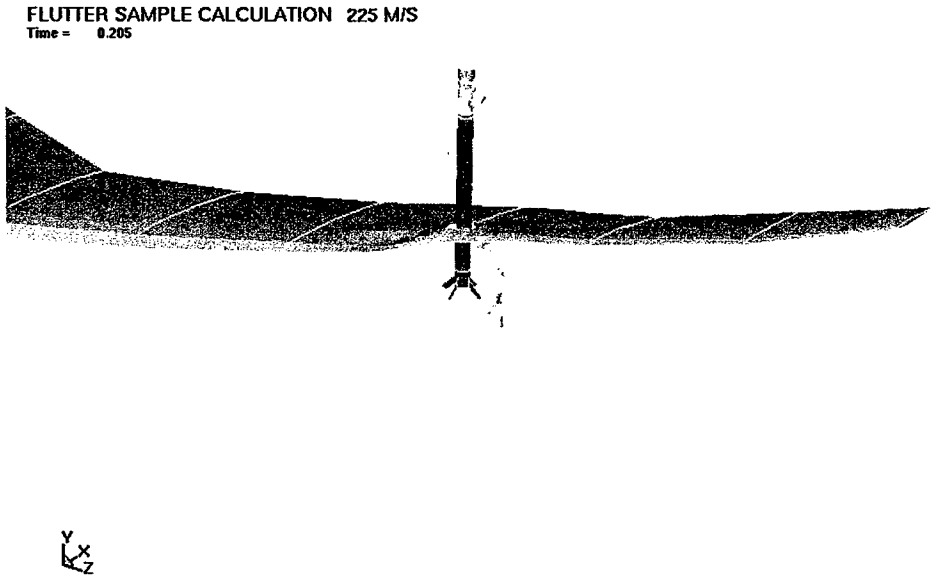

Figure 3.2.2-6. Wing Flutter (time=0.205 s)

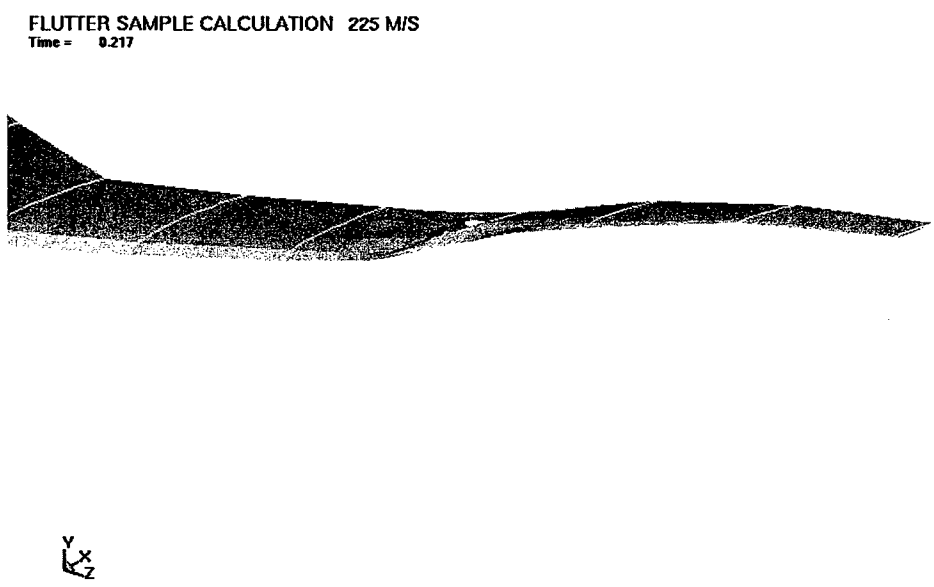

Figure 3.2.2-7. Wing Flutter (time=0.217 s)

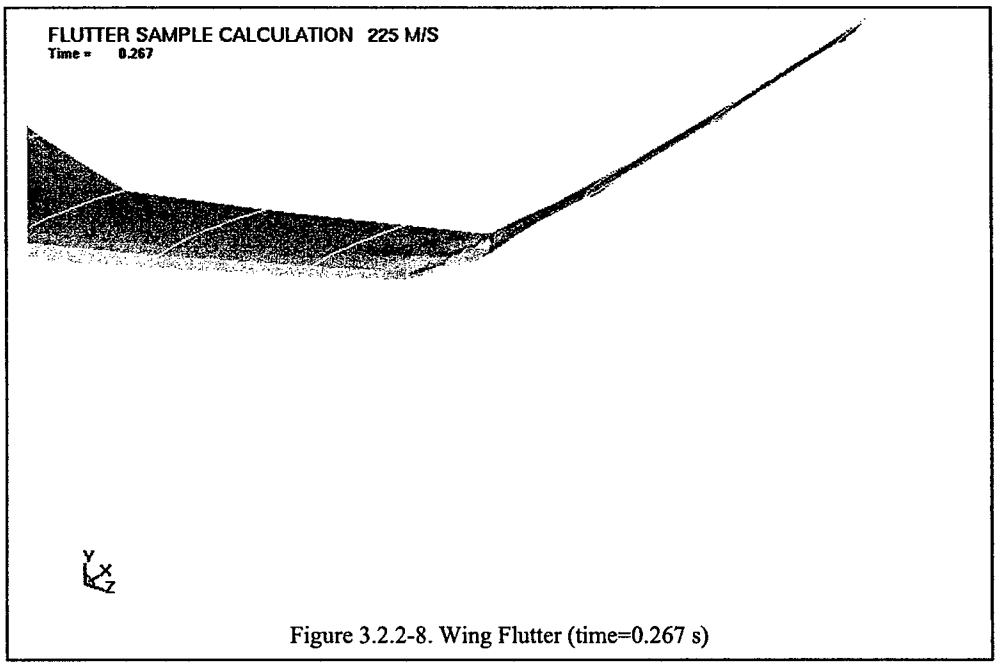

Figure 3.2.2-8. Wing Flutter (time=0.267 s)

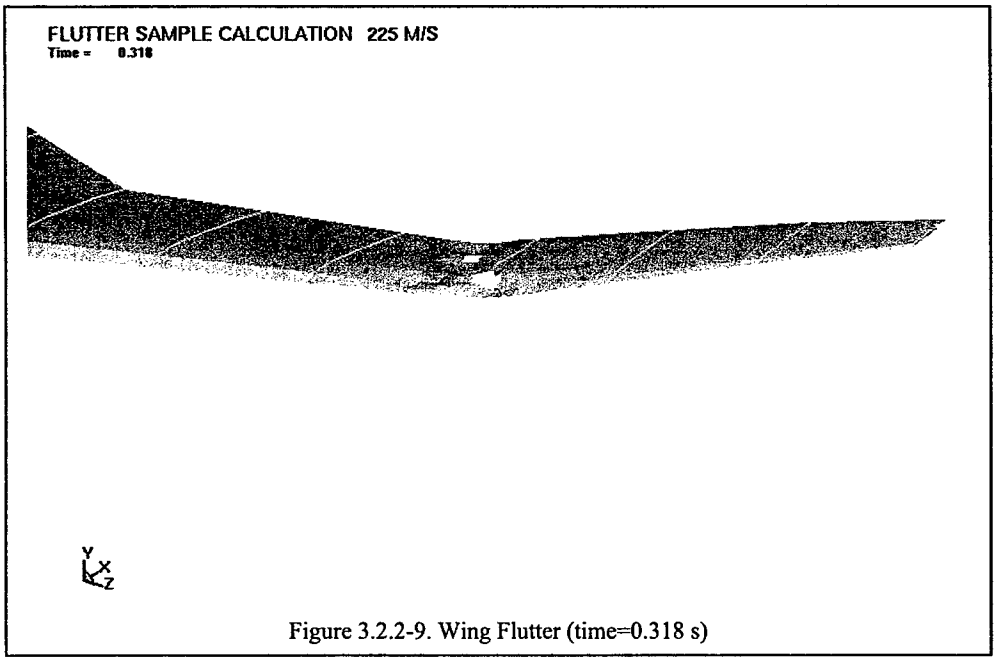

Figure 3.2.2-9. Wing Flutter (time=0.318 s)

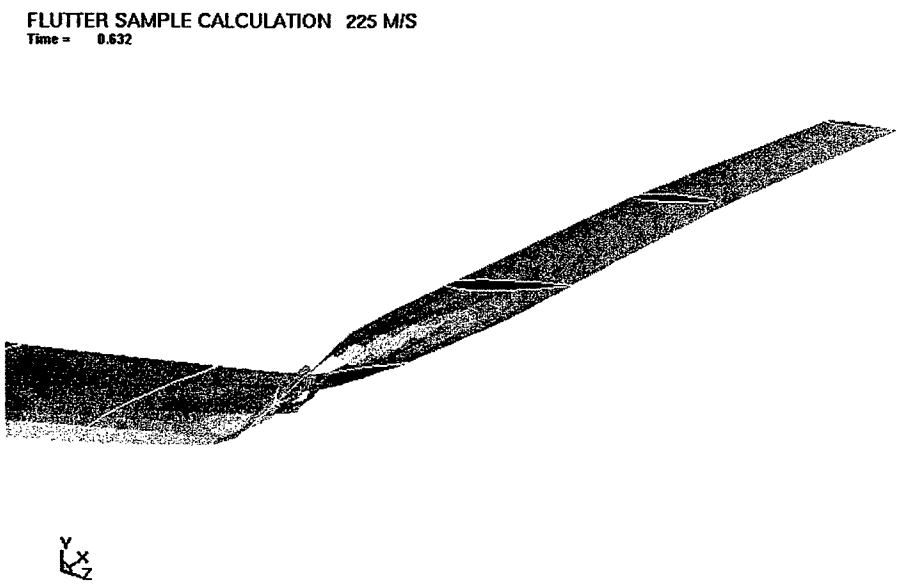

Figure 3.2.2-10. Wing Flutter with Large Deformation (time=0.632 s)

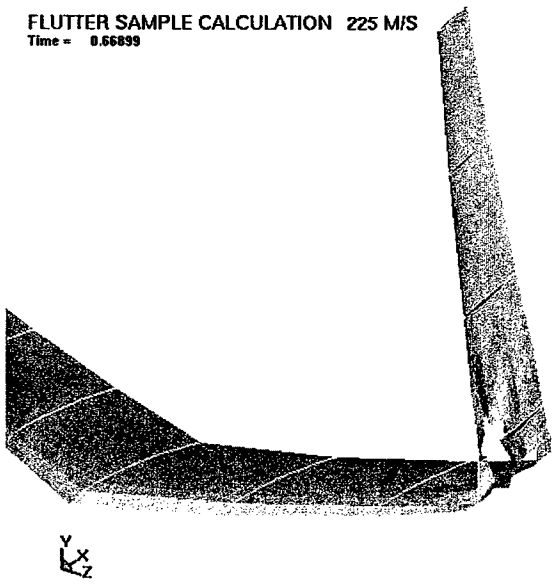

Figure 3.2.2-11. Wing Flutter with Large Deformation (time=0.669 s)

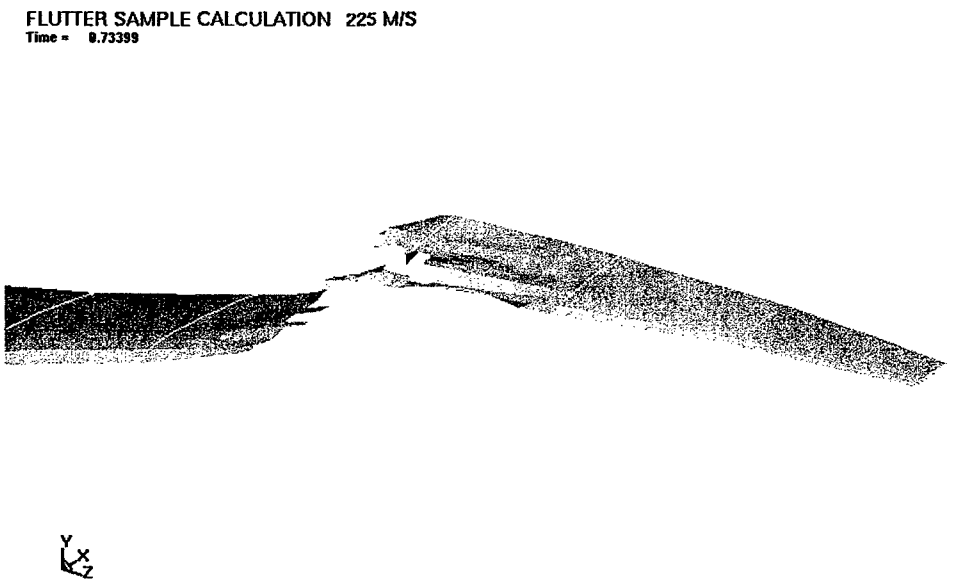

Figure 3.2.2-12. Wing Flutter with Complete Separation of Wing (time=0.734 s)

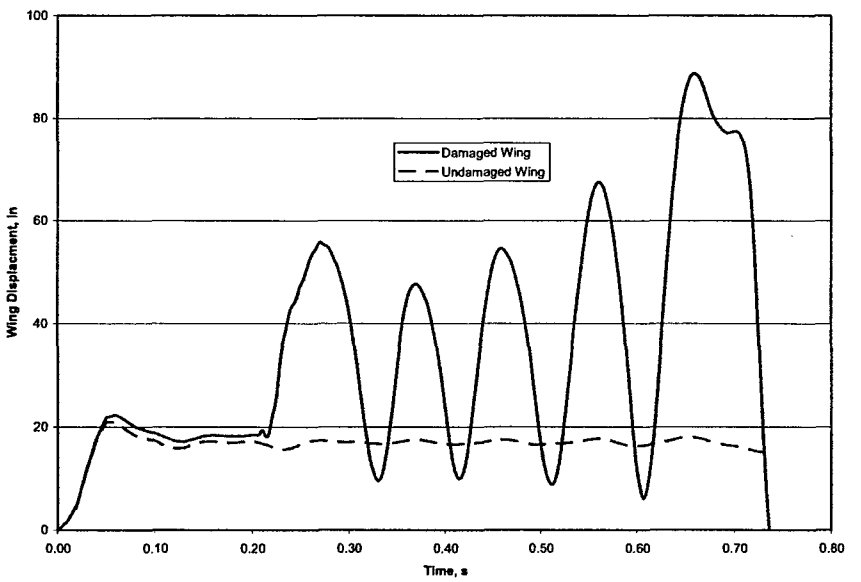

Figure 3.2.2-13. Wing Leading Edge Tip Displacements versus Time

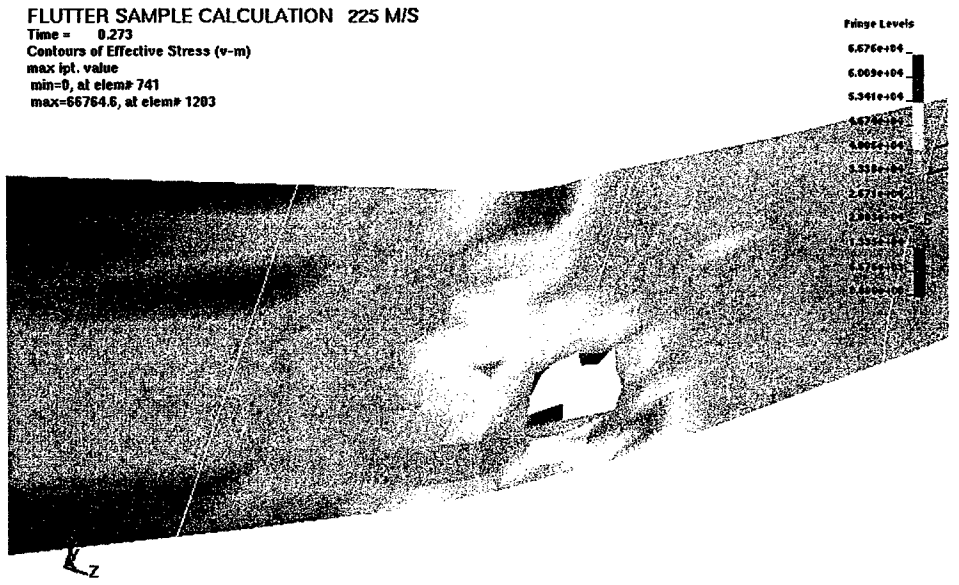

Figure 3.2.2-14. Wing Flutter Von Mises Stresses (time=0.273 s)

3.3 MANPADS Damage on Transport Aircraft Wing Structures

This section shows samples of each of the steps described in section 2.3. The first samples are of the missile impact on a target without detonation. Secondly, samples are shown of the missile passing nearby the target and detonating as well as impacting and detonating. The last sample shown is of the missile impacting and detonating on a full wing section.

Step One -- No Detonation

Results presented here show the body-on-body impact damages caused by a missile on a stiffened panel and a wing section. LS-DYNA was used to simulate the impact and study the size and pattern of the damage caused by the impact of the projectile at incident angles. The stiffened panel, shown in Figure 3.3-1, was impacted by the missile with various incident angles at two different locations. One of the impact points is at the midpoint of the panel where there is a stiffener, and the other is at a mid-bay between two stiffeners. The wing section shown in Figure 3.3-2 was impacted by the missile at a stiffened point on the lower skin. Analysis results are discussed in the following sections. These studies and other missile impact cases will help identify the worst case damage scenario for the prediction of the residual strength of damaged wing structures.

A. Stiffened panels impacted by missile with various incident angles at a mid-bay

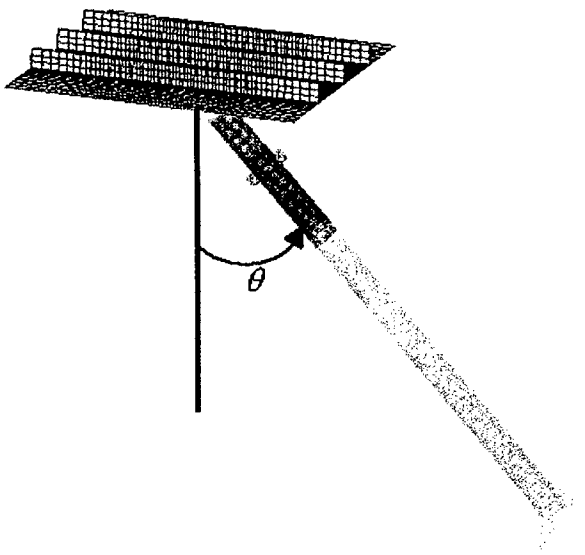

Figure 3.3-1. Finite Element Model Of A Missile Impacting On A Stiffened Wing Panel Effects.

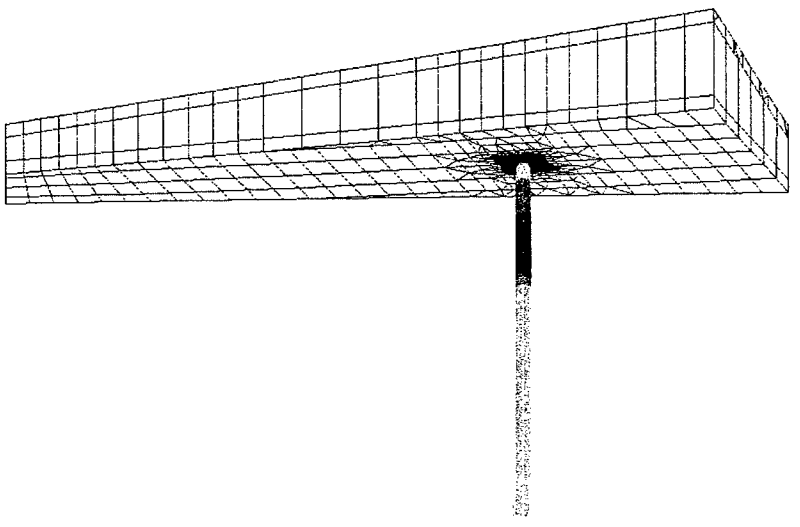

Figure 3.3-2. Finite Element Model Of A Projectile Impacting On A Wing Section.

The damage caused by the missile impacting at a mid-bay of the stiffened panel with a zero degree incident angle is shown in Figure 3.3-3. The missile body created a nearly circular hole in the plate approximately 3.8 inches in diameter. The impact of the fins

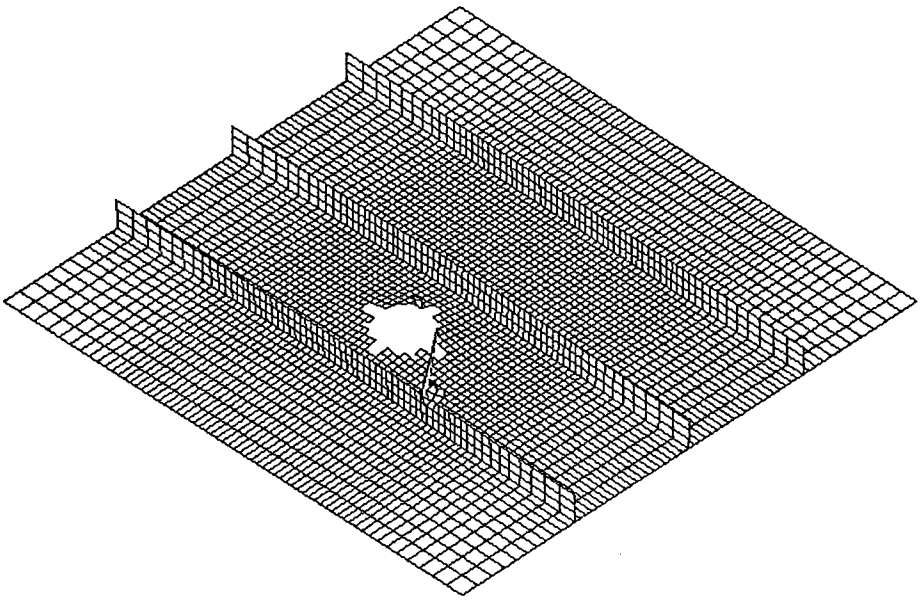

Figure 3.3-3. Damage From 0° Incident Angle Impacting At Mid-Bay.

created cracks of a total length of 4.6 inches normal to the stiffener and 5.3 inches in length in the direction of the stiffener. There was almost no deformation of either the plate or the stiffener, and the deformation was limited to only the edge of the hole.

The damage caused by the missile impacting at a mid-bay of the stiffened panel with a forty-five degree incident angle is shown in Figure 3.3-4. The projectile body impact created an elliptical hole of 4.6 inches wide and 7.6 inches long, large enough for the fins to pass through without causing any additional damage. There was significant deformation of the plate, extending to the stiffeners on either side of the impact. This deformation caused the center stiffener to bend upward and twist away from the impact, creating a gap in the stiffener of 0.4 inches.

The damage caused by the missile impacting at a mid-bay of the stiffened panel with a seventy-five degree incident angle is shown in Figure 3.3-5. There does not appear to be any permanent damage from this impact. The section of the plate between the stiffeners is flexible enough to absorb the energy of the projectile through elastic deformation, while deflecting the projectile to move along the plate without any penetration.

B. Stiffened panels impacted by missile with various incident angles at the middle of the center stiffener

The damage caused by the missile with a zero degree incident angle is shown in Figure 3.3-6. The missile body created a nearly circular hole in the plate approximately 3.25 inches in diameter. The impact of the fins created cracks of a total length of 4.6

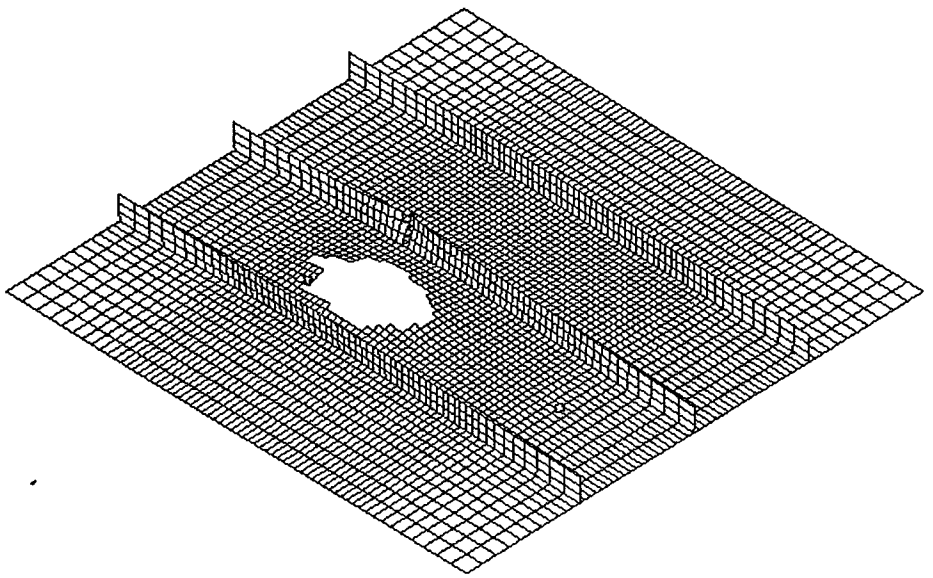

Figure 3.3-4. Damage From 45° Incident Angle Impacting At Mid-Bay.

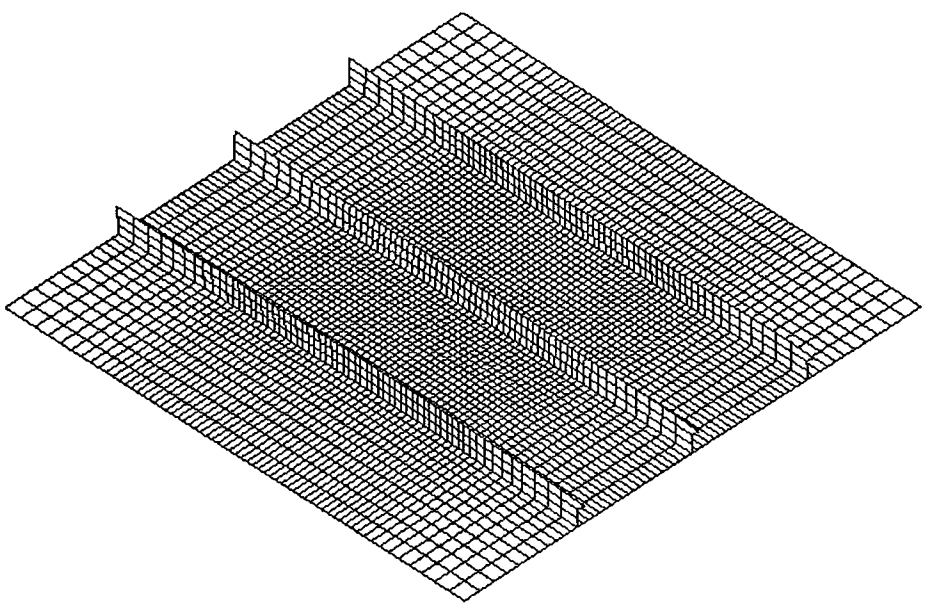

Figure 3.3-5. Damage From 75° Incident Angle Impacting At Mid-Bay.

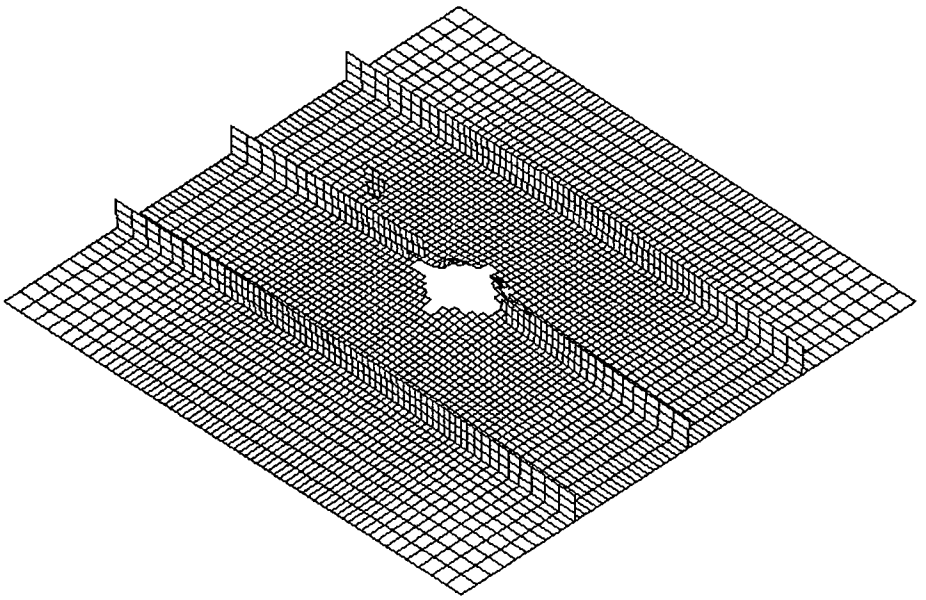

Figure 3.3-6. Damage From 0° Incident Angle Impacting At The Center Stiffener.

inches normal to the stiffener and 5.3 inches in length in the direction of the stiffener. The resulting gap in the stiffener was 5.1 inches in length. There was almost no deformation of either the plate or the stiffener.

The damage caused by the missile with a forty-five degree incident angle is shown in Figure 3.3-7. The impact of the missile body created a rectangular hole approximately 3.1 inches wide and 5 inches long. The impact of the fins created an additional 1.8 inch x 1.1 inch rectangular hole to the right of the main damage area and an additional 1.1 inch x 1.1 inch hole to the left of the main damage. The stiffener remained intact throughout the impact, absorbing the kinetic energy of the projectile through deformation. The upward bending of the stiffener tore cracks in the plate measuring 2.6 inches long in front of the projectile impact, and 2.25 inches long behind the impact. The section of the stiffener that was impacted by the projectile was greatly damaged, with numerous cracks forming and a large amount of deformation.

The damage caused by the missile with a seventy-five degree incident angle is shown in Figure 3.3-8. The missile impact split the plate forming a 25 inch long crack extending from 8.2 inches behind the point of impact to the edge of the plate. The width of the crack at the point of impact was 3.6 inches, and the width of the crack at the edge of the plate was 8.25 inches. Both the plate and the stiffener experience a significant amount of upward bending. The stiffener broke at the constrained end at the edge of the plate 2.6

milliseconds after the impact, when the motor portion of the missile struck the stiffener. The stiffener then began to twist, tearing a crack in the stiffener near the point of initial impact. The 15.2 inch section of the stiffener between the crack and the edge of the plate then pivoted upward, away from the projectile.

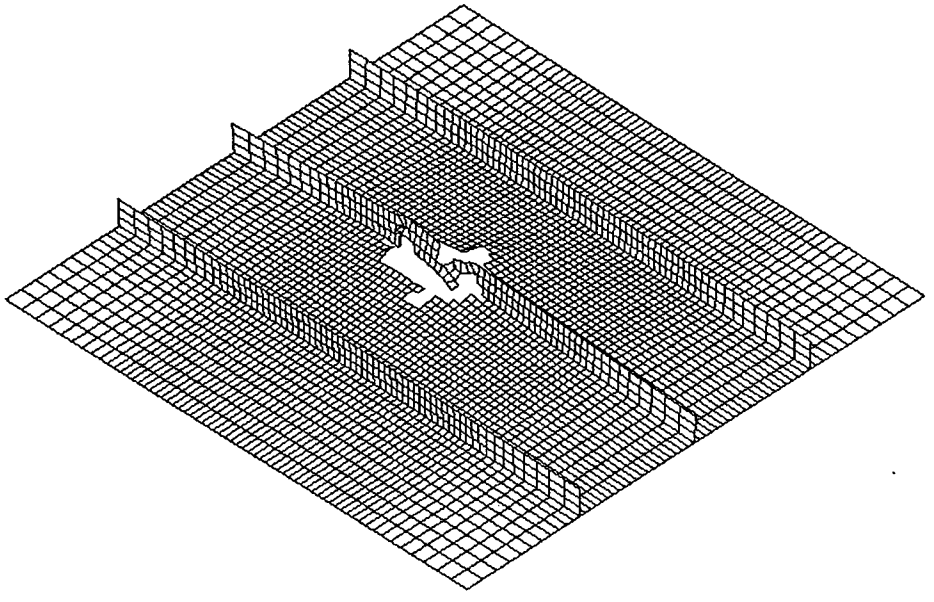

Figure 3.3-7. Damage From 45° Incident Angle Impacting At The Center Stiffener.

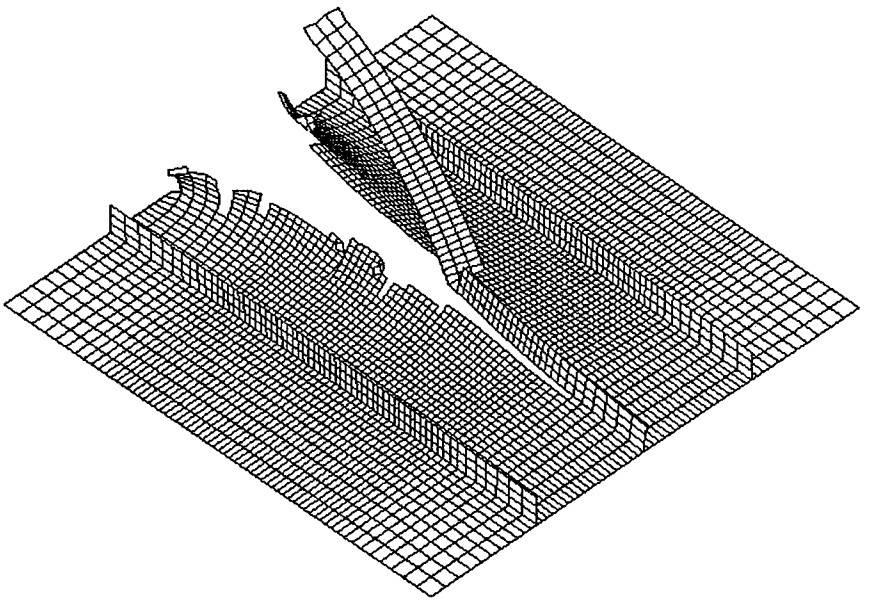

Figure 3.3-8. Damage From 75° Incident Angle Impacting At The Center Stiffener.

C. Projectile damage of a wing section

The model used for studying the effect of a projectile impact on a representative wing box is shown in Figure 3.3-2. Figure 3.3-9 shows the predicted damage for an impact

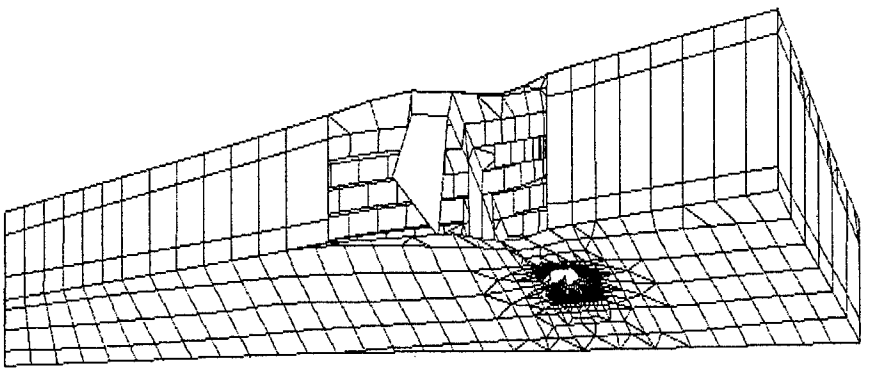

Figure 3.3-9. Predicted Damage To Wing Box Caused By A Projectile.

normal to the lower skin and with the impact point lying at a stringer. The projectile penetrated through both the lower skin and the upper skin, broke a stringer on the lower and upper skins, and caused significant deformation of the structure within the impacted bay. This deformation also caused damage to the other stringers, spars, and ribs.

Step 2 – Detonation and Fragmentation

In preparation for performing analysis of cases where detonation and fragmentation would occur, the meshes of the target models were refined. The refinement was necessary in order to capture the contact of the relatively small fragments with the target. If the target elements are large relative to the fragment size, the target appears artificially stiff to the fragment and damage is not properly simulated. Following the refinement, several cases were run.

The first case presented here shows the missile passing close by a stiffened plate target at a speed of 1200 fps and not impacting the target . Three cases were run:

1. Missile fragments impact target without blast effects.
2. Blast effects only impact target.
3. Combined blast and fragments impact target.

Figure 3.3-10 shows the model. Figures 3.3-11 through 3.3-13 show the damage due to each of the three cases. One observation that can be made from these figures is that for this very close range from threat to target, the blast effects are significant.

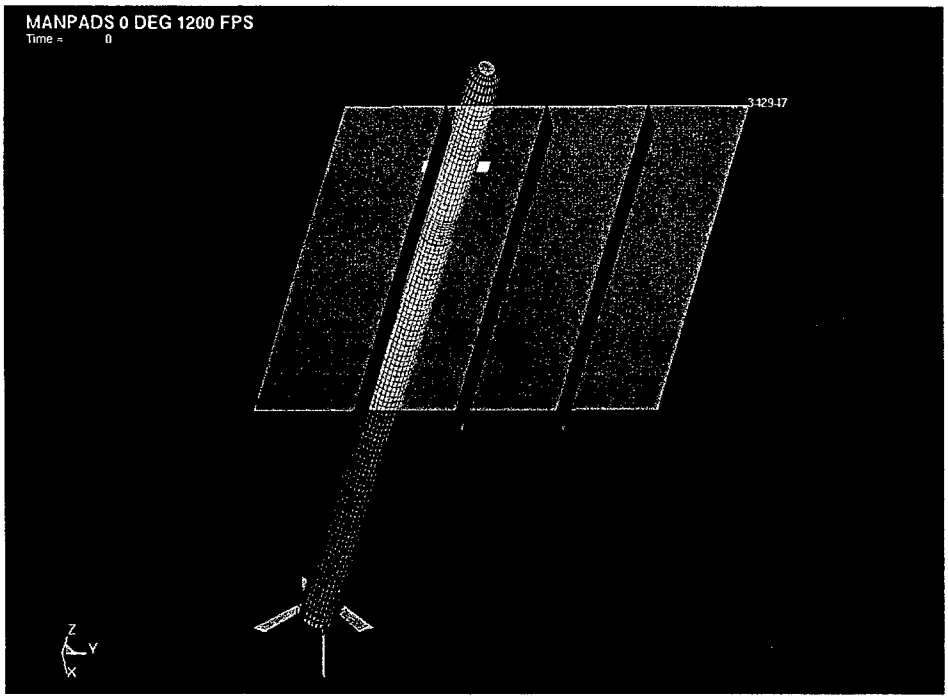

Figure 3.3-10. MANPADS Model Passing Close by Stiffened Plate Structure.

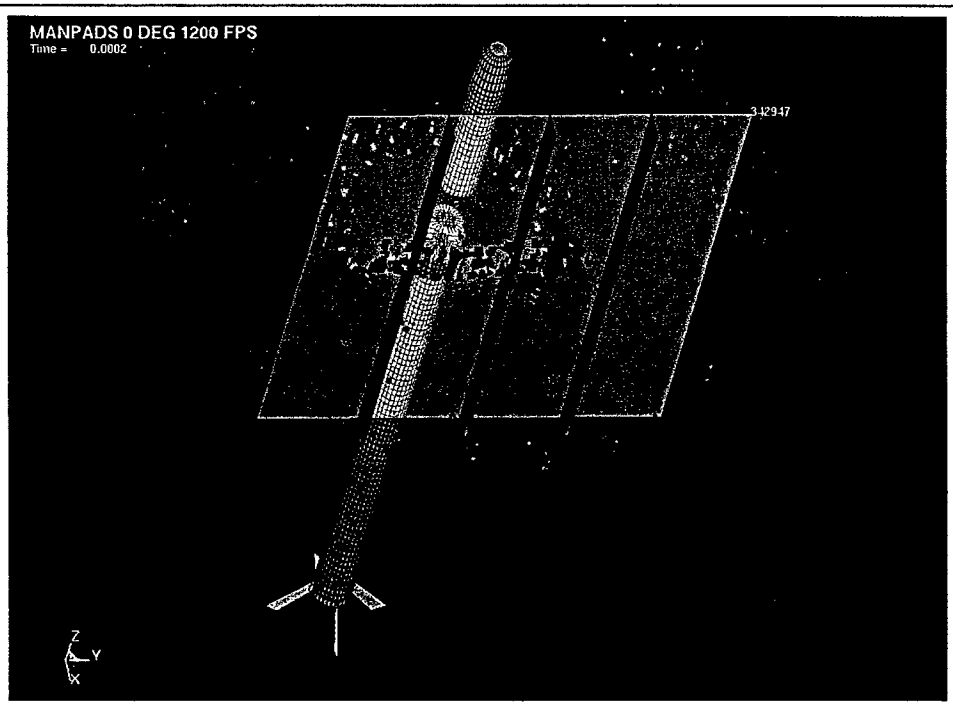

Figure 3.3-11. Damage Due To Fragmentation Only.

Furthermore one can observe the synergistic effects of the blast and fragmentation on the target.

From these quick look simulations, one immediately sees how significant the blast and fragmentation of the warhead are when the missile is in close proximity to the target.

Figure 3.3-12. Damage Due To Blast Only.

Whereas damage due to penetration-only is relatively small, the close-in detonation and fragmentation of the warhead leads to significant damage. Additional parametric studies are underway to progressively move the threat away from the target in order to understand the effects of range vs. damage including the blast and fragmentation effects.

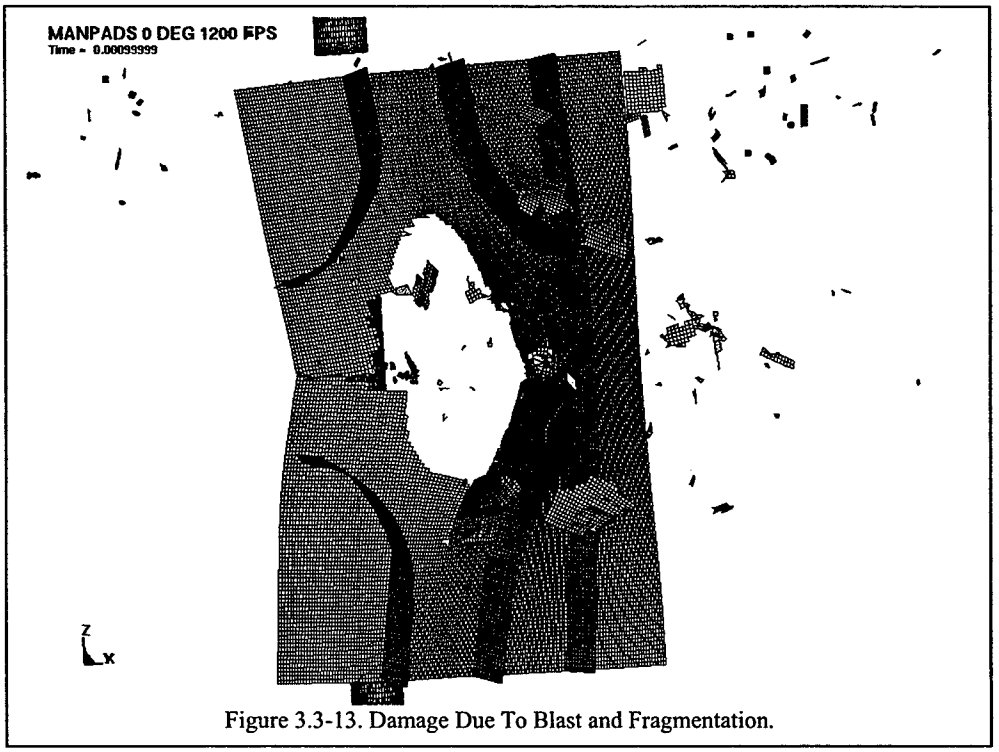

Figure 3.3-13. Damage Due To Blast and Fragmentation.

One other item that is significant to report is that the blast is moving relative to the target. Using the *LOAD_BLAST feature of LS-DYNA assumes that the blast is located at a fixed point in space. Therefore, in order to simulate the moving blast, the missile is held at a fixed point and the target is moved relative to it. The resulting effects are that the blast appears to move relative to the target. Figure 3.3-14 is a snapshot in time of the plastic strain produced by the blast only. One can observe that the strain at the top of the target is significantly greater than at the bottom, indicating that the blast is moving relative to the target.

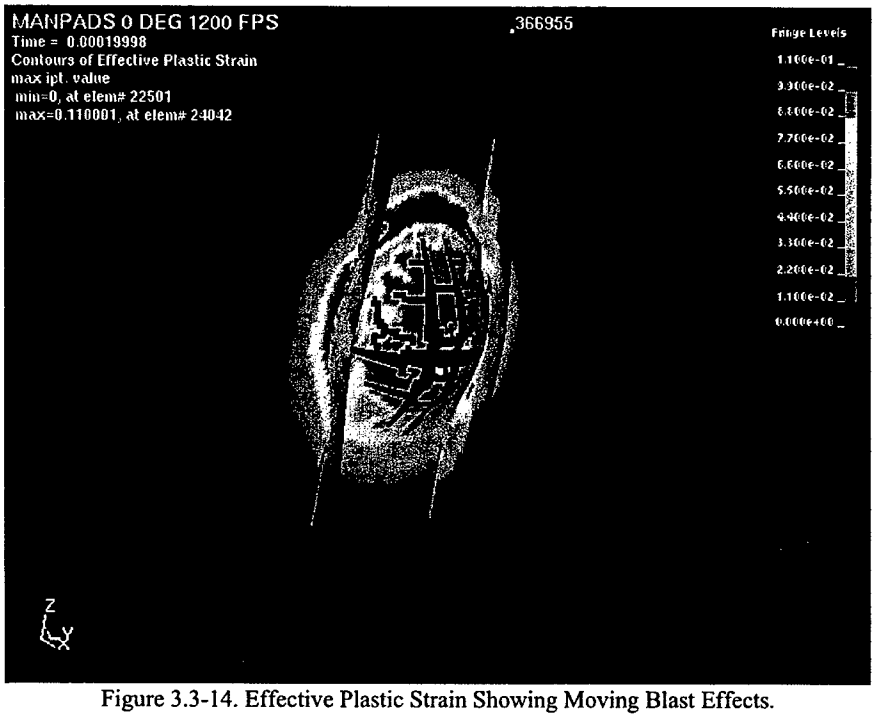

Figure 3.3-14. Effective Plastic Strain Showing Moving Blast Effects.

Another case of interest is presented here. This case was chosen, because the corresponding non-detonating case did not show any observable damage to the structure. The case of interest is the 75° incident angle impacting at mid-bay with detonation and fragmentation. Figure 3.3-15 shows the results of this case. Comparison of Figure 3.3-15 with Figure 3.3-5 reinforces the observation that close-in detonation of the warhead leads to much more significant damage than penetration alone.

The last problem presented here under this step is the impact and detonation of the missile at the center of a typical wing box structure where the threat hits the structure on a stiffener on the lower surface at approximately mid chord. Figures 3.3-16 and 3.3-17 show the results of this encounter at 0.0044 seconds after impact. At this time, the threat has impacted and detonated on the lower surface with the rocket body still traveling forward. One can observe that the rocket body is in the process of penetrating the upper surface. Figure 3.3-16 shows the damage observed from the lower side, while Figure 3.3-17 shows the damage observed from the upper side. Note that the damage on the lower side is

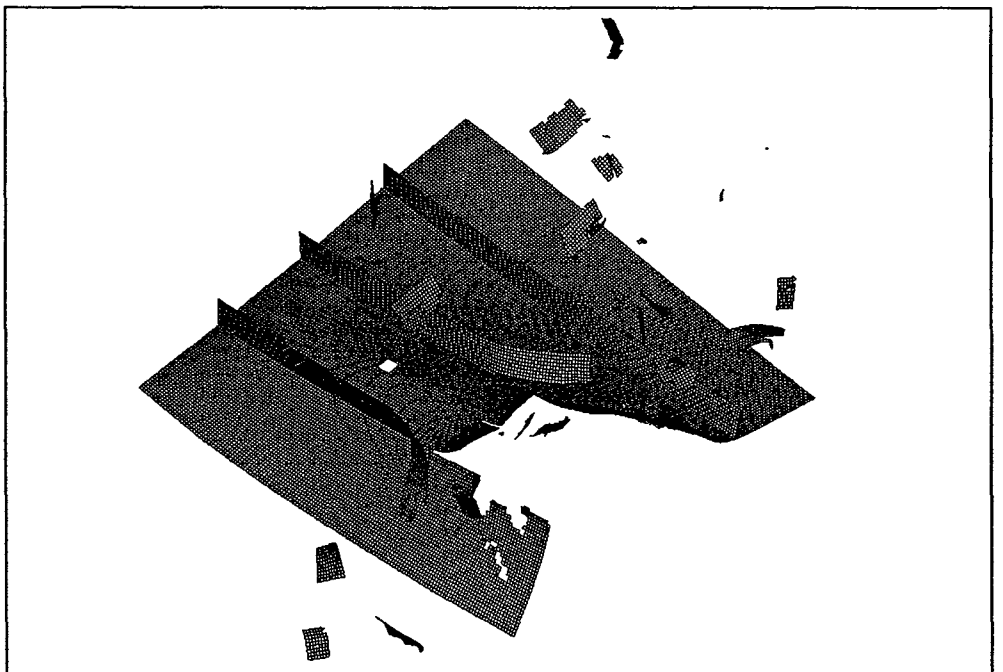

Figure 3.3-15. Damage From 75° Incident Angle Detonating At Mid-Bay.

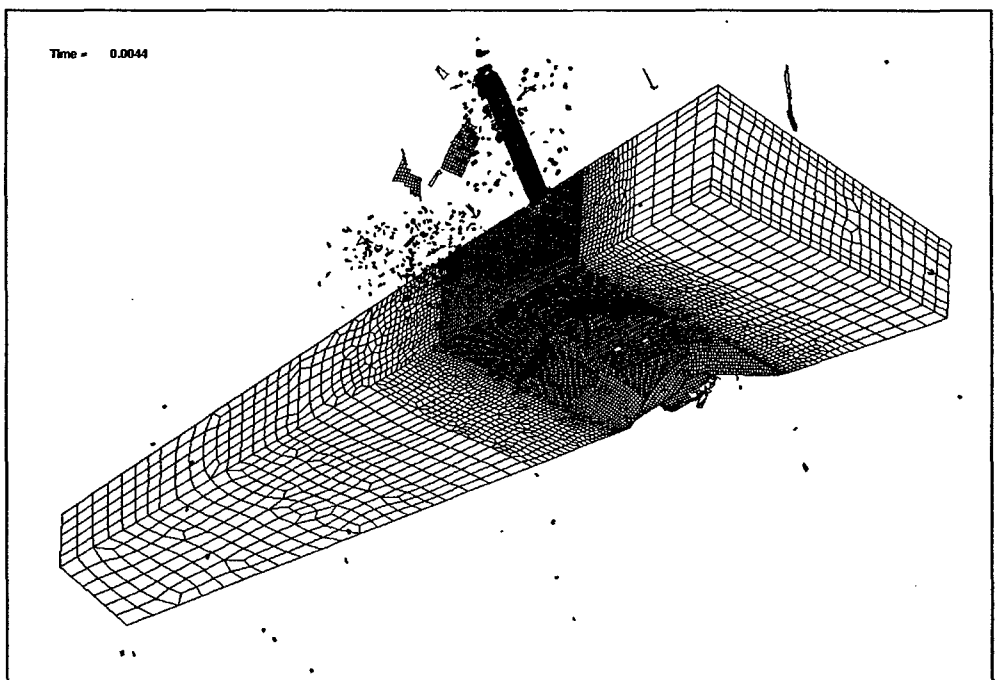

Figure 3.3-16. Damage From 60° Incident Angle Detonating on Wing Box (bottom).

extensive. The upper side damage is mainly the results of the kinetic energy imparted to the upper skin by some of the warhead fragments as well as the rocket body.

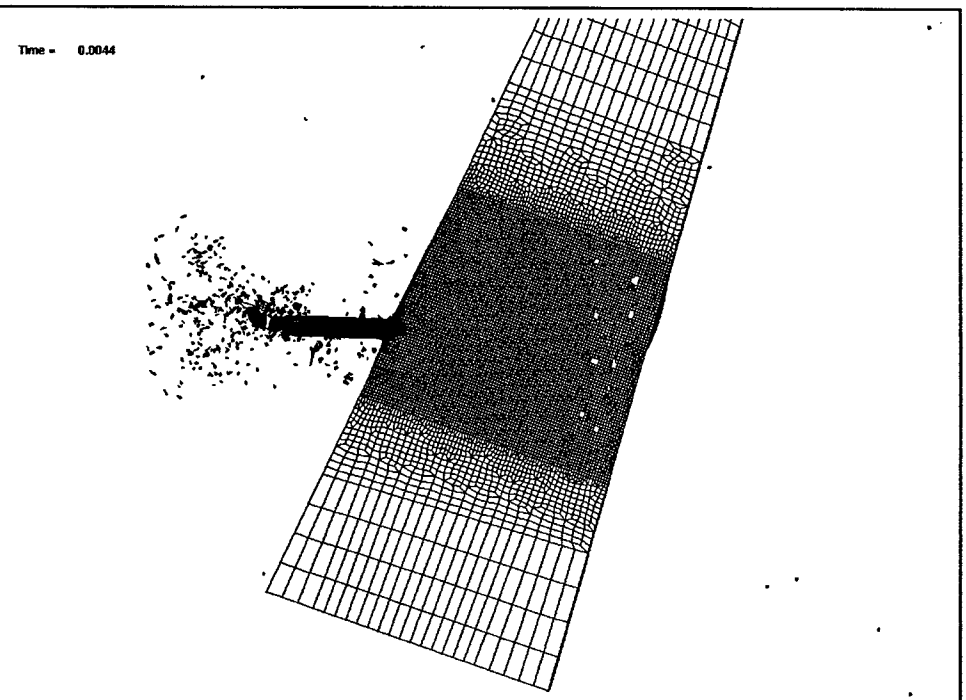

Figure 3.3-17. Damage From 60 ° Incident Angle Detonating on Wing Box (top).

Summary of Transport Aircraft Wingbox Study

This section presented the results of a study to investigate the extent of damage that could result from impact of a Man Portable Air Defense System (MANPADS) on a typical wing structure. The study was performed analytically using an explicit finite element code, LS-DYNA to do the simulations. The threat model was validated against experimental data and shows good agreement with the data.

The simulations show that if the threat impacts on a dry structure (no fuel) it will penetrate through both wing surfaces and produce hole sizes somewhat larger than the missile diameter. If the threat impacts on a wet structure (fuel tank) and does not detonate, the resulting hydrodynamic ram damage could be significant due to the high pressure generated in the fluid. If the threat impacts and detonates on a dry structure, the damage to the impact surface and much of the internal surface could be quite extensive. The case of detonation on a fuel-filled structure is being investigated and will be reported on in the future.

4 Conclusions

An enhanced MANPADS model has been created which now includes energetic materials and fragmentation effects including air drag. This model has been shown to effectively model blast and fragmentation damage. Fragment weight, distribution, initial velocity, and drag have been validated against static arena tests. Blast peak pressure vs. range as well as blast time of arrival vs. range have also been validated against static arena tests.

The authors have demonstrated the model's usefulness in simulating damage on selected targets that range from simple plate structures to complex composite wingbox structures. Wing flutter associated with typical wing structures has been demonstrated that includes the effects of damage progression.

Currently collaborative work with NASA is on-going to investigate probable damage associated with MANPADS impacts on commercial aircraft.

Other uses of the model will include pre- and post-test predictions against selected targets. Pre-test predictions will help aid in test design including sensor usage and assist in variation analyses. Post-test predictions will help the fidelity of other probability based codes currently in use.

5 Recommendations

While the latest model has been greatly improved over the previous body on body impact model, further refinements could greatly improve the event simulation. Also the lessons learned with the current MANPADS can be incorporated into other models of MANPADS as well as incorporate some of the findings into other probability based simulations. Some of those refinements will require additional static testing. Many of the assumptions made to create the current model were to reduce the simulation to a manageable size. As computers become faster and simulation codes become more stable additional features such as the air surrounding the target and flow boundary conditions can be included.

Also, as testing capabilities improve, more correlation to test data can be made. Currently, much of the data used to create the simulation was not created with the intent of incorporation into a full physics model. In the future, a set of tests could be defined that would be tailored to provide the type of data required to accurately model a MANPADS missile.

Finally, it is recommended that the dynamic test be redone. The lessons learned in the rail test at Eglin can be effectively used to ensure that the warhead detonates at the selected position. Furthermore, a redo of the test should be quite economical as the composite wingbox and much of the other associated structures and bundles are still intact and available for testing.

References

1. Ronald L. Hinrichsen, Monty A Moshier, Alex G. Kurtz, "MANPADS Penetration Methodology Development", AIAA 2002-1493, 43rd AIAA/ASME/ASCE/AHS/ASC Structures, Structural Dynamics, and Materials Conference, April 22-25, 2002, Denver, CO.

2. Ronald L. Hinrichsen, "Problems in Aircraft Survivability", ASC/MSRC Journal, Fall 2000, pp 25.

3. Alex G. Kurtz and Ronald L. Hinrichsen, "MANPADS Analysis Methodology Development", Aircraft Survivability, Fall 2001, pp 8-9.

4. Maskew, B., "Program VSAERO Theory Document," NASA CR-4023 (1987). Hallquist, J.O., "LS-DYNA Theoretical Manual," Livermore Software Technology Corporation (1998).

5. Felker, F., "Fluid-Structure Interaction Calculations Using the LS-Dyna Boundary Element Method," 5th International LS-DYNA Users Conference, Southfield,Michigan, 1998.

6. Negaard, G.R., "Finite Element Analysis of Ballistic Tests," USAF AFWAL-TR-88-3041.

Appendices

A1. List of Personnel Involved in Work

The following researchers at RHAMM Technologies, LLC were involved in this work:

Dr. Ronald L. Hinrichsen, Principle Investigator
Dr. Monty A. Moshier, Senior Scientist
Brian J. Barlow, Engineering Analyst
Mr. Steve Stratton, Engineering Analyst
Dr. Brian D. Choules, Senior Engineer

A2. Publications

R. L. Hinrichsen, A. G. Kurtz, MANPADS Analysis Methodology Development, 43rd AIAA/ASME/ASCE/AHS SDM Conference, 22 - 25 Apr 2002, Denver, Colorado.

R.L. Hinrichsen, M.A. Moshier, Using Coupled Fluid/structure Interaction Code to Predict Fighter Aircraft Wing Response to AAA Damage,COMPUTATIONAL FLUID AND SOLID MECHANICS, 2nd MIT Conference, 17-20 June 2003, Elsevier Ltd.

M. A. Moshier, R. L. Hinrichsen, G.J. Czarnecki, Dynamic Loading Methodologies, AIAA Journal, Vol. 41, Number 11, PP 2291-2294, Nov. 2003.

R.L. Hinrichsen, M.A. Moshier, A.G. Kurtz, High Velocity Impacts of Man Portable Air Defense Systems (MANPADS) on Selected Targets, 45th AIAA/ASME/ASCE/AHS SDM Conference, 19-23 Apr 2004,Palm Springs, CA.

Alex G. Kurtz, Gregory Czarnecki, Ronald L. Hinrichsen, Monty A. Moshier, Brian Barlow, MANPADS Modeling Update, Large Aircraft Survivability Initiative (LASI) IPT Meeting, Eglin AFB, FL, 2 February, 2005.

Alex G. Kurtz, Gregory Czarnecki, Ronald L. Hinrichsen, Brian Barlow, MANPADS Modeling Update Large Aircraft Survivability Initiative (LASI) IPT Meeting, Eglin AFB, FL, 18-20 March, 2006.

Alex G. Kurtz, Ronald L. Hinrichsen, MANPADS Analysis Methodology Development, Aircraft Survivability, Summer 2003.

Alex G. Kurtz, Ronald L. Hinrichsen, MANPADS Analysis Methodology Development, Aircraft Survivability, Fall 2006.

R. Hinrichsen, J. Wang, C. Belcastro, A. Kurtz, J. Parks, Modeling Projectile Damage in Transport Aircraft Wing Structures, 47th AIAA/ASME/ASCE/AHS/ASC Structures, Structural Dynamics, and Materials Conference, Newport, RI, May, 2006, AIAA-2006-2128.

Ronald L. Hinrichsen, Alex G. Kurtz, Brian Barlow, and Monty A. Moshier, High Velocity Impacts of Man Portable Air Defense Systems (MANPADS) on Selected Targets, 9th International LS-DYNA Users Conference, Detroit, MI, June, 2006.

A3. Acceleration Extraction Program

```
#include <stdlib.h>
#include <stdio.h>
#include <string.h>
#include <math.h>
#include "dynamicArrays.h"

void usage();
void ProcessCommandLineArgs(int *argc, char *argv[], char rdbout_filename[], char
d3hsp_filename[], double *offsetA, double *drag, char pMotion_filename[]);
int getKeyWordLine(char *s, FILE *Stream);
void smooth(int *listLength,  DynArray* tempArray);

#define    MAX_CHARS_PER_LINE 512


int main(int argc, char *argv[]) {

   /* File pointers */
   FILE *rbdoutFilePointer;
   FILE *d3hspFilePointer;
   FILE *pMotionFilePointer;

   /* Variables */
   int numberOfRigidBodies = 0;
   int itemCount = 0;
   int firstTimeStep = 1;
   int numberOfTimeSteps = 0;
   double offsetA = 0.0;
   double drag = 0.0;
   char d3hsp_filename[MAX_CHARS_PER_LINE];
   char rdbout_filename[MAX_CHARS_PER_LINE];
   char pMotion_filename[MAX_CHARS_PER_LINE];
   char currentLine[MAX_CHARS_PER_LINE];
   double* currentItem;
   double* current2Item;
   int i, j;
   int outputBodyCount = 1;
   double temp2Data[2];
   double tempDoubleArray[2];
   DynArray MassData;
   DynArray AccelerationData;
   double tempData[5];
   int listLength;
```

```
   DynArray tempArray;

   DynArrayCreate(&AccelerationData, 5*sizeof(double));
   DynArrayCreate(&MassData, 2*sizeof(double));

   /* Process Command Line arguements */
   printf("Processing Command Line Args \n");
   ProcessCommandLineArgs(&argc, argv, rdbout_filename, d3hsp_filename, &offsetA,
&drag, pMotion_filename);

   /* Open the rdbout file and d3hsp for reading and the perscribed motion file for
writing */

   d3hspFilePointer = fopen(d3hsp_filename, "r");
   if (d3hspFilePointer == NULL) {
      printf("Cannot open %s for input\n",d3hsp_filename);
      return (1);
   }

   /* ********************************************************/
   /* Read d3hsp File until the line with the m a s s is reached */
   printf("Read the d3hsp file \n");
   while (0 == getKeyWordLine(currentLine, d3hspFilePointer)) {
   /*printf(" got here \n");*/
      if(strncmp(currentLine, "  m a s s", 9) == 0) {
         /* Read the rigid body number */
            sscanf(&currentLine[60], "%le", &temp2Data[0]);
        /* printf("%e \n", temp2Data[0]);*/
         } else if(strncmp(currentLine, "     mass of rigid", 18) == 0) {
          /* Read the mass */
          sscanf(&currentLine[35], "%le", &temp2Data[1]);
       /*   printf("%e \n", temp2Data[1]); */
          /* Write the current "objectNum, Mass" to the dynamic array */
            /*printf("test \n");*/
          DynArrayInsert(&MassData,itemCount, temp2Data);
            itemCount = itemCount + 1;
      }

   }


   /* Close the d3hsp file */
   fclose(d3hspFilePointer);


   numberOfRigidBodies=itemCount ;
```

```
   itemCount = 0;

 /* Open the rdbout file for reading and the perscribed motion file for writing */
   printf("Opening Files for reading and writing \n");
   rbdoutFilePointer = fopen(rdbout_filename, "r");
   if (rbdoutFilePointer == NULL) {
      printf("Cannot open %s for input\n",rdbout_filename);
      return (1);
   }

   /* Read rdbout File until the line with the time is reached */
   printf("Read the rbdout file \n");
   while (0 == getKeyWordLine(currentLine, rbdoutFilePointer)) {
      if(strncmp(currentLine, "  r i g i d", 11) == 0) {
         /* Read the time */
            sscanf(&currentLine[67], "%le", &tempData[0]);
      } else if(strncmp(currentLine, " rigid body", 11) == 0) {
         /* Read the rigid body number */
         sscanf(&currentLine[12], "%le", &tempData[1]);

         /* Read lines until the line with the Acceleration is reached */
         while (0 == getKeyWordLine(currentLine, rbdoutFilePointer)) {
            if(strncmp(currentLine, " accelerations", 14) == 0) {
               /* Read the Acceleration in */
                     sscanf(&currentLine[16], "%le%le%le", &tempData[2],
&tempData[3], &tempData[4]);
                     break;
            }
            }

         /* Write the current "time, objectNum, Acelx, Acely, Acelz" to the dynamic
array */
            /*printf("%e %e %e %e %e \n", tempData[0], tempData[1], tempData[2],
tempData[3], tempData[4]);*/
         DynArrayInsert(&AccelerationData, itemCount, tempData);
            itemCount = itemCount + 1;
      }

   }
   printf("itemCount: %d \n number of rigidBodies %d \n", itemCount,
numberOfRigidBodies);
   /* Calculate the number of timeSteps read in */
   numberOfTimeSteps = itemCount/numberOfRigidBodies;
   /*printf("Item Count: %d \n", itemCount);*/
   printf("number of TimeSteps: %d \n number of rigidBodies %d \n",
numberOfTimeSteps, numberOfRigidBodies);
```

```
   /* Close the rdbout file */
   fclose(rbdoutFilePointer);



   pMotionFilePointer = fopen(pMotion_filename, "w");
   if (pMotionFilePointer == NULL) {
      printf("Cannot open %s for output of the pbs script file\n",pMotion_filename);
   return (1);
   }



   /* Write out the perscribed motion file */
   printf("write out the perscribed motion file \n");
   fprintf(pMotionFilePointer,"*DEFINE_VECTOR_TITLE \n" );
   fprintf(pMotionFilePointer,"prescribed object vector \n" );
   fprintf(pMotionFilePointer,"$#    vid       xt       yt       zt       xh       yh       zh \n" );
   fprintf(pMotionFilePointer,"         1  1.000000      0.0      0.0      0.0      0.0      0.0
\n" );

   fprintf(pMotionFilePointer,"*DEFINE_CURVE \n" );
   fprintf(pMotionFilePointer,"$#   lcid      sidr       sfa       sfo      offa      offo    dattyp
\n" );
   fprintf(pMotionFilePointer,"   9999999         0   1.00000  1.000000       0.0\n");

   fprintf(pMotionFilePointer,"     0.000     0.000      \n");
   fprintf(pMotionFilePointer," %3.3e     0.000 \n", (offsetA + .000398));
   fprintf(pMotionFilePointer," %3.3e     1.000 \n", (offsetA + .000399));
   fprintf(pMotionFilePointer," 1.0000000     1.000 \n");



   while (outputBodyCount < (numberOfRigidBodies + 1)) {
      currentItem = (double*) DynArrayLookup(&AccelerationData, (outputBodyCount
- 1));
      fprintf(pMotionFilePointer,"*LOAD_RIGID_BODY \n" );
      fprintf(pMotionFilePointer,"$#     pid      dof     lcid    scalef \n" );
      fprintf(pMotionFilePointer,"  %8d         1  %8d  1.000000 10\n",
(int)currentItem[1], (((outputBodyCount-1)*3)+1) );

      fprintf(pMotionFilePointer,"*LOAD_RIGID_BODY \n" );
      fprintf(pMotionFilePointer,"$#     pid      dof     lcid    scalef \n" );
```

```
        fprintf(pMotionFilePointer," %8d       2 %8d 1.000000 10\n",
(int)currentItem[1], (((outputBodyCount-1)*3)+2) );

        fprintf(pMotionFilePointer,"*LOAD_RIGID_BODY \n" );
        fprintf(pMotionFilePointer,"$#    pid     dof     lcid   scalef \n" );
        fprintf(pMotionFilePointer," %8d       3 %8d 1.000000 10\n",
(int)currentItem[1], (((outputBodyCount-1)*3)+3) );

        fprintf(pMotionFilePointer,"*DAMPING_PART_MASS \n" );
        fprintf(pMotionFilePointer,"$#    pid     lcid       sf \n" );
        fprintf(pMotionFilePointer," %8d  9999999 %3.3e", (int)currentItem[1], drag );

        current2Item = (double*) DynArrayLookup(&MassData, (outputBodyCount - 1));
        fprintf(pMotionFilePointer,"      %12.6e      %12.6e \n", currentItem[0],
currentItem[1] );
          /*printf("my stuff %d \n", (((outputBodyCount-1)*3)+3) );*/
       /* Write out Acceleration curves */
          for (i = 0; i < 3; ++i) {
           fprintf(pMotionFilePointer,"*DEFINE_CURVE \n" );
           fprintf(pMotionFilePointer,"$#   lcid     sidr      sfa      sfo      offa      offo
dattyp \n" );
           fprintf(pMotionFilePointer," %8d       0 1.000000  1.000000 %3.3e \n",
(((outputBodyCount-1)*3)+1+i), offsetA);
           fprintf(pMotionFilePointer,"$#              a1              o1 \n" );
           DynArrayCreate(&tempArray, 2*sizeof(double));
           for (j = 0; j < numberOfTimeSteps; ++j){
              currentItem = (double*) DynArrayLookup(&AccelerationData,
((outputBodyCount - 1) + (j*numberOfRigidBodies)));
              tempDoubleArray[0] = currentItem[0];
              tempDoubleArray[1] = (currentItem[2+i]*current2Item[1]);
              DynArrayInsert(&tempArray, j, tempDoubleArray);
      /* printf("works to here\n");*/
           }
           listLength = numberOfTimeSteps;
        /*Loops through the numner of items in the original array */
          smooth(&listLength, &tempArray);
           for (j = 0; j < listLength; ++j) {
                    currentItem = (double*) DynArrayLookup(&tempArray, j);
              fprintf(pMotionFilePointer,"      %12.6e      %12.6e \n", currentItem[0],
currentItem[1] );
             /* printf("   %12.6e    %12.6e %12.6e %12.6e \n", currentItem[0],
currentItem[2+i], current2Item[1], current2Item[0]);*/
           }
           DynArrayDelete(&tempArray);
          }
       outputBodyCount = outputBodyCount + 1;
```

```
    }
    /* Close the perscribed motion file */
    fclose(pMotionFilePointer);


    /* clean up the dynamic array */
    DynArrayDelete(&AccelerationData);

    /* clean up the dynamcic mass array */
    DynArrayDelete(&MassData);
    printf("Done! \n");
    return 0;
    }

void usage() {
    fprintf(stderr,"\n\n Usage is: pMotion.exe rdbout_filename d3hsp_filename offsetA
drag output_filename\n");
    exit(8);
    }

void ProcessCommandLineArgs(int *argc, char *argv[], char
rdbout_filename[MAX_CHARS_PER_LINE], char
d3hsp_filename[MAX_CHARS_PER_LINE], double *offsetA, double *drag, char
pMotion_filename[MAX_CHARS_PER_LINE]) {
    char * pEnd;
    switch ( argv[1][0]) {
        case 'h':
            /* check for help request */
            usage();
            break;
        default:
                strcpy(rdbout_filename, &argv[1][0]);
                strcpy(d3hsp_filename, &argv[2][0]);
                *offsetA =  strtod(strcpy(pEnd,&argv[3][0]),&pEnd);
            *drag = strtod(strcpy(pEnd,&argv[4][0]),&pEnd);
                strcpy(pMotion_filename, &argv[5][0]);
            break;
        }
    }

int getKeyWordLine(char *s, FILE *Stream) {
    int i;
    int keepLine = 0;
    char testChar;
    char currentLine[MAX_CHARS_PER_LINE];
```

```
/* This function essentially reads lines from the keyword file until it reads a line */
/* That is not a comment and is not blank.  The non-comment line is then returned */
while(NULL != fgets(currentLine, sizeof(currentLine), Stream))
   {

   for(i = 0; i < MAX_CHARS_PER_LINE; i = i + 1)
      {
      testChar = currentLine[i];

      if((testChar == '\0') || ( testChar == '$' ))
         {
         break;
         }
      else if(( isalnum((unsigned char)testChar) ) || ( testChar == '*' ) )
         {
         keepLine = 1;
         break;
         }
      }

   if(keepLine)
      {
      strcpy(s, currentLine);
      return(0);
      }

   }

return(1);
```

A4. LS-DYNA Wing Flutter Input File

```
*KEYWORD  30000000
$---+---1----+---2----+---3----+---4----+---5----+---6----+---7----+---
8
*TITLE
Simple 2 Spar Wing 625 Ft/s (190 m/s)
*CONTROL_CONTACT
$---+---1----+---2----+---3----+---4----+---5----+---6----+---7----+---
8
$   slsfac    rwpnal    islchk    shlthk    penopt    thkchg     orien
enmass
  1.000000     0.000         2         0         1         1         1
$#  usrstr    usrfrc     nsbcs    interm     xpene     ssthk      ecdt
tiedprj
         0        10         0         0     0.000
$#   sfric     dfric       edc       vfc        th     th_sf    pen_sf
     0.000     0.000     0.000     0.000     0.000     0.000     0.000
$#  ignore    frceng   skiprwg    outseg   spotstp   spotdel
         1
*CONTROL_ENERGY
$     hgen      rwen    slnten     rylen
         2         2         1         1
*CONTROL_OUTPUT
$    npopt    neecho    nrefup    iaccop     opifs    ipnint    ikedit
iflush
         1         3         0         0     0.000         0       100
5000
$    iprtf
         0
*CONTROL_PARALLEL
$#    ncpu    numrhs     const      para
         4         0         2
*CONTROL_SHELL
$   wrpang    itrist     irnxx    istupd    theory       bwc     miter
proj
 20.000000         1        -1         0         2         2         1
$# rotascl    intgrd    lamsht    cstyp6    tshell    nfail1    nfail4
  1.000000         0         0         1
*CONTROL_TERMINATION
$#  endtim    endcyc     dtmin    endeng    endmas
  0.209000         0     0.000     0.000     0.000
*CONTROL_TIMESTEP
$#  dtinit    tssfac      isdo    tslimt     dt2ms      lctm     erode
mslst
 1.0000E-7  0.900000         0     0.000     0.000         0         1
$       dt
$#  dt2msf   dt2mslc
     0.000
*DATABASE_GLSTAT
$       dt
$#      dt    binary
 1.0000E-4
*DATABASE_MATSUM
```

```
$       dt
$#      dt    binary
 1.0000E-7
*DATABASE_RCFORC
$       dt
$#      dt    binary
 1.0000E-4
*DATABASE_SLEOUT
$       dt
$#      dt    binary
 1.0000E-4
*DATABASE_BINARY_D3PLOT
$  dt/cycl      lcdt      beam     npltc
$#      dt      lcdt      beam     npltc
  0.001000
*DATABASE_EXTENT_BINARY
$    neiph     neips    maxint    strflg    sigflg    epsflg    rltflg
engflg
         0         0         0         0         0         0         0
0
$   cmpflg    ieverp    beamip     dcomp      shge     stssz    n3thdt
         0         0         0         0         0         0         0
0
*BOUNDARY_ELEMENT_METHOD_CONTROL
$---+---1----+---2----+---3----+---4----+---5----+---6----+---7----+---
8
$#   lwake     dtbem    iupbem    farbem
        40 5.0000E-4     10000 10.000000
*BOUNDARY_ELEMENT_METHOD_FLOW
$#    ssid        vx        vy        vz        ro   pstatic      mach
         1 7500.0000 435.00000     0.000 1.1230E-7     0.000  0.570000
*BOUNDARY_ELEMENT_METHOD_WAKE
$#   nelem     nside
       120         2
       130         2
       139         2
       149         2
       159         2
       169         2
       179         2
       189         2
       199         2
       209         2
       219         2
*BOUNDARY_SPC_SET
$#    nsid       cid      dofx      dofy      dofz     dofrx     dofry
dofrz
         1         0         1         1         1         1         1
1
*SET_NODE_LIST
$#     sid       da1       da2       da3       da4
         1     0.000     0.000     0.000     0.000
$#    nid1      nid2      nid3      nid4      nid5      nid6      nid7
nid8
       101       102       103       104       105       106       107
120
```

```
       109       110       111       112       113       114       115
116
       117       118       119
*BOUNDARY_SPC_NODE
$#     nid       cid      dofx      dofy      dofz     dofrx     dofry
dofrz
       108         0         1         1         1         1         1
1
*CONTACT_AUTOMATIC_SURFACE_TO_SURFACE_ID
$---+---1----+---2----+---3----+---4----+---5----+---6----+---7----+---
8
$#     cid
title
         2
$#    ssid      msid     sstyp     mstyp    sboxid    mboxid       spr
mpr
        16        17         2         2
$#      fs        fd        dc        vc       vdc    penchk        bt
dt
     0.000     0.000     0.000     0.000     0.000         0  0.200000
1.000000
$#     sfs       sfm       sst       mst      sfst      sfmt       fsf
vsf
  1.000000  1.000000     0.000     0.000  1.000000  1.000000  1.000000
1.000000
*SET_PART_LIST
$#     sid       da1       da2       da3       da4
        16     0.000     0.000     0.000     0.000
$#    pid1      pid2      pid3      pid4      pid5      pid6      pid7
pid8
     11007     11008     11009     11010     11011     11013     11014
11015
     11016     11017     11018     11019     11021     11022     11023
11024
     11025     11026     11032     11080     11081
*PART
$# title
null shell lower surface
$#     pid     secid       mid     eosid      hgid      grav    adpopt
tmid
         1         1         1
*SECTION_SHELL
$---+---1----+---2----+---3----+---4----+---5----+---6----+---7----+---
8
$CardName:S0000001
$    secid    elform      shrf       nip     propt   qr/irid     icomp
setyp
$#   secid    elform      shrf       nip     propt   qr/irid     icomp
setyp
         1         2  0.833330         3         1     0.000         0
1
$#      t1        t2        t3        t4      nloc     marea
  0.050000  0.050000  0.050000  0.050000         0     0.000
*MAT_NULL
$---+---1----+---2----+---3----+---4----+---5----+---6----+---7----+---
8
$CardName:M0000001
```

```
$      mid        ro        pc        mu     terod     cerod        ym
pr
$#     mid        ro        pc        mu     terod     cerod        ym
pr
         1 2.5900E-4     0.000     0.000     0.000     0.000 1.0000E
0.300000
*PART
$# title
null shell upper surface
$#     pid     secid       mid     eosid      hgid      grav    adpopt
tmid
         2         1         1
*PART
$# title
aluminum shell lower surface
$#     pid     secid       mid     eosid      hgid      grav    adpopt
tmid
         3         2         3
*SECTION_SHELL
$---+---1----+---2----+---3----+---4----+---5----+---6----+---7----+---
8
$CardName:S0000001
$    secid    elform      shrf       nip     propt   qr/irid     icomp
setyp
$#   secid    elform      shrf       nip     propt   qr/irid     icomp
setyp
         2        16  0.833330         3         1     0.000         0
1
$#      t1        t2        t3        t4      nloc     marea
  0.070000  0.070000  0.070000  0.070000         0     0.000
*MAT_PIECEWISE_LINEAR_PLASTICITY
$---+---1----+---2----+---3----+---4----+---5----+---6----+---7----+---
8
$CardName:AL 7075
$      mid        ro         e        pr      sigy      etan      fail
tdel
         3 2.6140E-4 1.0300E  0.330000 70000.000 50000.000  0.090000
8.0000E-8
$        c         p      lcss      lcsr        vp
     0.000     0.000         0         0     0.000
$     eps1      eps2      eps3      eps4      eps5      eps6      eps7
eps8
     0.000     0.000     0.000     0.000     0.000     0.000     0.000
0.000
$      es1       es2       es3       es4       es5       es6       es7
es8
     0.000     0.000     0.000     0.000     0.000     0.000     0.000
0.000
*PART
$# title
aluminum shell upper surface
$#     pid     secid       mid     eosid      hgid      grav    adpopt
tmid
         4         2         3
*PART
$# title
aluminum shell ribs
```

```
$#     pid     secid       mid     eosid      hgid      grav    adpopt
tmid
         5         3         3
*SECTION_SHELL
$---+---1----+---2----+---3----+---4----+---5----+---6----+---7----+---
8
$CardName:S0000001
$    secid    elform      shrf       nip     propt   qr/irid     icomp
setyp
$#   secid    elform      shrf       nip     propt   qr/irid     icomp
setyp
         3        16  0.833330         3         1     0.000         0
1
$#      t1        t2        t3        t4      nloc     marea
  0.085000  0.085000  0.085000  0.085000         0     0.000
*PART
$# title
aluminum shell shear webs
$#     pid     secid       mid     eosid      hgid      grav    adpopt
tmid
         6         3         3
*PART
$# title
FIN_BEAM
$#     pid     secid       mid     eosid      hgid      grav    adpopt
tmid
     11007     11004     11006
*SECTION_BEAM
$CardName:S0011001
$    secid    elform      shrf   qr/irid       cst     scoor
$#   secid    elform      shrf   qr/irid       cst     scoor       nsm
     11004         1  1.000000         2         0     0.000     0.000
$      ts1       ts2       tt1       tt2     nsloc     ntloc
$#     ts1       ts2       tt1       tt2     nsloc     ntloc
 8.4400E-4 1.2000E-5 1.2000E-5  0.031250
*MAT_PIECEWISE_LINEAR_PLASTICITY
$CardName:M0011004
$      mid        ro         e        pr      sigy      etan      fail
tdel
     11006 7.4000E-4 2.7000E  0.330000 1.6970E 1.1840E  0.187000
8.0000E-8
$        c         p      lcss      lcsr        vp
     0.000     0.000         0         0     0.000
$     eps1      eps2      eps3      eps4      eps5      eps6      eps7
eps8
     0.000  0.187000     0.000     0.000     0.000     0.000     0.000
0.000
$      es1       es2       es3       es4       es5       es6       es7
es8
 1.6970E 1.9184E     0.000     0.000     0.000     0.000     0.000
0.000
*PART
$# title
G_C
$#     pid     secid       mid     eosid      hgid      grav    adpopt
tmid
     11008     11005     11004
```

```
*SECTION_SHELL
$CardName:S0011002
$    secid    elform      shrf       nip     propt   qr/irid     icomp
setyp
     11005         1  1.000000         2         0     0.000         0
1
$       t1        t2        t3        t4      nloc
$#      t1        t2        t3        t4      nloc     marea
  0.062000  0.062000  0.062000  0.062000         0     0.000
*MAT_PIECEWISE_LINEAR_PLASTICITY
$CardName:M0011002
$      mid        ro         e        pr      sigy      etan      fail
tdel
$#     mid        ro         e        pr      sigy      etan      fail
tdel
     11004 2.5400E-4 9.7440E  0.330000 68000.000 50000.000  0.110000
8.0000E-8
$        c         p      lcss      lcsr        vp
     0.000     0.000         0         0     0.000
$     eps1      eps2      eps3      eps4      eps5      eps6      eps7
eps8
     0.000  0.110000     0.000     0.000     0.000     0.000     0.000
0.000
$      es1       es2       es3       es4       es5       es6       es7
es8
 68000.000 73500.000     0.000     0.000     0.000     0.000     0.000
0.000
*PART
$# title
G_C_GAS_GENERATOR
$#     pid     secid       mid     eosid      hgid      grav    adpopt
tmid
     11009     11006     11006
*SECTION_SHELL
$CardName:S0011003
$    secid    elform      shrf       nip     propt   qr/irid     icomp
setyp
     11006         1  1.000000         2         0     0.000         0
1
$       t1        t2        t3        t4      nloc
  0.100000  0.100000  0.100000  0.100000         0     0.000
*PART
$# title
G_C_PHENOLIC
$#     pid     secid       mid     eosid      hgid      grav    adpopt
tmid
     11010     11007     11003
*SECTION_SOLID
$CardName:S0011004
$    secid    elform       aet
$#   secid    elform       aet
     11007         1
*MAT_ISOTROPIC_ELASTIC_FAILURE
$#     mid        ro         g      sigy      etan      bulk
     11003 9.3500E-5 1.0000E 10000.000 8000.0000 83300.000
$#     epf       prf       rem      trem
  0.005000     0.000     0.000     0.000
```

```
*PART
$# title
HMX
$#     pid     secid       mid     eosid      hgid      grav    adpopt
tmid
     11011     11008     11003
*SECTION_SOLID
$CardName:S0011005
$#   secid    elform       aet
     11008         1
*PART
$# title
TDD_1
$#     pid     secid       mid     eosid      hgid      grav    adpopt
tmid
     11013     11010     11006
*SECTION_SOLID
$CardName:S0011007
$#   secid    elform       aet
     11010         1
*PART
$# title
ALUMINUM_LINER
$#     pid     secid       mid     eosid      hgid      grav    adpopt
tmid
     11014     11011     11004
*SECTION_SOLID
$CardName:S0011008
$#   secid    elform       aet
     11011         1
*PART
$# title
BOOSTER
$#     pid     secid       mid     eosid      hgid      grav    adpopt
tmid
     11015     11012     11003
*SECTION_SOLID
$CardName:S0011009
$#   secid    elform       aet
     11012         1
*PART
$# title
FIN
$#     pid     secid       mid     eosid      hgid      grav    adpopt
tmid
     11016     11013     11006
*SECTION_SHELL
$CardName:S0011010
$    secid    elform      shrf       nip     propt   qr/irid     icomp
setyp
$#   secid    elform      shrf       nip     propt   qr/irid     icomp
setyp
     11013         1  1.000000         2         0     0.000         0
1
$       t1        t2        t3        t4      nloc
$#      t1        t2        t3        t4      nloc     marea
  0.100000  0.100000  0.100000  0.100000         0     0.000
```

```
*PART
$# title
FUZE_HOUSING
$#     pid      secid        mid      eosid       hgid       grav    adpopt
tmid
     11017      11014      11004
*SECTION_SOLID
$CardName:S0011011
$    secid     elform        aet
$#   secid     elform        aet
     11014          1
*PART
$# title
FUZE_SHELLS
$#     pid      secid        mid      eosid       hgid       grav    adpopt
tmid
     11018      11015      11004
*SECTION_SHELL
$CardName:S0011012
$    secid     elform      shrf       nip      propt   qr/irid     icomp
setyp
$#   secid     elform      shrf       nip      propt   qr/irid     icomp
setyp
     11015          1  1.000000         2          0     0.000         0
1
$       t1         t2         t3         t4      nloc
$#      t1         t2         t3         t4      nloc     marea
  0.015000   0.015000   0.015000   0.015000         0     0.000
*PART
$# title
FUZE_SHELLS_THICK
$#     pid      secid        mid      eosid       hgid       grav    adpopt
tmid
     11019      11016      11004
*SECTION_SHELL
$CardName:S0011013
$    secid     elform      shrf       nip      propt   qr/irid     icomp
setyp
     11016          1  1.000000         2          0     0.000         0
1
$       t1         t2         t3         t4      nloc
  0.020000   0.020000   0.020000   0.020000         0     0.000
*PART
$# title
GLASS
$#     pid      secid        mid      eosid       hgid       grav    adpopt
tmid
     11021      11018      11005
*SECTION_SHELL
$CardName:S0011015
$    secid     elform      shrf       nip      propt   qr/irid     icomp
setyp
     11018          1  1.000000         2          0     0.000         0
1
$       t1         t2         t3         t4      nloc
  0.020000   0.020000   0.020000   0.020000         0     0.000
*MAT_PIECEWISE_LINEAR_PLASTICITY
```

```
$CardName:M0011003
$      mid        ro         e        pr      sigy      etan      fail
tdel
     11005 2.1500E-4 1.0000E  0.220000 24660.000 1.0000E  0.002500
8.0000E-8
$        c         p      lcss      lcsr        vp
     0.000     0.000         0         0     0.000
$     eps1      eps2      eps3      eps4      eps5      eps6      eps7
eps8
     0.000  0.025000     0.000     0.000     0.000     0.000     0.000
0.000
$      es1       es2       es3       es4       es5       es6       es7
es8
 24660.000 50000.000     0.000     0.000     0.000     0.000     0.000
0.000
*PART
$# title
ROCKET_MOTOR
$#     pid     secid       mid     eosid      hgid      grav    adpopt
tmid
     11022     11019     11006
*SECTION_SHELL
$CardName:S0011016
$    secid    elform      shrf       nip     propt   qr/irid     icomp
setyp
$#   secid    elform      shrf       nip     propt   qr/irid     icomp
setyp
     11019         1  1.000000         2         0     0.000         0
1
$       t1        t2        t3        t4      nloc
$#      t1        t2        t3        t4      nloc     marea
  0.080000  0.080000  0.080000  0.080000         0     0.000
*PART
$# title
ROCKET_MOTOR_SOLID
$#     pid     secid       mid     eosid      hgid      grav    adpopt
tmid
     11023     11020     11006
*SECTION_SOLID
$CardName:S0011017
$    secid    elform       aet
$#   secid    elform       aet
     11020         1
*PART
$# title
SEEKER_BOARDS
$#     pid     secid       mid     eosid      hgid      grav    adpopt
tmid
     11024     11021     11004
*SECTION_SHELL
$CardName:S0011018
$    secid    elform      shrf       nip     propt   qr/irid     icomp
setyp
     11021         1  1.000000         2         0     0.000         0
1
$       t1        t2        t3        t4      nloc
  0.050000  0.050000  0.050000  0.050000         0     0.000
```

```
*PART
$# title
SEEKER_BODY
$#     pid     secid       mid     eosid      hgid      grav    adpopt
tmid
     11025     11022     11004
*SECTION_SHELL
$CardName:S0011019
$    secid    elform      shrf       nip     propt   qr/irid     icomp
setyp
$#   secid    elform      shrf       nip     propt   qr/irid     icomp
setyp
     11022         1  1.000000         2         0     0.000         0
1
$       t1        t2        t3        t4      nloc
$#      t1        t2        t3        t4      nloc     marea
  0.040000  0.040000  0.040000  0.040000         0     0.000
*PART
$# title
SEEKER_HEAD
$#     pid     secid       mid     eosid      hgid      grav    adpopt
tmid
     11026     11023     11004
*SECTION_SHELL
$CardName:S0011020
$    secid    elform      shrf       nip     propt   qr/irid     icomp
setyp
     11023         1  1.000000         2         0     0.000         0
1
$       t1        t2        t3        t4      nloc
  0.040000  0.040000  0.040000  0.040000         0     0.000
*PART
$# title
WARHEAD_WALLS
$#     pid     secid       mid     eosid      hgid      grav    adpopt
tmid
     11032     11029     11006
*SECTION_SOLID
$CardName:S0011026
$    secid    elform       aet
$#   secid    elform       aet
     11029         3
*PART
$# title
nozzle
$#     pid     secid       mid     eosid      hgid      grav    adpopt
tmid
     11080     11077     11006
*SECTION_SHELL
$CardName:S0011074
$    secid    elform      shrf       nip     propt   qr/irid     icomp
setyp
     11077         1  1.000000         2         0     0.000         0
1
$       t1        t2        t3        t4      nloc
  0.250000  0.250000  0.250000  0.250000         0     0.000
*PART
```

```
$# title
rear_fin
$#     pid     secid       mid     eosid      hgid      grav    adpopt
tmid
     11081     11078     11004
*SECTION_SHELL
$CardName:S0011075
$    secid    elform      shrf       nip     propt   qr/irid     icomp
setyp
     11078         1  1.000000         2         0     0.000         0
1
$       t1        t2        t3        t4      nloc
  0.150000  0.150000  0.150000  0.150000         0     0.000
*INITIAL_VELOCITY_GENERATION
$---+---1----+---2----+---3----+---4----+---5----+---6----+---7----+---
8
$       id      styp     omega        vx        vy        vz
$#nsid/pid      styp     omega        vx        vy        vz
        16         1     0.000     0.000 14400.000     0.000
$#      xc        yc        zc        nx        ny        nz     phase
     0.000     0.000     0.000     0.000     0.000     0.000
*DEFINE_CURVE
$#    lcid      sidr       sfa       sfo      offa      offo    dattyp
     11032         0  1.000000  1.000000     0.000     0.000
$#                a1                  o1
              0.000        300.00000000
         10.00000000        300.00000000
*SET_PART_LIST_TITLE
Wing
$#     sid       da1       da2       da3       da4
        17     0.000     0.000     0.000     0.000
$#    pid1      pid2      pid3      pid4      pid5      pid6      pid7
pid8
         3         4         5         6
*SET_SHELL_LIST_GENERATE
$---+---1----+---2----+---3----+---4----+---5----+---6----+---7----+---
8
$      sid       da1       da2       da3       da4
$#     sid       da1       da2       da3       da4
         1     0.000     0.000     0.000     0.000
$#   b1beg     b1end     b2beg     b2end     b3beg     b3end     b4beg
b4end
         1       220
*DAMPING_PART_MASS
$#     pid      lcid        sf      flag
     11015     11032  1.000000         1
$#     stx       sty       stz       srx       sry       srz
  1.000000  0.100000  1.000000  1.000000  1.000000  1.000000
*DAMPING_PART_MASS
$#     pid      lcid        sf      flag
     11017     11032  1.000000         1
$#     stx       sty       stz       srx       sry       srz
  1.000000  0.100000  1.000000  1.000000  1.000000  1.000000
*DAMPING_PART_MASS
$#     pid      lcid        sf      flag
     11018     11032  1.000000         1
$#     stx       sty       stz       srx       sry       srz
```

```
  1.000000  0.100000  1.000000  1.000000  1.000000  1.000000
*DAMPING_PART_MASS
$#     pid      lcid        sf      flag
     11019     11032  1.000000         1
$#     stx       sty       stz       srx       sry       srz
  1.000000  0.100000  1.000000  1.000000  1.000000  1.000000
*DAMPING_PART_MASS
$#     pid      lcid        sf      flag
     11032     11032  1.000000         1
$#     stx       sty       stz       srx       sry       srz
  1.000000  0.100000  1.000000  1.000000  1.000000  1.000000
*ELEMENT_SOLID
$---+---1----+---2----+---3----+---4----+---5----+---6----+---7----+---
8
$    eid     pid      n1      n2      n3      n4      n5      n6
n7      n8
...
*ELEMENT_SHELL
$#   eid     pid      n1      n2      n3      n4
...
*ELEMENT_BEAM
$---+---1----+---2----+---3----+---4----+---5----+---6----+---7----+---
8
$    eid     pid      n1      n2      n3     rt1     rr1     rt2
rr2   local
..
*NODE
$#   nid               x               y               z      tc
rc
...excluded for brevity
$
$Unrecognized cards
$
*STRESS_INITIALIZATION
         1         0
         2         0
         3         0
         4         0
         5         0
         6         0
*END
```

A5. Transport Aircraft Outer Wingbox

```
*KEYWORD 30000000
*TITLE
MANPADS Lethality Characterization
$$ HM_OUTPUT_DECK created 10:39:42 03-03-2006 by HyperMesh Version 7.0
$$ Ls-dyna Input Deck Generated by HyperMesh Version  : 7.0
$$ Generated using HyperMesh-Ls-dyna 970 Template Version : 7.0
*CONTROL_TERMINATION
$$  ENDTIM    ENDCYC     DTMIN    ENDENG    ENDMAS
      0.01         0       0.0       0.0       0.0
*CONTROL_TIMESTEP
$$  DTINIT    TSSFAC      ISDO    TSLIMT     DT2MS      LCTM     ERODE
MSIST
1.0000E-07       0.9         0       0.0       0.0         0         1
       0.0
*CONTROL_SHELL
$$  WRPANG     ESORT     IRNXX    ISTUPD    THEORY       BWC     MITER
PROJ
      20.0         1        -1         0         2         2         1
       1.0         0         0         1
*CONTROL_CONTACT
$$  SLSFAC    RWPNAL    ISLCHK    SHLTHK    PENOPT    THKCHG     ORIEN
ENMASS
      10.0       0.0         2         0         1         1         1
$$  USRSTR    USRFRC     NSBCS    INTERM     XPENE     SSTHK      ECDT
TIEDPRJ
         0        10         0         0       0.0
$$   SFRIC     DFRIC       EDC    INTVFC        TH     TH_SF  TIPEN_SF
       0.0       0.0       0.0       0.0       0.0       0.0       0.0
$$  IGNORE    FRCENG
         0         0         0         0         0         0
*CONTROL_PARALLEL
$$    NCPU    NUMRHS      ACCU
         4         0         2
*CONTROL_OUTPUT
$$   NPOPT    NEECHO    NREFUP    IACCOP     OPIFS    IPNINT    IKEDIT
         1         3         0         0       0.0         0       100
5000
         0
*CONTROL_ENERGY
$$    HGEN      RWEN    SLNTEN     RYLEN
         2         2         1         1
$$DATABASE_OPTION -- Control Cards for ASCII output
*DATABASE_GLSTAT
1.0000E-04         1
*DATABASE_MATSUM
1.0000E-07         1
*DATABASE_RCFORC
1.0000E-04         1
*DATABASE_SLEOUT
1.0000E-04         1
*DATABASE_BINARY_D3PLOT
$$ DT/CYCL      LCDT      BEAM     NPLTC
2.0000E-04
```

```
         0
*DATABASE_BINARY_D3DUMP
$$ DT/CYCL
   20000.0
*DATABASE_EXTENT_BINARY
$$   NEIPH     NEIPS    MAXINT    STRFLG    SIGFLG    EPSFLG    RLTFLG
ENGFLG
         0         0         0         0         0         0         0
0
$$  CMPFLG    IEVERP    BEAMIP     DCOMP      SHGE     STSSZ    N3THDT
         0         0         0         0         0         0         0
$$ NINTSLD

*NODE
  332775    377.76998901    -52.68299866     15.79699993
  332782    388.17001343    -32.61600113      16.9260006
.
.
.
  332785     407.6000061    -32.61000061     17.85499954
  384953 379.66150182237 -85.91665906484 13.052420972553
  384954 378.05136946763 -85.38977899395 13.072202190137
*MAT_ELASTIC
$HMNAME MATS       1MATL1_1
         1     0.10210200000.0     0.308       0.0       0.0
*MAT_PIECEWISE_LINEAR_PLASTICITY
$HMNAME MATS   11004MATL24_11004
     110047.4000E-0427000000.0      0.33  169700.0  118400.0
0.1878.0000E-08
       0.0       0.0         0         0         0
$$ HM Entries in Stress-Strain Curve =         8
       0.0     0.187       0.0       0.0       0.0       0.0       0.0
0.0
  169700.0  191840.0       0.0       0.0       0.0       0.0       0.0
0.0
*MAT_PIECEWISE_LINEAR_PLASTICITY
$HMNAME MATS   11002MATL24_11002
     110022.5400E-04 9744000.0      0.33   68000.0   50000.0
0.118.0000E-08
       0.0       0.0         0         0         0
$$ HM Entries in Stress-Strain Curve =         8
       0.0      0.11       0.0       0.0       0.0       0.0       0.0
0.0
   68000.0   73500.0       0.0       0.0       0.0       0.0       0.0
0.0
*MAT_PIECEWISE_LINEAR_PLASTICITY
$HMNAME MATS      21MATL24_21
        212.6140E-0410300000.0      0.33   70000.0   50000.0
0.118.0000E-08
       0.0       0.0         0         0         0
$$ HM Entries in Stress-Strain Curve =         8
       0.0       0.0       0.0       0.0       0.0       0.0       0.0
0.0
   70000.0   75500.0       0.0       0.0       0.0       0.0       0.0
0.0
*PART
$HMNAME COMPS       1plate_1
```

```
$HMCOLOR COMPS        1        1
plate_1
         1          1          1
$HMNAME COMPS    11001FIN_BEAM
$HMCOLOR COMPS    11001        9
FIN_BEAM
     11001     11001     11004
$HMNAME COMPS    11075rear_fin
$HMCOLOR COMPS    11075        3
rear_fin
     11075     11075     11002
$HMNAME COMPS    11078plate_11078
$HMCOLOR COMPS    11078        6
plate_11078
     11078     11078        21
$HMNAME COMPS    11079plate_11079
$HMCOLOR COMPS    11079        7
plate_11079
     11079     11079        21
$HMNAME COMPS    11080plate_11080
$HMCOLOR COMPS    11080        8
plate_11080
     11080     11080        21
$HMNAME COMPS    11081plate_11081
$HMCOLOR COMPS    11081        9
plate_11081
     11081     11081        21
$HMNAME COMPS    11082plate_11082
$HMCOLOR COMPS    11082       10
plate_11082
     11082     11082        21
$HMNAME COMPS    11083plate_11083
$HMCOLOR COMPS    11083       11
plate_11083
     11083     11083        21
$HMNAME COMPS    11084plate_11084
$HMCOLOR COMPS    11084       12
plate_11084
     11084     11084        21
$HMNAME COMPS    11085plate_11085
$HMCOLOR COMPS    11085       13
plate_11085
     11085     11085        21
$HMNAME COMPS    11086plate_11086
$HMCOLOR COMPS    11086       14
plate_11086
     11086     11086        21
$HMNAME COMPS    11087plate_11087
$HMCOLOR COMPS    11087       15
plate_11087
     11087     11087        21
$HMNAME COMPS    11088plate_11088
$HMCOLOR COMPS    11088        1
plate_11088
     11088     11088        21
*SECTION_BEAM
$HMNAME PROPS    11001SectBeam_11001
```

```
     11001         1       1.0       2.0       0.0       0.0
8.4400E-041.2000E-051.2000E-05   0.03125
*SECTION_SHELL
$HMNAME PROPS       1SectShll_1
         1         1      0.87         5       2.0       0.0         0
      0.25      0.25      0.25      0.25       0.0       0.0
*SECTION_SHELL
$HMNAME PROPS   11075SectShll_11075
     11075         1       1.0         2       0.0       0.0         0
      0.15      0.15      0.15      0.15       0.0       0.0
*SECTION_SHELL
$HMNAME PROPS   11078SectShll_11078
     11078         1      0.87         5       2.0       0.0         0
      0.25      0.25      0.25      0.25       0.0       0.0
*SECTION_SHELL
$HMNAME PROPS   11079SectShll_11079
     11079         1      0.87         5       2.0       0.0         0
      0.25      0.25      0.25      0.25       0.0       0.0
*SECTION_SHELL
$HMNAME PROPS   11080SectShll_11080
     11080         1      0.87         5       2.0       0.0         0
      0.25      0.25      0.25      0.25       0.0       0.0
*SECTION_SHELL
$HMNAME PROPS   11081SectShll_11081
     11081         1      0.87         5       2.0       0.0         0
      0.25      0.25      0.25      0.25       0.0       0.0
*SECTION_SHELL
$HMNAME PROPS   11082SectShll_11082
     11082         1      0.87         5       2.0       0.0         0
      0.25      0.25      0.25      0.25       0.0       0.0
*SECTION_SHELL
$HMNAME PROPS   11083SectShll_11083
     11083         1      0.87         5       2.0       0.0         0
      0.25      0.25      0.25      0.25       0.0       0.0
*SECTION_SHELL
$HMNAME PROPS   11084SectShll_11084
     11084         1      0.87         5       2.0       0.0         0
      0.25      0.25      0.25      0.25       0.0       0.0
*SECTION_SHELL
$HMNAME PROPS   11085SectShll_11085
     11085         1      0.87         5       2.0       0.0         0
      0.25      0.25      0.25      0.25       0.0       0.0
*SECTION_SHELL
$HMNAME PROPS   11086SectShll_11086
     11086         1      0.87         5       2.0       0.0         0
      0.25      0.25      0.25      0.25       0.0       0.0
*SECTION_SHELL
$HMNAME PROPS   11087SectShll_11087
     11087         1      0.87         5       2.0       0.0         0
      0.25      0.25      0.25      0.25       0.0       0.0
*SECTION_SHELL
$HMNAME PROPS   11088SectShll_11088
     11088         1      0.87         5       2.0       0.0         0
      0.25      0.25      0.25      0.25       0.0       0.0
*INITIAL_VELOCITY_GENERATION
$HMNAME LOADCOLS       1InitialVelGen_1
$HMCOLOR LOADCOLS       1       1
```

```
        16         1       0.0       0.0       0.0  -14400.0
       0.0       0.0       0.0       0.0       0.0       0.0
*DEFINE_BOX
$HMNAME BLOCKS       1DefineBox_0
$HMCOLOR BLOCKS       1       1
         1 331.70001 385.29999-155.39999-98.650002     -55.0     181.0
*CONTACT_ERODING_SINGLE_SURFACE_ID
$HMNAME GROUPS       1ESingSurf_1
$HMCOLOR GROUPS       1       1
         1
         0                   5                   1
       0.0       0.0       0.0       0.0       0.0         0       0.0
0.0
       1.0       1.0       0.0       0.0       1.0       1.0       1.0
1.0
         0         1         1
         0       0.0         0       0.0       0.0
       0.0         0         0         0         0         0       0.0
0.0
         0         0
*ELEMENT_SHELL
  288921   11078  348081  348080  348082  348083
  288920   11078  348076  348081  348083  348077
  288002   11078  347016  347006  347023  347021
.
.
.
  310554   11088  371515  371516  371578  371514
  310555   11088  371516  355955  355956  371578
*END
```

Symbols

A	=	fragment area
A	=	constant for JWL equation of state
B	=	constant for JWL equation of state
C_d	=	drag coefficient
E	=	specific internal energy
P	=	predicted pressure
R_1	=	constant for JWL equation of state
R_2	=	constant for JWL equation of state
V_i	=	initial velocity
V_f	=	final velocity
$a_0 \ldots a_7$	=	constants for Gruneisen equation of state
e	=	specific internal energy, and
k	=	drag coefficient
m	=	mass
x	=	distance traveled
η	=	ρ/ρ_0,
μ	=	η-1
ω	=	constant for JWL equation of state
ρ	=	overall material density,
ρ_0	=	reference density (initial density),

Abbreviations

CONWEP	=	Conventional Weapons

Acronyms

ALE	=	Arbitrary Lagrangian Eulerian
CEL	=	Coupled Euler Lagrange
FEA	=	Finite Element Analysis
FEM	=	Finite Element Method
FFT	=	Fast Fourier Transform
JLF	=	Joint Live Fire
JSF	=	Joint Strike Fighter
JTCG/AS	=	Joint Technical Coordinating Group for Aircraft Survivability
JWL	=	Jones-Wilkins-Lee
LFT&E	=	Live Fire Test and Evaluation
MANPADS	=	Man Portable Air Defense Systems